Improvement of Accuracy and Reliability on BWR Thermal-Hydraulic Analysis Code by Newly Modified Interfacial Drag Force Models

by Tetsuhiro Ozaki

A dissertation submitted in partial fulfillment of requirements for the
Degree of Doctor of Philosophy in Engineering

Division of Energy and Environmental Systems
Graduate School of Engineering
Hokkaido University
Sapporo, JAPAN

August 2018

Table of Contents

Nomenclature

a	coefficient
a_i	interfacial area concentration
b	coefficient
C	Chisholm's parameter
C_i	interfacial drag coefficient
C_0	distribution parameter
C_D	drag coefficient
C_{wf}	wall drag coefficient of liquid phase
C_{wg}	wall drag coefficient of gas phase
C_α	void fraction covariance
C'_α	relative velocity covariance
C''_α	drift velocity covariance
C_∞	asymptotic distribution parameter
d_B	bubble departure diameter
D_{base}	drag diameter of cap bubble
D_d	drag diameter
D_H	hydraulic equivalent diameter
D_{Sm}	Sauter mean diameter
DR	dumping ratio
F_w	pressure drop due to wall friction
f	Fanning friction factor
g	gravitational acceleration
g_1	factor
G	mass flux
j	mixture volumetric flux
j_f	superficial liquid velocity
j_g	superficial gas velocity
La, Lo	Laplace length
M_{ik}	interfacial drag force

$M_{\tau k}$	viscous and turbulent shear stress
m_d	mean absolute error
m_{rel}	mean relative deviation
$m_{rel.ab}$	mean absolute relative deviation
n	exponent
N_{a_i}	non-dimensional interfacial area concentration
N_{La}	non-dimensional Laplace length
N_{Re_b}	bubble Reynolds number
N_{vr}	relative velocity ratio
$N_{\mu f}$	viscosity number
N_{ρ}	density ratio
p , P	pressure
p_c	critical pressure
Q	bundle power
r	radial distance
R_w	radius of a pipe
Re	Reynolds number
$Re_{2\phi,f}$	liquid phase Reynolds number
s_d	standard deviation
t	time
v	velocity
v_{gj}	drift velocity
v_r	relative velocity between phases
V_{gj}^{+}	non-dimensional drift velocity
$\left\langle\left\langle v_{gj}^{*}\right\rangle\right\rangle$	drift velocity ratio
W	mass flow rate
X	Martinelli's parameter
X_{+3}	specific value of positive third peak

X_{+4}	specific value of positive fourth peak
X_{steady}	specific value at an initial steady-state condition
$\left\langle x_f \right\rangle_{exit}$	area-averaged flow quality at the exit of heated region
z	axial position

Greek symbols

α	void fraction
α_0	void fraction at center of a pipe
$\left\langle \alpha_{target} \right\rangle$	target void fraction predicted by drift-flux model
$\Delta\rho$	density difference
ε	energy dissipation rate per unit mass
ε_{BI}	bubble induced energy dissipation
ε_{sh}	shear induced energy dissipation
ε_w	wall surface roughness
ϕ	momentum source defined in chapter 3
ϕ^2	two-phase wall friction multiplier
ϕ_S	correction factor
$\Phi_{Phase\ Change}$	sink/source term of interfacial area concentration due to phase change
$\Phi_{Pressure\ Change}$	sink/source term of interfacial area concentration due to pressure change
Φ_{sink}	sink term of interfacial area concentration due to bubble coalescence
Φ_{source}	source term of interfacial area concentration due to bubble breakup
η	factor
μ	viscosity
ν	kinematic viscosity

ρ	density
σ	surface tension
τ_w	wall shear stress
ψ	shape factor
ξ	uncertainty factor for drag coefficient
ζ	factor for relative velocity ratio

Subscripts

1	value for group 1 bubble
2	value for group 2 bubble
B	bubbly flow condition
BB	bulk boiling condition
$crit$	critical value
f	liquid phase
$film$	liquid film
g	gas phase
init	initial value
k	liquid or gas phase
L	laminar region
$L-T$	transition region between laminar and turbulent regions
m	mixture
max	maximum value
P	pool condition
SB	subcooled boiling condition
T	turbulent region
w	wall
w cov	With covariance
w/o cov	Without covariance

Superscripts

$+$	non-dimensional value

Mathematical symbols

$\langle\ \rangle$	area-averaged quantity
$\langle\langle\ \rangle\rangle$	void-fraction-weighted mean quantity
∞	asymptotic value

1. Introduction

1.1 Historical background of thermal-hydraulic safety analysis codes

Since the first nuclear power plant, Dresden-1, began commercial operation in the United States, ensuring a high level of safety has been a primary concern. Sophisticated analytical methodology and system calculation codes have always been explored to accurately predict thermal hydraulic behavior within various components of a nuclear power plant, such as the reactor core, steam separator, steam generator, jet pump, pipe, and so on. Nuclear energy is attractive, compared to other power generation methods, due to high energy density, low fuel costs, and suppression of CO_2 emissions. However, limited public acceptance of nuclear power exists due to significant safety concerns, especially after the severe accidents occurring at TMI-2 in 1979, Chernobyl in 1986, and the Fukushima Daiichi nuclear power plant in 2011. Therefore, the implementation of thermal-hydraulic simulations in the analysis of nuclear power plants is crucial to ensure design integrity, develop countermeasures to prevent reactor meltdowns in accident scenarios, and to provide useful information for reactor operators.

In the 1960's, low computational performance restricted the selection of the analytical method to a homogenous approach. Under the homogeneous flow assumption, equal temperature and velocity in the gas and liquid phases are assumed. This approximation allows for three fundamental equations of mass, momentum, and energy to be solved when determining the thermal-hydraulic behavior of two-phase flow. The idea of the drift-flux model, later proposed by Zuber and Findlay [1-1], allowed the gas-phase velocity to be approximated by a drift velocity and distribution parameter, which represent the difference between gas velocity and mixture volumetric flux, the spatial covariance of mixture volumetric flux and void fraction, respectively. Ishii [1-2] extended the drift-flux model to develop the distribution parameter and the drift velocity models, which enhanced the applicability of the drift-flux model in thermal-hydraulic simulations. In the 1970's, thermal-hydraulic codes implemented the drift-flux model through the use of four fundamental equations. In the 1980's, increases in computational performance became evident and codes, such as RELAP5, TRAC, etc., began to implement the two-fluid model. The two-fluid model uses separate mass, momentum, and energy equations for the gas and liquid phase, respectively. The individual treatment of the gas and liquid phase allows for the elimination of the homogenous flow assumption. Therefore, this more rigorous evaluation can provide more precise calculation results, but the complexity of the analysis increases significantly. Since the two-fluid model solves six conservation equations, several constitutive equations representing mass,

momentum, and energy transfer terms between gas-liquid interface are needed to close the model. Interfacial transport of mass, momentum, and energy is dependent on the interfacial area concentration and flow structure of two-phase flow, which depend on flow velocity, void fraction, geometrical condition, etc. Two-fluid analysis codes developed around the 2000's introduced a flow regime map model, which allowed for specification of appropriate constitutive equations in accordance with specific two-phase flow regimes, such as the dispersed bubbly flow, churn flow, annular flow, and droplet flow regimes.

Recently, high-performance computers have allowed for the prediction of two-phase flow behavior to be refined by implementing an interfacial area concentration equation in two-fluid codes. The interfacial area concentration equation can estimate the time and spatial dependent value of interfacial area concentration by accounting for the change of interfacial structure in two-phase flow through introducing source terms to model bubble breakup, coalescence, expansion, and phase change. Traditionally, a flow regime map model is not necessary if the interfacial area concentration equation is introduced in a two-fluid code because the value of interfacial area concentration is obtained through mechanistically formulated models representing physical processes of bubble interfacial behavior. However, many experimental works must be required to develop reliable constitutive relations for source terms and to obtain sufficient databases over the wide range of flow conditions needed to evaluate the relations. High computational costs, compared to the existing flow regime map based two-fluid model, are associated with two-fluid codes because additional conservation equations are needed to solve the interfacial area transport equation.

The historical evolution of thermal-hydraulic simulation codes shows that as computational performance has increased the implementation of more rigorous methodology has improved prediction of two-phase flow behaviors. This improved accuracy has allowed us to increased safety and economic efficiency of a nuclear power plant. However, the number of constitutive relations required to close the conservation equations have increased, resulting in the credibility of results obtained by analysis codes to become largely dependent on the fidelity of the implemented constitutive relations. It is important to utilize a computational code that determines the applicability of implemented constitutive relations to the problem of interest and selects proper methodology to achieve the highest level of safety possible. Relevant physical phenomena and computational behavior should be studied and compared to realize improved accuracy in future safety analysis codes. The developed constitutive relations should then be carefully selected based on the recognition of real physical mechanisms and model sensitivity.

1.2 Application of best estimate codes and its reliability

Two-fluid thermal-hydraulic codes like TRAC-BF1, TRACE, RELAP5, and so on are classified as best estimate codes and are expected to improve code accuracy compared to codes using the homogenous flow approach. These codes have been utilized to simulate nuclear power plant behavior during AOOs (Anticipated Operational Occurrences) or anticipated severe accident scenarios. Such best-estimate codes solve the six basic conservation equations with many constitutive equations, which are required to couple the conservation equations. Therefore, the relationship between inputs and results of simulations become quite complicated, and the effect of each constitutive equation on simulation outputs is unclear. The credibility of an analysis code, for the simulation of an anticipated operating scenario, should be assessed through confirmation of proper code design with the intended algorithms (verification) and the ability to simulate the required physical phenomena through proper mathematical models (validation).

The code validation process begins by identifying a specific power plant and scenario. Then the important phenomena to be considered must be identified and summarized in a PIRT (Phenomena Identification and Ranking Table) [1-3]. Highly ranked phenomena, determined by a PIRT, have a significant influence on safety parameters when licensing criteria assessed for a specific simulation scenario. The eligibility of the physical models to a real power plant and a specific scenario in highly ranked phenomena determines the credibility of the code. Therefore, it is necessary to validate the physical models of highly ranked phenomena based on appropriate experimental databases. Ideally, these experimental databases should be obtained by reproducing practical conditions. Otherwise, the scalability of a database should be assessed by considering whether the experiment and physical model can be extended to realistic flow conditions for the use in the simulation of actual phenomena. Moreover, EMDAP (Evaluation Model Development and Assessment Process), ruled by the US regulatory guide 1.203 and V&V methodology require the identification of model uncertainties based on the information about fidelity and pedigree of each physical model, and interaction with the other phenomena.

As can be seen in V&V methodology [1-4], the following confirmation process should be performed to assure the model credibility and identification of model uncertainty.

1) The physical concept of the model
2) Adequacy of the experimental database
3) Model prediction ability to various experimental data
4) Scalability of experiment and model

5) Effect of approximated and neglected phenomena

Mechanistic models of physical phenomena implemented in simulation codes are becoming more detailed and complicated, which necessitates increased analysis to determine code credibility. Methodology such as CSAU (Code Scaling, Applicability and Uncertainty), EMDAP, and V&V provide procedures to enhance overall code credibility by selecting the most important physical phenomena that need elaboration, and allow for prevention of time and resource consumption caused by reckless development.

1.3 Thesis objectives

Based on the background to enhance the reliability of a nuclear safety analysis code, it becomes necessary to confirm the fidelity of the code and to identify how precisely the code can simulate the anticipated scenario. Traditionally, safety analysis codes have been developed to simulate specific experimental data. The code models are not rigorous containing approximation and compensating errors may exist if the model parameters have been adjusted to simulate experimental data. Additionally, if the experimental data with prototypic conditions are not available to develop the codes, the scalability of the code models are the problem to assure the codes can simulate prototypic plant behavior as well as the experimental data. Eliminating the approximation of the codes is one of an approach to resolve this problem. Therefore, it is required to improve the reliability of a nuclear safety analysis code by means of the proper usage of basic equation and selection of constitutive equations.

Study of a rigorous interfacial drag model and improvement of the momentum equation used in one-dimensional two-fluid analysis codes are the focus of this thesis. Figure 1-1 schematically shows the relationship between the research topic of this thesis and existing research about interfacial drag models utilized in one-dimensional two-fluid analysis codes.

A momentum transfer term between the liquid and gas phases has a significant role in two-fluid analysis codes and is used to calculate void fraction, a characteristic parameter of two-phase flow. It is well known that void fraction impacts nuclear thermal power feedback, pressure loss, flow distribution within a core, two-phase water level, flow induced vibration, etc. in a light water reactor. Depending on the scenarios to be simulated, the phenomenon of interfacial momentum transfer in a core region may be highly-ranked in a PIRT for many anticipated scenarios.

One-dimensional two-fluid analysis codes are typically selected to perform the safety analysis of nuclear power plants, since detailed three-dimensional codes, such as 3D-CFD codes, are

inappropriate to simulate such a large and complicated system due to extremely high computational demand. In one-dimensional two-fluid analysis codes, the conservation equations are solved, to simulate two-phase flow behavior, through use of physical quantities that are area-averaged over a specific geometrical flow area. Therefore, each source term implemented in the area-averaged conservation equations must account for the effect of area-averaging.

The interfacial drag term, which is an important source term in the momentum equation, can be formulated based on parameters such as relative velocity between gas and liquid phase, drag coefficient, interfacial area concentration, and so on. It is also necessary to consider the effect of void fraction and velocity spatial distribution on the area averaged value of the interfacial drag term. Andersen and Chu [1-5] proposed an area-averaged interfacial drag model based on Ishii and Mishima[1-6]'s formulation of area-averaged relative velocity through the introduction of distribution parameter and drift velocity. Namely, this area-averaged interfacial drag model is utilized in one-dimensional two-fluid analysis codes by applying the idea of the drift-flux model to consider the void fraction and mixture volumetric flux profiles. On the other hand, Brooks et al. [1-7, 1-8] indicates the necessity of introducing void fraction covariance (spatial auto-covariance of void fraction), which is a result of the rigorous area-averaging of relative velocity. Additionally, Hibiki and Ozaki [1-9], Ozaki and Hibiki [1-10] developed constitutive equations of void fraction covariance for piping and rod bundle, respectively. The approximation of uniform void fraction profile, pointed out by Brooks et al. [1-7, 1-8], can be excluded by implementing these developed covariance models into one-dimensional two-fluid analysis codes, which contributes to an improvement in the rigorous treatment of safety analysis. However, the other problem still needs to be solved. The wall shear friction term included in the momentum equation of a current existing one-dimensional two-fluid analysis code is derived based on the assumption of uniform void fraction profile. No existing knowledge has been found, regarding the proper expression of the momentum equation with consideration of the void fraction covariance model. Additionally, the effect of the uniform void fraction profile approximation should be assessed by comparing the obtained results with a rigorous formulation treating void fraction covariance. These discussions are necessary to judge the validity and credibility of the current code approximation.

Since the interfacial drag force term is dependent on the geometrical interfacial structure of two-phase flow, consideration of flow regime allows for the determination of this term. Kelley [1-11], however, pointed out that discontinuity of calculation results and numerical instability was caused by constitutive equation transition as two-phase flow changes flow regime. In response, to address this problem, the interfacial area concentration transport equation (IATE) has been

developed. IATE can represent the interfacial structure of two-phase flow without using a flow regime map model, so Talley et al. [1-12, 1-13] implemented IATE in the TRACE code to assess its applicability. The usage of IATE still has the following problems to overcome when accounting for its compatibility to V&V methodology, namely,

1) Results of IATE are strongly dependent on an initial value which cannot readily be determined.
2) Sink/source terms included in IATE require many coefficients, whose validity cannot readily be confirmed.
3) Coefficients of source terms are dependent on the geometrical condition of the flow path.
4) Constitutive relations to determine source terms are not scalable to the prototypic operational conditions in a light water reactor (LWR) because these correlations have been developed based on databases obtained under steady-state air-water flow at atmospheric pressure.

Recently, Ozar et al. [1-14], Schlegel and Hibiki [1-15], and Shen and Hibiki [1-16] developed constitutive equations for predicting interfacial area based on the idea of a two-group model. Bubbles in two-phase flow are categorized according to a characteristic difference of interfacial drag, and thus spherical bubbles in dispersed bubbly flow are considered as group-1 bubbles. Whereas, Taylor bubbles in slug flow, cap bubbles in cap bubbly or cap turbulent flow, and bubbles in churn turbulent flow regimes are considered as group-2 bubbles. The interfacial area for group-1 and group-2 bubbles can be identified by the proposed constitutive equations and possibly by providing an interfacial drag force term in a one-dimensional two-fluid analysis code. Although the introduction of these interfacial area concentration correlations can resolve some IATE problems, such as the complexity of equations and increased computational cost, the existing work is needed to determine the adequacy of the constitutive equations when implemented in a one-dimensional two-fluid code and the effect of uncertainty on the prediction of void fraction. Discussion of how the interfacial area concentration affects the results of a two-fluid analysis code is another goal of this thesis. Sink/source terms implemented in IATE shall be modeled based on physical phenomena like coalescence and breakup of bubbles, bubble expansion due to pressure gradient, phase change, and so on. The existing databases are insufficient to scale the data to the prototypic operating conditions of a real power plant, so the databases should be extended to a range comparable to prototypic flow conditions, geometrical condition, etc. In general, the cost to obtain such databases is significant. Therefore it should be carefully discussed whether the investments for IATE

development will contribute to improved accuracy in safety analysis codes.

Based on the above mentioned existing works and unresolved issues, the following studies have been performed to determine useful knowledge about the importance of the interfacial drag model in a one-dimensional two-fluid analysis code.

1) A rigorous formulation of the momentum equation for a one-dimensional two-fluid analysis code, considering void fraction covariance.
2) A comparison between the existing model based on Andersen and Chu [1-5] and the above rigorous approach to clarify the effect of the approximation on uniform void fraction distribution.
3) Development of an interfacial drag model for a one-dimensional two-fluid analysis code, based on the two-group interfacial area concentration correlation models developed by Ozar et al. [1-14] and Schlegel and Hibiki [1-15], and confirmation of the newly developed model's applicability.
4) Clarify the effect of interfacial area concentration and drag coefficient on void fraction through uncertainty analysis of the interfacial drag model, based on the two-group interfacial area concentration correlation model.

1.4 Outline of the thesis

The following chapters discuss void fraction covariance, momentum equation development, and the interfacial drag force term. Chapter 2 reviews existing constitutive equations applied to rod bundle geometry in two-fluid analysis codes. The effect of void distribution covariance on a one-dimensional two-fluid analysis code has been studied for pipe and rod bundle and is discussed in chapter 3 and chapter 4, respectively. The appropriate formulation of the momentum equation, with consideration of a void fraction covariance model, is also discussed in these chapters. Additionally, the interfacial drag force term may affect transient behavior due to the difference of characteristics in momentum coupling between phases. Therefore, differences in calculation results for transient scenarios are investigated to compare cases with and without consideration of covariance.

Chapter 5 discusses the formulation of the interfacial drag force term, based on the two-group interfacial area concentration correlations. This methodology, a so-called "C_D approach," is validated against several representative separate effect tests and determination of numerical instability, which might occur due to flow regime transition, is discussed. Chapter 5 also investigates the influence of uncertainties in interfacial area concentration and drag coefficient, since

these uncertainties are normally considered to be significant. The sensitivity of interfacial area concentration and drag coefficient is also quantified to provide useful information to determine further development required in safety analysis codes. Lastly, the findings obtained in these studies are summarized and concluded in chapter 6.

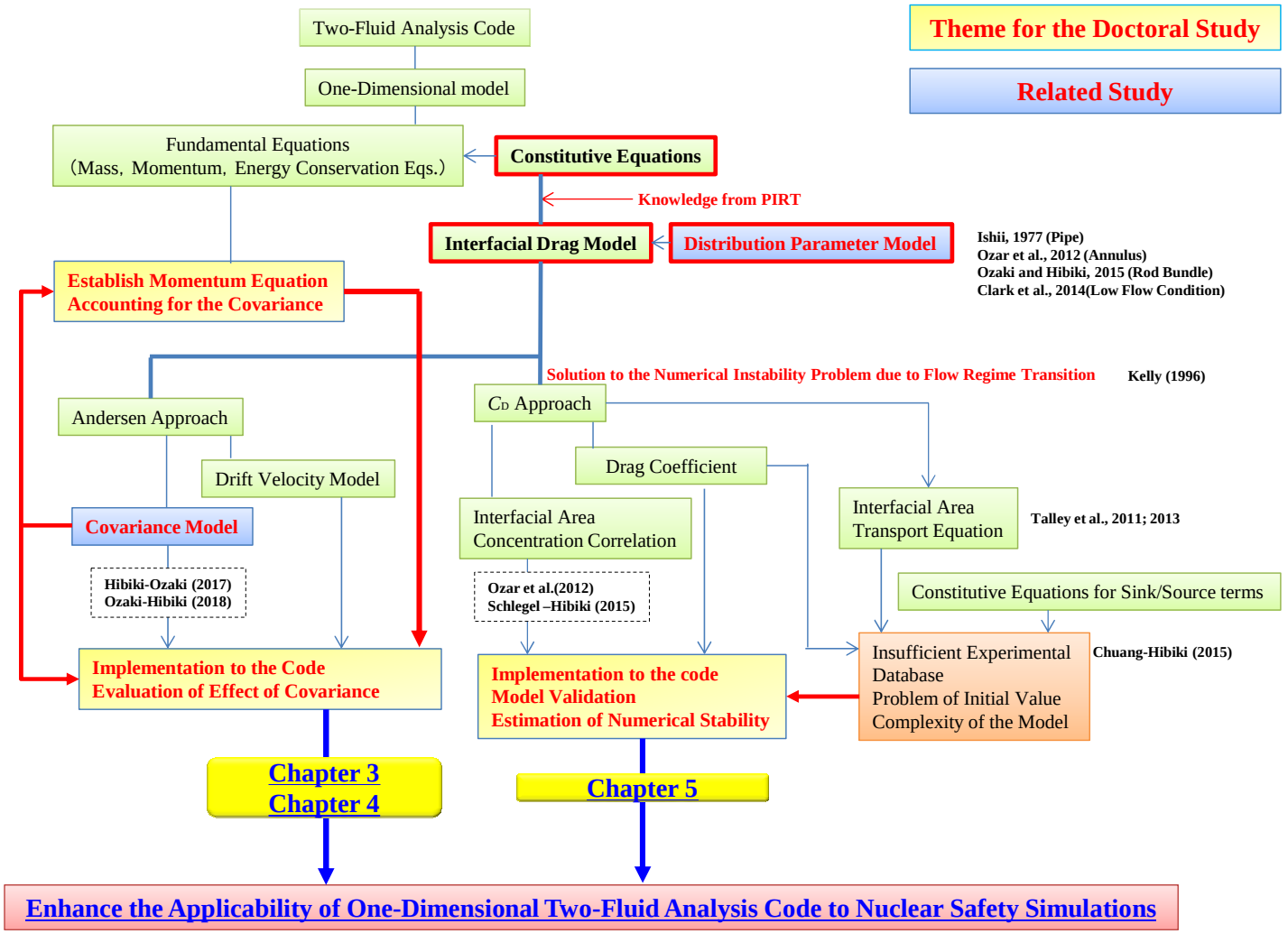

Figure 1-1 Schematic of the relation between this research and existing research related to one-dimensional interfacial drag model.

References

[1-1] Zuber N, Findlay JA. Average volumetric concentration in two-phase flow systems. Journal of Heat Transfer 1965; 87: 453-468.

[1-2] Ishii M. One-dimensional drift-flux model and constitutive equations for relative motion between phases in various two-phase flow regimes. USA: Argonne National Laboratory; 1979. (ANL-77-47).

[1-3] Boyack B, Duffey R, Griffith P ,et al. Quantifying reactor safety margins: Application of code scaling, applicability, and uncertainty evaluation methodology to a large-break, loss-of-coolant accident. USA: US NRC; 1989. (NUREG/CR-5249/EGG-2552).

[1-4] Atomic Energy Society of Japan. Guidline for credibility assessment of nuclear simulations: 2015. Tokyo: AESJ; 2016. (AESJ-SC-A008:2015). Japanese.

[1-5] Andersen JGM, Chu KH. BWR refill-reflood program constitutive correlations for shear and heat transfer for the BWR version of TRAC. Washington DC: US NRC; 1983. (NURG/CR-2134/GEAP-24940).

[1-6] Ishii M, Mishima K. Two-fluid model and hydrodynamic constitutive relations. Nuclear Engineering and Design 1984;82:107-126.

[1-7] Brooks CS, Ozar B, Hibiki T, et al. Two-group drift-flux model in boiling flow. International Journal of Heat and Mass Transfer 2012;55:6121-6129.

[1-8] Brooks CS, Liu Y, Hibiki T, et al. Effect of void fraction covariance on relative velocity in gas-dispersed two-phase flow. Progress in Nuclear Energy 2014;70:209-220.

[1-9] Hibiki T, Ozaki T. Modeling of distribution parameter, void fraction covariance and relative velocity covariance for upward steam-water boiling flow in vertical pipe. International Journal of Heat and Mass Transfer 2017;112:620-629.

[1-10] Ozaki T, Hibiki T. Modeling of distribution parameter, void fraction covariance and relative velocity covariance for upward steam-water boiling flow in vertical rod bundle. Journal of Nuclear Science and Technology 2018;55:386-399.

[1-11] Kelley JM. Thermal-hydraulic modeling needs for passive reactors. Proceedings of the OECD/CSNI Workshop on Transient Thermal-Hydraulic and Neutronic Codes Requirements, Annapolis, Maryland, USA, Nov. 5-8, 1996.

[1-12] Talley JD, Kim S, Mahaffy J, et al. Implementation and evaluation of one-group interfacial area transport equation in TRACE. Nuclear Engineering and Design 2011;241:865-873.

[1-13] Talley JD, Worosz T, Kim S, Bajorek S, Tien K. Effect of bubble interactions on the prediction of interfacial area in TRACE. Nuclear Engineering and Design 2013;264:135-145.

[1-14] Ozar, B., Dixit, A., Chen, S.W., Hibiki, T., Ishii, M., Interfacial area concentration in gas-liquid bubbly to churn-turbulent flow regime. International Journal of Heat and Fluid Flow 38 (2012) 168-179.

[1-15] Schlegel, J.P., Hibiki, T., A correlation for interfacial area concentration in high void fraction flows in large diameter channels. Chemical Engineering Science 31 (2015) 172-186.

[1-16] Shen X, Hibiki T. Interfacial area concentration in gas-liquid bubbly to churn flow regimes in large diameter pipes. International Journal of Heat and Fluid Flow 2015;54:107-118.

2. Constitutive Equations for Vertical Upward Two-Phase Flow in Rod Bundle

2.1 Introduction

Two-phase flows are encountered in various industrial apparatuses such as chemical reactors, boilers, heat exchangers and nuclear reactors. Detailed three-dimensional two-phase flow analyses using two-phase computational fluid dynamics (two-phase flow CFD) codes have been advanced for design and performance analyses of industrial apparatuses [2-1]. However, the prediction accuracy of the two-phase flow CFD does not reach sufficient level for these purposes due to the difficulty of modeling in interfacial area concentration, two-phase flow turbulence, non-drag force and wall nucleation source [2-2, 2-3] as well as lack of local two-phase flow data to be used for validating the two-phase flow CFD [2-4].

In a practical use of two-phase flow analyses, one-dimensional analyses are common. For example, a nuclear reactor system is composed of many components such as reactor core, piping and safety components which make the system complicated. In order to simulate some accident scenario, the nuclear system behavior is the focus. A flow channel in each component is area-averaged and one-dimensional formulation is used in a nuclear thermal-hydraulic system analysis code. In the nuclear thermal-hydraulic system analysis code, the two-fluid model is often utilized as modeled two-phase conservation equations [2-5]. The one-dimensional two-fluid model is formulated by averaging local time-averaged two-fluid model over a flow channel and is composed of six equations, namely mass, momentum and energy balance equations for gas and liquid phases. The two-fluid model is considered one of most accurate two-phase flow balance equations because it can treat thermal and kinematic non-equilibrium between two phases. In order to close the mathematical system of the two-fluid model, numerous constitutive equations should be given. Figure 2-1 shows a typical code structure and important constitutive equations. Since constitutive equations are often flow-regime-dependent, accurate flow regime transition boundaries should be identified. A drift-flux type correlation is often used for calculating the area-averaged relative velocity between phases. An interfacial area correlation is important for calculating an available area for mass, momentum and energy transfers. A correlation to predict a wall friction is indispensable in closing the momentum equation. Continuous efforts have been made to improve the prediction accuracy of these correlations and constitutive correlations have been well-established for a simple geometry such as a pipe.

Due to the requirement to use best-estimate codes, CSAU (Code Scalability, Applicability,

and Uncertainty) methodology has been established. In the CSAU methodology, the scalability of constitutive correlations in terms of channel geometry (size and shape) and thermal-hydraulic conditions (pressure, temperature and velocity) should be assessed and the uncertainty of the correlations should be evaluated. One cornerstone of the CSAU methodology is to develop the Phenomenon Identification and Ranking Table (PIRT) [2-7]. Some PIRT evaluation suggests that constitutive equations in a nuclear reactor core analysis may have a significant impact on the safety measure. In view of this, important constitutive equations for a rod bundle should be re-assessed and be improved to enhance the prediction accuracy. Recently, several improved constitutive equations have been proposed for flow regime transition criteria, void fraction, void fraction covariance and relative velocity covariance and interfacial area concentration in a rod bundle. This chapter discusses the state-of-the-art constitutive equations for flow regime transition criteria, void fraction, void fraction covariance and relative velocity covariance and interfacial area concentration in a rod bundle and reviews the constitutive equation for wall frictional pressure drop used in legacy one-dimensional nuclear thermal-hydraulic system analysis codes such as TRACE, RELAP5 and TRAC codes.

2.2 Flow regime map

In a dynamic two-phase flow, an interfacial structure evolves spatially and temporally. Since the interaction between two phases occurs through the interface, the interfacial structure significantly affects the mass, momentum and energy transfers between two phases. The dependence of the interfacial structure on flow parameters is expressed as a flow regime map or a flow pattern map. Typical two-phase flow regimes observed in a vertical channel are bubbly, slug, churn and annular flow. In a large size channel, slug bubbles cannot exist due to its surface instability and the slug flow regime is replaced with cap bubbly flow and cap turbulent flow regimes [2-8]. In a nuclear thermal-hydraulic system analysis code, a two-phase flow regime is commonly determined by two parameters such as void fraction and mass flux, and flow-regime-dependent constitutive equations are used with some interpolation scheme between two different flow regimes.

Table 2-1 lists existing experimental studies in observing two-phase flow regime map in vertical rod bundles. From the overall viewpoint, observed two-phase flow regimes in the vertical rod bundles are bubbly, finely dispersed bubbly, cap bubbly, cap turbulent, churn and annular flow regimes. It should be noted here that Venkateswararao et al. [2-9] adopted slug flow regime instead of cap bubbly and cap turbulent flow regimes. This may be due to a limited understanding of two-phase flow characteristics in a large channel such as large bubble disintegration due to its

surface instability as of 1982. The two-phase flow regimes observed in a relatively small bundle such as a 3×3 rod bundle may be different from these in a large bundle such as an 8×8 rod bundle, because slug bubbles spanning over the bundle casing can exist in the small bundle.

Venkateswararao et al. [2-9] proposed a phenomenological model to predict the transition boundaries between two-phase flow regimes including slug flow regime. As discussed above, the slug flow regime should be replaced with cap bubbly and cap turbulent flow regimes. Liu and Hibiki [2-15] performed extensive literature survey of existing experimental flow regime maps and existing two-phase flow regime transition criteria model. They developed a phenomenological model to predict the two-phase flow regime transition boundaries and demonstrated its validity by comparing their model with existing data taken in vertical rod bundles. The brief summary of the Liu and Hibiki's model is given below.

Bubbly-to-cap bubbly flow transition

The bubbly-to-cap bubbly flow transition criterion given by Eq. (2-1) was derived by assuming a significant increase in the bubble coalescence rate at the distance between bubbles being smaller than the bubble diameter.

$$\left\langle j_f \right\rangle = \left\{ \frac{1}{\left(0.234 + 0.066\sqrt{\rho_g / \rho_f}\right) C_0} - 1 \right\} \left\langle j_g \right\rangle - \frac{\left\langle\left\langle v_{gj} \right\rangle\right\rangle}{C_0} \tag{2-1}$$

where j_f, j_g, v_{gj}, C_0, ρ_g and ρ_f are the superficial liquid velocity, superficial gas velocity, drift velocity, distribution parameter, gas density and liquid density, respectively. $\langle\ \rangle$ and $\langle\langle\ \rangle\rangle$ are the area-averaged quantity and void-fraction-weighted mean quantity, respectively. The distribution parameter and drift velocity are calculated by Ozaki and Hibiki's correlation [2-16] and Hibiki and Ishii's correlation [2-17], respectively.

Cap bubbly-to-cap turbulent flow transition

The cap bubbly-to-cap turbulent flow transition criterion considered "two-group" bubbles, namely, small bubble (group-1) and large-cap bubble (group-2). The transition criterion given by Eq. (2-2) was derived by assuming a significant increase in the small bubble coalescence rate at the distance between small bubbles being smaller than the small bubble diameter as well as a significant increase in the large bubble coalescence rate at the distance between large bubbles being smaller

than the large bubble diameter.

$$\left\langle j_f \right\rangle = \left(\frac{1}{0.51 C_0} - 1 \right) \left\langle j_g \right\rangle - \frac{\left\langle \left\langle v_{gj} \right\rangle \right\rangle}{C_0} \tag{2-2}$$

Bubbly-to-dispersed bubbly flow and dispersed bubbly-to-cap bubbly flow transitions

Two flow transition criteria were proposed based on critical Weber number and a maximum allowable void fraction.

Criterion based on critical Weber number:

$$\left(\frac{\rho_f}{\sigma} \right) \left(\frac{\sigma}{\Delta \rho g} \right)^{5/6} N_{\mu f}^{5/9} \left\langle \varepsilon \right\rangle^{2/3} = 0.0849 \tag{2-3}$$

where σ, $\Delta\rho$, g and ε are the surface tension, density difference, gravitational acceleration and energy dissipation rate per unit mass. The viscous number, $N_{\mu f}$, is defined by:

$$N_{\mu f} \equiv \frac{\mu_f}{\left(\rho_f \sigma \sqrt{\frac{\sigma}{\Delta \rho g}} \right)^{1/2}} \tag{2-4}$$

where μ_f is the liquid viscosity.

Criterion based on maximum allowable void fraction:

$$\left\langle \alpha_{crit} \right\rangle = 0.52 \tag{2-5}$$

where α is the void fraction.

Cap turbulent-to-churn flow transition

The cap turbulent-to-churn flow transition criterion was derived by assuming the void fraction averaged over the entire region being larger than that averaged over the cap-bubble section as:

$$\left\langle \alpha_{crit} \right\rangle \geq 1 - 0.813 \left[\frac{\left(C_0 - 1\right)\left\langle j \right\rangle + \left\langle \left\langle v_{gj} \right\rangle \right\rangle}{\left\langle j \right\rangle + 0.94\sqrt{\Delta\rho g D_H / \rho_f}\left\{ \Delta\rho g D_H^3 / \rho_f \nu_f^2 \right\}^{1/18}} \right]^{0.75} \tag{2-6}$$

where j, D_H and ν_f are the mixture volumetric flux, hydraulic equivalent diameter and liquid kinematic viscosity, respectively.

Churn-to-annular flow transition

Two transition criteria were proposed based on flow reversal in the liquid film section along large bubbles and destruction of large cap-bubbles or large waves by entrainment or deformation.

Criterion based on flow reversal:

$$\left\langle j_g \right\rangle = \sqrt{\frac{3\Delta\rho g D_H}{2\rho_g}}\left(\left\langle \alpha \right\rangle - 0.11\right) \tag{2-7}$$

Criterion based on destruction of large cap-bubbles or large waves by entrainment or deformation:

$$\left\langle j_g \right\rangle \geq \left(\frac{\Delta\rho g \sigma}{\rho_g^2} \right)^{1/4} N_{\mu f}^{-0.2} \tag{2-8}$$

Figure 2-2 compares Liu and Hibiki's model with a vertical upward air-water flow regime map observed in an 8×8 rod bundle under an atmospheric pressure condition [2-15]. Open square, solid diamond, open triangular and solid triangular in Fig. 2-2 indicate bubbly, cap bubbly, cap turbulent and churn flow regimes, respectively. Liu and Hibiki's model predicts the observed two-phase flow regime transition boundaries well. The validity of Liu and Hibiki's model at the boundaries between bubbly and finely dispersed bubbly flow regimes and between churn and annular flow regimes are also demonstrated using the data taken by Liu et al. [2-13] and Venkateswararao et al. [2-9], respectively. Liu and Hibiki's model adopts the state-of-the-art two-phase flow regime definitions in a vertical rod bundle and has been validated by several experimental two-phase flow regime maps. In view of these, Liu and Hibiki's model is considered

the state-of-the-art model to predict two-phase flow regime boundaries in a vertical rod bundle. However, since its validation has been done using data taken under atmospheric pressure conditions, the applicability of Liu and Hibiki's model to high pressure conditions should be examined using data to be taken in a future study.

2.3 Void fraction

Void fraction is one of most important two-phase flow parameters in characterizing gas fraction of a two-phase flow. The accurate prediction of void fraction is a key to estimate actual coolant level in a nuclear reactor core under an accident. Void fraction is also an important design parameter in various industrial apparatuses. A correlation based on the drift-flux model [2-18], namely a drift-flux correlation, is often used for predicting area-averaged or one-dimensional void fraction. The drift-flux model considers the relative velocity between phases through the drift velocity defined by:

$$v_{gj} \equiv v_g - j \tag{2-9}$$

where v_g is the gas velocity. Averaging Eq. (2-9) over a flow channel yields one-dimensional drift-flux model as:

$$\left\langle\left\langle v_g \right\rangle\right\rangle \left(\equiv \frac{\left\langle j_g \right\rangle}{\left\langle \alpha \right\rangle} \right) = C_0 \left\langle j \right\rangle + \left\langle\left\langle v_{gj} \right\rangle\right\rangle \tag{2-10}$$

One-dimensional nuclear thermal-hydraulic system analysis codes use a drift-flux correlation to calculate area-averaged relative velocity between phases from void-fraction-weighted mean gas and liquid velocities, $\left\langle\left\langle v_g \right\rangle\right\rangle$ and $\left\langle\left\langle v_f \right\rangle\right\rangle$ [2-19]. The distribution parameter is modeled by considering a scaling parameter such as a density ratio and a channel geometry. The drift velocity is modeled by a drag law for multi-particles.

Table 2-2 lists existing experimental studies in measuring void fraction in vertical rod bundles. Based on these existing data, several drift-flux type correlations were developed. Ozaki et al. [2-36] and Ozaki and Hibiki [2-16] performed an extensive review of the existing drift-flux type correlations including Bestion's correlation [2-37], Chexal and Lellouche's correlation [2-38], Inoue et al.'s correlation [2-39], Maier and Coddington's correlation [2-40] and Julia et al.'s correlation [2-41]. Ozaki and Hibiki [2-16] developed a drift-flux type correlation based on

vertical upward boiling water flow data taken in an 8×8 rod bundle under prototypic high pressure and temperature conditions as:

$$C_0 = 1.1 - 0.1\sqrt{\frac{\rho_g}{\rho_f}} \tag{2-11}$$

$$V_{gj}^{+} = V_{gj,B}^{+}\, exp\left(-1.39\left\langle j_g^{+}\right\rangle\right) + V_{gj,P}^{+}\left\{1 - exp\left(-1.39\left\langle j_g^{+}\right\rangle\right)\right\} \tag{2-12}$$

where

$$V_{gj}^{+} \equiv \frac{\left\langle\left\langle v_{gj}\right\rangle\right\rangle}{\left(\frac{\Delta\rho g\sigma}{\rho_f^2}\right)^{1/4}} \quad \text{and} \quad j_g^{+} \equiv \frac{\left\langle j_g\right\rangle}{\left(\frac{\Delta\rho g\sigma}{\rho_f^2}\right)^{1/4}} \tag{2-13}$$

The subscripts of B and P denote the bubbly flow and pool condition. The drift velocities for bubbly flow and pool condition are calculated by Ishii's correlation [2-42] and Kataoka and Ishii's correlation [2-43].

Ozaki et al. [2-36] demonstrated no significant effects of the power distribution of a rod bundle on the distribution parameter. They also revealed that the spacer grid effect on the distribution parameter goes away within a short distance from the spacer grid. Ozaki and Hibiki [2-16] discussed the effect of an unheated rod in a rod bundle on the distribution parameter and recommended Eq. (2-14) for a rod bundle with a large unheated rod.

$$C_0 = 1.08 - 0.08\sqrt{\frac{\rho_g}{\rho_f}} \tag{2-14}$$

Figure 2-3 compares Ozaki and Hibiki's correlation with void fraction measured in a vertical 8×8 rod bundle. Blue broken and red solid lines indicate the calculated values using Eqs. (2-11) and (2-14), respectively. Ozaki and Hibiki's correlation agrees with the data well. The average relative error of Ozaki and Hibiki's correlation is determined to be ±4.36 % based on data taken under a wide range of test conditions such as pressure from 0.1-12 MPa, mass flux from 5-2000 kg/m^{2}s, rod bundle casing size from 79-140 mm, hydraulic equivalent diameter from 9.8-21.7 mm and adiabatic and boiling flows.

Ozaki and Hibiki [2-44] used a bubble-layer thickness model [2-45] for deriving the distribution parameter of a subcooled boiling flow in a rod bundle as:

$$C_0 = \left(1.1 - 0.1\sqrt{\frac{\rho_g}{\rho_f}}\right)\left\{1 - exp\left(-12.1\left\langle\alpha\right\rangle^{0.701}\right)\right\} \tag{2-15}$$

which is applicable to $D_0/P_0 = 0.7 \sim 0.9$. D_0 and P_0 are the rod diameter and pitch between neighboring rods, respectively. Equation (2-15) indicates that enhanced wall peaking in void fraction distribution due to subcooled void near the rod lowers the distribution parameter in a subcooled boiling region and asymptotically approaches Eq. (2-11) in a bulk boiling region.

Liu et al. [2-46] performed an experiment using a vertical upward air-water bubbly flow in a 5×5 rod bundle under an atmospheric pressure condition and collected void fraction data. They developed the following correlation to predict the distribution parameter of an adiabatic bubbly flow in a rod bundle as:

$$C_0 = \left(1.1 - 0.1\sqrt{\frac{\rho_g}{\rho_f}}\right)\left\{1 - exp\left(-17\frac{\left\langle D_{Sm}\right\rangle}{D_H}\right)\right\} \tag{2-16}$$

where D_{Sm} is the bubble Sauter mean diameter. Equation (2-16) indicates that a lift force acting on relatively small bubbles pushes bubbles towards the rod resulting in lowered distribution parameter.

Chen et al. [2-33] and Clark et al. [2-47] performed an experiment using a vertical upward air-water flow in an 8×8 rod bundle under pool conditions and low liquid flow conditions, respectively. As shown in Fig. 2-4, Clark et al. [2-47] found that the distribution parameter increased due to a secondary flow formed in the rod bundle at low flow conditions. Figure 2-4 indicates that the distribution parameter asymptotically approaches Eq. (2-11) with increased mixture volumetric flux. Clark et al. [2-47] developed a drift-flux type correlation applicable to low flow conditions. Schlegel and Hibiki [2-48] and Kinoshita et al. [2-49] modified the Clark et al.'s correlation by considering a proper pressure scaling as:

$$C_0 = C_\infty - \left(C_\infty - 1\right)\sqrt{\frac{\rho_g}{\rho_f}} \tag{2-17}$$

$$C_\infty = \begin{cases} C_{\infty L} & \text{for} \quad \left\langle j^+\right\rangle \le \left\langle j^+\right\rangle_{C_\infty \max} \\ C_{\infty H} & \text{for} \quad \left\langle j^+\right\rangle > \left\langle j^+\right\rangle_{C_\infty \max} \end{cases} \tag{2-18}$$

$$C_{\infty H} = 1.1 + \left(1.84 e^{-0.1\left\langle j^+ \right\rangle}\right) \cdot F\left(\frac{\rho_g}{\rho_f}\right) \tag{2-19}$$

$$F = \min\left\{1,\ \max\left\{1.70 - 582\left(\frac{\rho_g}{\rho_f}\right),\ 0\right\}\right\} \tag{2-20}$$

$$C_{\infty L} = \left[\frac{C_{\infty H}\left(\left\langle j^+ \right\rangle_{C_\infty \max}\right) - 1}{\left\langle j^+ \right\rangle_{C_\infty \max} - \left\langle j_f^+ \right\rangle}\right]\left(\left\langle j_g^+ \right\rangle\right) + 1 \tag{2-21}$$

$$\left\langle j^+ \right\rangle_{C_\infty \max} = m\left\langle j_f^+ \right\rangle + b;\ \ m = \frac{1}{1 - \langle\alpha\rangle_{crit} C_0};\ \ b = \frac{\left\langle\left\langle V_{gj}^+ \right\rangle\right\rangle \langle\alpha\rangle_{crit}}{1 - \langle\alpha\rangle_{crit} C_0};$$

$$\left\langle j^+ \right\rangle \equiv \frac{\left\langle j \right\rangle}{\left(\frac{\Delta\rho g\sigma}{\rho_f^2}\right)^{1/4}};\quad \left\langle j_f^+ \right\rangle \equiv \frac{\left\langle j_f \right\rangle}{\left(\frac{\Delta\rho g\sigma}{\rho_f^2}\right)^{1/4}} \tag{2-22}$$

$$\left\langle\alpha\right\rangle_{crit} = \min\left(0.0284\left\langle j_f^+ \right\rangle + 0.125,\ 0.52\right) \tag{2-23}$$

The notations of the symbols used in Eqs. (2-18) to (2-23) are given in Fig. 2-5.

2.4 Void fraction and relative velocity covariance

Brooks et al. [2-19, 2-50] have pointed out the importance of void fraction covariance, C_α, and relative velocity covariance, C'_α, in one-dimensional two-phase flow analyses. In current one-dimensional nuclear thermal-hydraulic system analysis codes, the area-averaged relative velocity between phases is calculated by:

$$\left\langle v_r \right\rangle = \frac{1 - C_0\left\langle\alpha\right\rangle}{1 - \left\langle\alpha\right\rangle}\left\langle\left\langle v_g \right\rangle\right\rangle - C_0\left\langle\left\langle v_f \right\rangle\right\rangle \tag{2-24}$$

Brooks et al. [2-19] pointed out that void fraction covariance or relative velocity covariance is missing in Eq. (2-24) and provided the correct form of Eq. (2-24) as:

$$\left\langle v_r \right\rangle = C'_\alpha \left(\frac{1 - C_0 \left\langle \alpha \right\rangle}{1 - \left\langle \alpha \right\rangle} \left\langle \left\langle v_g \right\rangle \right\rangle - C_0 \left\langle \left\langle v_f \right\rangle \right\rangle \right) \tag{2-25}$$

$$C'_\alpha \equiv \frac{1 - \left\langle \alpha \right\rangle}{1 - C_\alpha \left\langle \alpha \right\rangle} \tag{2-26}$$

$$C_\alpha \equiv \frac{\left\langle \alpha^2 \right\rangle}{\left\langle \alpha \right\rangle \left\langle \alpha \right\rangle} \tag{2-27}$$

Since the interfacial drag force term in momentum equations is proportional to the square of the area-averaged relative velocity, the correct form of the area-averaged relative velocity should be used for an accurate prediction of void fraction. In view of this, Ozaki and Hibiki [2-44] developed correlations of void fraction covariance and relative velocity covariance for vertical upward two-phase flows in a rod bundle as:

$$\begin{cases} C_\alpha \left(\left\langle \alpha \right\rangle \right) = \max \left(C_{\alpha,SB}, C_{\alpha,BB} \right) & \text{for } \left\langle \alpha_{crit} \right\rangle > \left\langle \alpha \right\rangle \\ C_\alpha \left(\left\langle \alpha \right\rangle \right) = \dfrac{1 - C_\alpha \left(\left\langle \alpha_{crit} \right\rangle \right)}{1 - \left(\left\langle \alpha_{crit} \right\rangle \right)} \left(\left\langle \alpha \right\rangle - 1 \right) + 1 & \text{for } \left\langle \alpha_{crit} \right\rangle \le \left\langle \alpha \right\rangle \end{cases} \tag{2-28}$$

where

$$C_{\alpha,BB} = 1 + \left\{ 9.38 \left(\left\langle \alpha \right\rangle - 0.5 \right)^4 + 0.414 \right\} \left\{ 1 - \left(\frac{\rho_g}{\rho_f} \right)^2 \right\} \left(1 - \left\langle \alpha \right\rangle \right) \tag{2-29}$$

$$C_{\alpha,SB} = \frac{0.190}{\left\langle \alpha \right\rangle^{0.855}} \tag{2-30}$$

$$\left\langle \alpha_{crit} \right\rangle = 0.84 \tag{2-31}$$

Figure 2-6 compares Ozaki and Hibiki's correlation with relative velocity covariance measured in a vertical 8×8 rod bundle. The figure shows that the relative velocity covariance reaches 2 at the area-averaged void fraction of about 0.8. Ozaki and Hibiki's correlation agrees with the data well. The mean absolute error (bias) and standard deviation (random error) of Ozaki and Hibiki's correlation for the relative velocity covariance are determined to be -0.00241 and 0.0452 based on steam-water data taken under a wide range of test conditions such as pressure from

1.0-8.6 MPa, mass flux from 280-2000 kg/m^{2}s and exit quality from 0.0-0.25. Ozaki et al. [2-51] derived gas and liquid momentum equations by considering the void fraction distribution.

2.5 Interfacial area concentration

Interfacial area concentration, a_i, is one of most important two-phase flow parameters in characterizing available interfacial area for mass, momentum and energy transfer between two phases. The inverse of the interfacial area concentration is one of the important length scales in a two-phase flow characterizing a bubble size. The accurate prediction of the interfacial area concentration is a key to estimate mass, momentum and energy transfer in a two-phase flow analysis. An interfacial area correlation is often used for predicting area-averaged interfacial area concentration and the introduction of an interfacial area transport equation into a code is also considered for predicting the dynamic behavior of the interfacial area concentration [2-52, 2-53]. However, limited work has been conducted on developing an interfacial area correlation and an interfacial area transport equation in a rod bundle. The existing interfacial area correlations and interfacial area transport equation developed for simple geometries such as a pipe has been tested for their applicability to a two-phase flow in a vertical rod bundle.

2.5.1 Interfacial area correlations

Hibiki and Ishii [2-54] simplified an interfacial area transport equation and developed a simple interfacial area correlation for adiabatic bubbly flows. The developed interfacial area correlation predicted 459 adiabatic bubbly flow data taken in flow channels including pipes and rectangular channels with an average relative deviation of ±22.0 %. Hibiki and Ishii's correlation was also compared with boiling bubbly flow data taken in a vertical 3×3 rod bundle and its agreement with the data was fairly well. Hibiki et al. [2-55] extended Hibiki and Ishii's correlation [2-54] to boiling bubbly flows. The developed interfacial area correlation predicted 569 adiabatic bubbly flow data and 343 boiling bubbly flow data with averaged relative deviations of ±21.1 % and 31.0 %, respectively. The boiling database included R-12 data taken at 1.46 MPa, which simulated subcooled bubbly flow under prototypic PWR condition. The correlations are given by:

$$N_{a_i} = 3.02\eta N_{La}^{0.335} \left\langle \alpha \right\rangle N_{Re_b}^{0.239}$$
$$\begin{cases} \eta = 1 & \text{for adiabatic bubbly flow [2-54]} \\ \eta = 1.22 \left\langle \alpha \right\rangle^{-0.170} N_{\rho}^{-0.138} & \text{for boiling bubbly flow [2-55]} \end{cases} \quad (2\text{-}32)$$

where

$$N_{a_i} \equiv a_i La,\ N_{Re_b} \equiv \frac{\left\langle \varepsilon \right\rangle^{1/3} La^{4/3}}{\nu_f},\ N_\rho \equiv \frac{\rho_f}{\rho_g},\ La \equiv \sqrt{\frac{\sigma}{\Delta \rho g}} \tag{2-33}$$

As shown in Fig. 2-7, Hibiki et al.'s correlation agreed with the boiling bubbly flow data taken in a vertical 3×3 rod bundle fairly well.

Ozar et al. [2-56] examined the prediction accuracy of interfacial area correlations implemented in one-dimensional nuclear thermal-hydraulic safety analysis codes such as RELAP5 and TRAC-P codes using three databases (air-NaOH two-phase flow in a 25.4 mm pipe, air-water two-phase flow in a 48.3 mm pipe, air-water two-phase flow in an annulus with the hydraulic equivalent diameter of 19.1 mm). A total number of the data points was 127. A comparison between the correlations and the data demonstrated that the interfacial area correlations in RELAP5 and TRAC-P codes failed to predict the interfacial area concentration in bubbly-to-churn flow regimes. Ozar et al. [2-56] extended Hibiki and Ishii's correlation [2-54, 2-55] to high void fraction region including slug and churn flow regimes. The set of the correlation is given in Table 2-3. The notations of the symbols used in Ozar et al.'s correlation are given in Fig. 2-8. Ozar et al.'s correlation agreed with the above three datasets with an averaged relative deviation of ±30 %.

Schlegel and Hibiki [2-48] simplified an interfacial area transport equation and developed a simple interfacial area correlation for cap bubbly, cap turbulent-to-churn flow in a large diameter pipe. The set of the correlation is given in Table 2-4. Schlegel and Hibiki's correlation agreed with the data taken in large diameter pipes with a bias and root mean square of -4.29 % and 22.6 %, respectively. As shown in Fig. 2-9, Schlegel and Hibiki's correlation was also compared with adiabatic two-phase flow data taken in a vertical 8×8 rod bundle and its agreement with the data was fairly well.

2.5.2 Interfacial area transport equation

A general form of one-dimensional interfacial area transport equation is expressed as:

$$\frac{\partial \left\langle a_i \right\rangle}{\partial t} + \frac{\partial \left\langle a_i \right\rangle \left\langle \left\langle v_i \right\rangle \right\rangle_a}{\partial z} = \left\langle \Phi_{Source} \right\rangle - \left\langle \Phi_{Sink} \right\rangle + \left\langle \Phi_{Phase\ Change} \right\rangle + \left\langle \Phi_{Pressure\ Change} \right\rangle \tag{2-34}$$

where t, v_i and z are the time, interfacial velocity and axial location, respectively. $\left\langle \Phi_{Source} \right\rangle$ is the interfacial area concentration source term due to bubble breakup accompanied by the increase

of the bubble number density, whereas $\left\langle \Phi_{Sink} \right\rangle$ is the interfacial area concentration sink term due to bubble coalescence accompanied by the decrease of the bubble number density. $\left\langle \Phi_{Phase\ Change} \right\rangle$ is the interfacial area concentration source or sink term due to phase change including boiling and condensation. Wall nucleation is accompanied by the increase of the bubble number density but bubble expansion and contraction through interfacial heat transfer are not accompanied by the change of the bubble number density. $\left\langle \Phi_{Pressure\ Change} \right\rangle$ is the interfacial area concentration source or sink term due to pressure change along a flow direction, which is not accompanied by the change of the bubble number density.

Yang et al. [2-57] assumed similarities between a narrow rectangular channel and a sub-channel in a rod bundle, and applied the models of interfacial area concentration sink and source terms developed for a vertical narrow rectangular channel [2-58] with some modifications to a rod bundle. Five bubble interaction mechanisms considered in the model were bubble coalescence due to (1) bubble-bubble random collision induced by liquid turbulence and (2) due to wake entrainment and bubble breakup due to (3) turbulent impact on bubbles, (4) sharing off and (5) surface instability. The bubbles were treated in two-group, namely small bubbles or group-1 bubbles and large bubbles or group-2 bubbles. Figure 2-10 compares the axial development of interfacial area concentration calculated by the interfacial area transport equation with adiabatic two-phase flow data taken in a vertical 8 × 8 rod bundle and its agreement with the data was fairly well. However, the interfacial area transport equation may not predict accurate interfacial area concentration unless the initial condition is accurately given.

2.6 Wall friction

Wall friction is one of important key parameters in momentum equations. In what follows, constitutive correlations adopted in one-dimensional nuclear thermal-hydraulic safety analysis codes [2-59, 2-60, 2-61] are briefly reviewed. In the codes, the pressure gradient due to wall friction is expressed as:

$$-\left.\frac{dp}{dz}\right|_{friction} = C_{wf}\left|\left\langle\left\langle v_f \right\rangle\right\rangle\right|\left\langle\left\langle v_f \right\rangle\right\rangle + C_{wg}\left|\left\langle\left\langle v_g \right\rangle\right\rangle\right|\left\langle\left\langle v_g \right\rangle\right\rangle \tag{2-35}$$

where C_{wf} and C_{wg} are, respectively, the liquid and gas friction factors where $C_{wg} = 0$ for a

Pre-CHF (Critical Heat Flux) regime and $C_{wf} = 0$ for a Post-CHF regime. The pressure gradient in the Pre-CHF regime is given as:

$$-\left.\frac{dp}{dz}\right|_{friction} = C_{wf}\left|\left\langle\left\langle v_f \right\rangle\right\rangle\right|\left\langle\left\langle v_f \right\rangle\right\rangle = \phi_f^2\left(\frac{2f\left|G_f\right|G_f}{D_H\rho_f}\right) \tag{2-36}$$

where ϕ_f^2, f and G_f are the two-phase multiplier, Fanning friction factor and liquid mass flux, respectively. The liquid friction factor is expressed by:

$$C_{wf} = \phi_f^2\left\{\frac{2f\left(1-\left\langle\alpha\right\rangle\right)^2\rho_f}{D_H}\right\} \tag{2-37}$$

Constitutive correlations for a single-phase friction factor and a two-phase multiplier are necessary to calculate the pressure gradient.

2.6.1 Single-phase friction factor

TRACE code adopts Churchill's correlation [2-62], which is applicable to laminar, transition and turbulent regimes as:

$$f = 2\left\{\left(\frac{8}{Re}\right)^{12} + \frac{1}{\left(a+b\right)^{3/2}}\right\}^{1/12} \tag{2-38}$$

where

$$a = \left[2.457\cdot\log\left\{\frac{1}{\left(\frac{7}{Re}\right)^{0.9} + 0.27\left(\frac{\varepsilon_w}{D_H}\right)}\right\}\right]^{16} \quad \text{and} \quad b = \left(\frac{3.753\times10^4}{Re}\right)^{16} \tag{2-39}$$

Re and ε_w are the Reynolds number and wall roughness, respectively. Churchill's correlation asymptotically approaches the theoretical laminar single-phase friction factor in $Re < 2100$ and an empirical turbulent single-phase friction coefficient in $Re > 3000$.

RELAP5/MOD3.3 code classifies the single-phase flow regime into three regions: (1) Laminar region ($Re \le 2200$), (2) Transition region ($2200 < Re \le 3000$) and (3) Turbulent

region ($Re > 3000$). The single-phase friction factor in the laminar region, f_L, is given by:

$$f_L = \frac{16}{Re \cdot \phi_S} \tag{2-40}$$

where ϕ_S is a correction factor considering the geometrical difference between a pipe and other flow channels, which is given by a user input. The single-phase friction factor in the turbulent region, f_T, is calculated by Zigrang and Sylvester's correlation [2-63] as:

$$\frac{1}{\sqrt{f_T}} = -4\log_{10}\left[\frac{\varepsilon_w}{3.7D_H} + \frac{2.51}{Re}\left\{1.14 - 2\log_{10}\left(\frac{\varepsilon_w}{D_H} - \frac{21.25}{Re^{0.9}}\right)\right\}\right] \tag{2-41}$$

The single-phase friction factor in the transition region, f_{L-T}, is given by an interpolation function as:

$$f_{L-T} = \left(3.75 - \frac{8250}{Re}\right)\left(f_{T,Re=3000} - f_{L,Re=2200}\right) + f_{L,Re=2200} \tag{2-42}$$

TRAC-BF1 code classifies the single-phase flow regime into four regions and the single-phase friction factor in each region is given by Pfann's correlation [2-64] as:

$$f = \frac{16}{Re} \quad , \quad \text{for} \quad Re < 2300 \tag{2-43}$$

$$f = \frac{1}{4}\left(\frac{0.28}{\log Re - 0.82}\right)^2 \quad , \quad \text{for} \quad 2300 < Re < \frac{60}{\left(\frac{2\varepsilon_w}{D_H}\right)^{1.111}} \tag{2-44}$$

$$f = \frac{1}{4}\left(\frac{0.25}{\left(3.393 - 0.805g_1\right)g_1 - 2.477 - \log\frac{2\varepsilon_w}{D_H}}\right)^2 \quad , \quad \text{for} \quad \frac{60}{\left(\frac{2\varepsilon_w}{D_H}\right)^{1.111}} < Re < 424\frac{0.87 - \log\frac{2\varepsilon_w}{D_H}}{\frac{2\varepsilon_w}{D_H}} \tag{2-45}$$

$$f = \frac{1}{4}\left(\frac{0.25}{0.87 - \log \frac{2\varepsilon_w}{D_H}} \right)^2 \quad , \quad \text{for} \quad Re > 424 \frac{0.87 - \log \frac{2\varepsilon_w}{D_H}}{\frac{2\varepsilon_w}{D_H}} \tag{2-46}$$

where

$$g_1 \equiv \log\left(\frac{Re \cdot \frac{2\varepsilon_w}{D_H}}{0.87 - \log \frac{2\varepsilon_w}{D_H}} \right) \tag{2-47}$$

2.6.2 Two-phase multiplier

TRACE code gives the two-phase multiplier with respect to each flow regime. The two-phase multiplier for adiabatic bubbly and slug flow regimes is given by:

$$\phi_f^2 = \frac{1}{\left(1 - \langle \alpha \rangle\right)^n} \tag{2-48}$$

where n is an exponent whose value is not specified in the TRACE manual but is expected to be between 1.72 and 1.8. The two-phase multiplier for boiling flow is formulated by considering increased "wall roughness" due to bubble nucleation as:

$$\phi_f' = \phi_f \left(1 + C_{NB}\right) \tag{2-49}$$

where

$$C_{NB} = \min\left[2,\ 155\left(\frac{d_B}{D_H} \right)\left\{ \langle \alpha \rangle \left(1 - \langle \alpha \rangle\right) \right\}^{0.62} \right] \tag{2-50}$$

The bubble departure diameter, d_B, is calculated by Levy's force balance model [2-65] as:

$$\frac{d_B}{D_H} = 0.015 \sqrt{\frac{\sigma}{\tau_w D_H}} \tag{2-51}$$

where τ_w is the wall shear stress.

The two-phase multiplier for annular flow regime is given by:

$$\phi_f^2 = \frac{1}{\left(1-\left\langle\alpha\right\rangle\right)^2} \tag{2-52}$$

The single-phase friction factor for a laminar liquid film in annular flow regime is given by:

$$f_{film} = \left(f_L^3 + f_T^3\right)^{1/3} \tag{2-53}$$

where

$$f_L = \frac{16}{Re_{2\phi,f}} \quad , \quad \text{for} \quad \left\langle\alpha\right\rangle < 0.95$$

$$f_L = \frac{\left\{16 + 8\left(\frac{\left\langle\alpha\right\rangle - 0.95}{0.99 - 0.95}\right)\right\}}{Re_{2\phi,f}} \quad , \quad \text{for} \quad 0.95 < \left\langle\alpha\right\rangle < 0.99 \tag{2-54}$$

$$f_L = \frac{24}{Re_{2\phi,f}} \quad , \quad \text{for} \quad \left\langle\alpha\right\rangle > 0.95$$

The single-phase friction factor for a turbulent liquid film in annular flow regime is given by Haaland's correlation [2-66] as:

$$f_T = \frac{1}{\left[3.6 \cdot \log_{10}\left\{\frac{6.9}{Re_{2\phi,f}} + \left(\frac{\varepsilon_w / D_H}{3.7}\right)^{1.11}\right\}\right]^2} \tag{2-55}$$

RELAP5/MOD3.3 code uses Lockhart and Martinelli's correlation [2-67] and Chisholm's correlation [2-68]. The frictional pressure gradient is expressed by:

$$\left(-\frac{\partial p}{\partial z}\right)_{friction} = \phi_g^2\left(-\frac{\partial p}{\partial z}\right)_g \quad \text{and} \quad \left(-\frac{\partial p}{\partial z}\right)_{friction} = \phi_f^2\left(-\frac{\partial p}{\partial z}\right)_f \tag{2-56}$$

Martinelli's parameter is defined by:

$$X \equiv \sqrt{\left(\frac{\partial p}{\partial z}\right)_f \Big/ \left(\frac{\partial p}{\partial z}\right)_g} = \phi_g^2 \Big/ \phi_f^2 \tag{2-57}$$

Chisholm [2-68] proposed the following simple correlation to calculate the two-phase multiplier as:

$$\phi_f^2 = 1 + \frac{C}{X} + \frac{1}{X^2} \tag{2-58}$$

The RELAP5 code calculates the parameter, C, using the following correlation developed based on HTFS tests [2-69].

$$C = -2 + f_1\left(G\right)T_1\left(\Lambda, G\right) \tag{2-59}$$

where

$$f_1\left(G\right) = 28 - 0.3\sqrt{G}$$

$$T_1\left(\Lambda, G\right) = \exp\left\{-\frac{\left(\log_{10}\Lambda + 2.5\right)^2}{2.4 - G/10^4}\right\} \tag{2-60}$$

$$\Lambda = \frac{\rho_g}{\rho_f}\left(\frac{\mu_f}{\mu_g}\right)^{0.2}$$

G, μ_f and μ_g are the mass flux, liquid viscosity and gas viscosity, respectively.

TRAC-BF1 code calculates the two-phase multiplier based on Lockhart-Marinelli's model. The two-phase multiplier is given by Hancox and Nicoll's correlation [2-70] as:

$$\phi_f^2 = \left[1 + \left\{\frac{1}{\Lambda} - 1\right\}X\right]\left\{1 + RX^{0.5}\left(1 - X\right)^{0.25}\right\} \tag{2-61}$$

where

$$R = 3.1\left(1 - \frac{p}{p_c}\right)\exp\left(5.65 \times 10^{-4} G\right) \tag{2-62}$$

p_c is the critical pressure.

2.7 Conclusions

In view of CSAU methodology and code V & V (Verification and Validation), the implementation of most advanced and accurate constitutive equations into a code is indispensable. This chapter reviews the state-of-the-art correlations for predicting key two-phase flow parameters in a vertical rod bundle. The reviewed correlations include flow regime map, void fraction, void fraction covariance and relative velocity covariance, interfacial area concentration and wall friction. Important conclusions are given as follows:

Flow regime map

The identified flow regimes in a rod bundle were bubbly, finely dispersed bubbly, cap bubbly, cap turbulent, churn and annular flows. Existing flow regime maps were taken under atmospheric pressure conditions. Liu and Hibiki [2-15] developed flow regime transition criteria for a rod bundle. Liu and Hibiki's model agreed with existing flow regime maps but its applicability to high pressure and temperature two-phase flow should be examined using data to be taken in a future study.

Void fraction

Five state-of-the-art drift-flux type correlations are identified. They are the drift-flux type correlations for (1) a rod bundle under prototypic nuclear reactor core conditions [2-16, 2-36], (2) a rod bundle with unheated rod at the bundle center [2-16], (3) a rod bundle under subcooled boiling conditions [2-44], (4) a rod bundle under adiabatic bubbly flow [2-46] and (5) a rod bundle at low liquid flow under low pressure conditions [2-47, 2-48, 2-49]. All correlations agreed with existing void fraction data but the correlation for a rod bundle at low liquid flow under low pressure conditions should be further examined using data to be taken in a future study.

Void fraction covariance and relative velocity covariance

Modeling of void fraction covariance and relative velocity covariance is indispensable for calculating area-averaged relative velocity accurately. Only one model of void fraction covariance and relative velocity covariance in a rod bundle [2-44] is identified. Ozaki and Hibiki's correlation agreed with existing data taken in a vertical 8×8 rod bundle under prototypic nuclear reactor core conditions.

Interfacial area concentration

Accurate modeling of interfacial area concentration is important for calculating interfacial drag force and interfacial heat transfer. The interface structure of large bubbles depends on a flow channel size. Slug bubbles spanning over a flow channel can exist in a relatively small size channel, whereas cap bubbles created by the disintegration of large bubbles due to their surface instability exist in a relatively large size channel. Two types of interfacial area correlations for relatively small and large size channels with simple geometries are identified [2-56, 2-48]. In bubbly flow, Ozar et al.'s correlation becomes identical to Hibiki and Ishii's correlation [2-54, 2-55]. The applicability of Hibiki and Ishii's correlation to a rod bundle was partly examined but the

applicability of Ozar et al.'s correlation to a rod bundle has not been tested. Schlegel and Hibiki's correlation agreed with existing data taken in a vertical 8×8 rod bundle under an atmospheric condition but its applicability to prototypic nuclear reactor core conditions should be tested by data to be taken in a future study.

Wall friction

Key constitutive correlations to calculate wall friction are single-phase friction factor and two-phase multiplier. The constitutive correlations used in one-dimensional nuclear thermal-hydraulic system analysis codes such as TRACE [2-59], RELAP5 [2-60] and TRAC-BF1 [2-61] were reviewed.

Code improvement by implementing the above state-of-the-art correlations is expected to enhance the code prediction accuracy for two-phase flow analyses in a rod bundle.

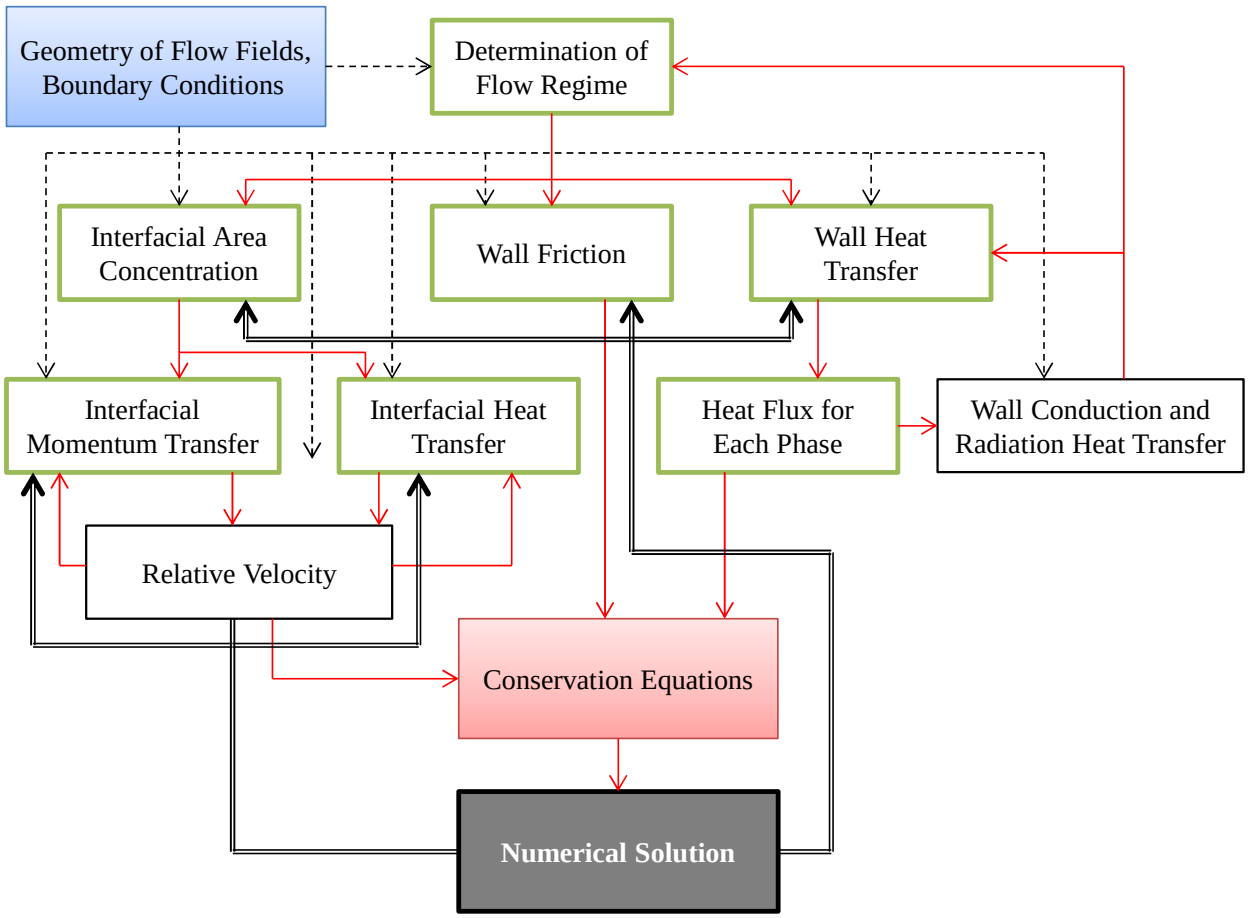

Figure 2-1 Schematic diagram of typical one-dimensional two-phase flow analysis code structure [2-6].

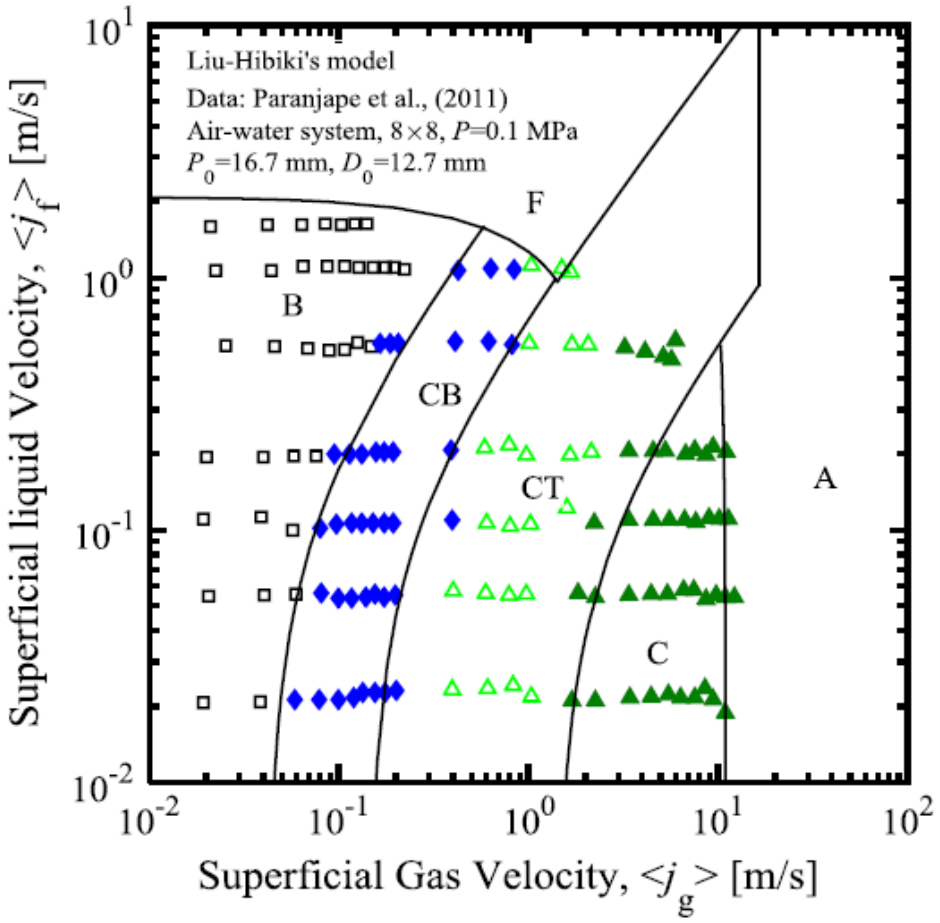

Figure 2-2 Comparison of Liu and Hibiki's model with two-phase flow regime maps observed in vertical 8×8 rod bundle [2-15].

Symbols: □: Bubbly, ◆: Cap Bubbly, △: Cap Turbulent, ▲: Churn

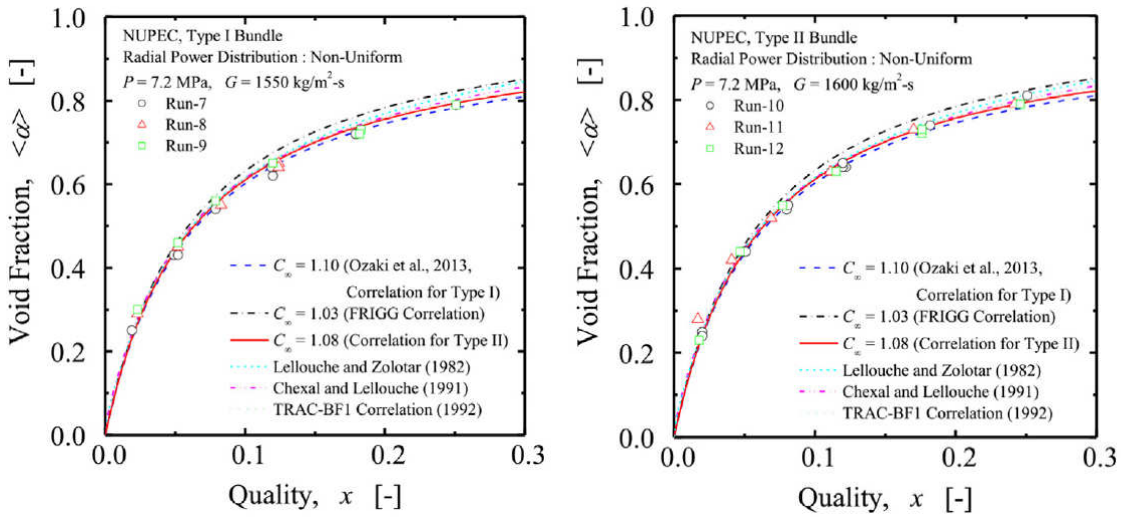

Figure 2-3 Comparison of Ozaki and Hibiki's correlation with void fraction measured in vertical 8×8 rod bundle [2-16].
(a) NUPEC Type I Bundle, (b) NUPEC Type II Bundle with large unheated rod at bundle center

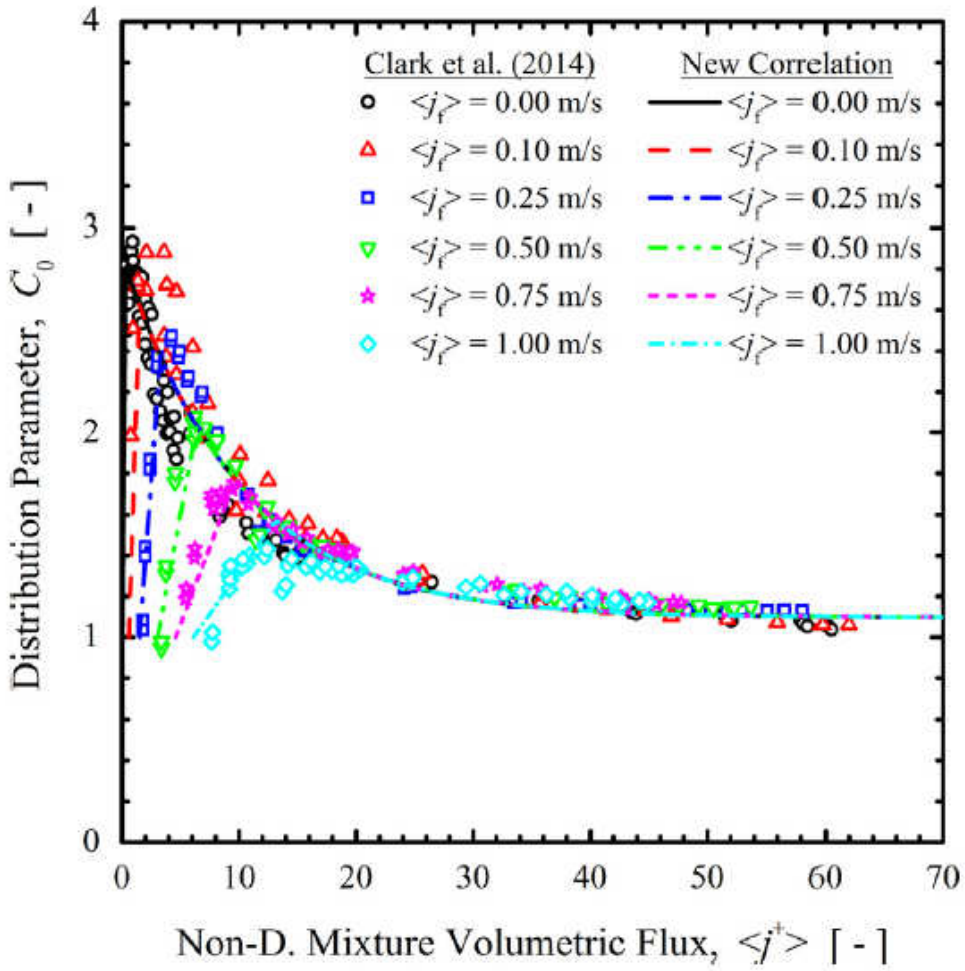

Figure 2-4 Enhanced distribution parameter in 8×8 rod bundle at low liquid flow rate under atmospheric pressure condition [2-47].

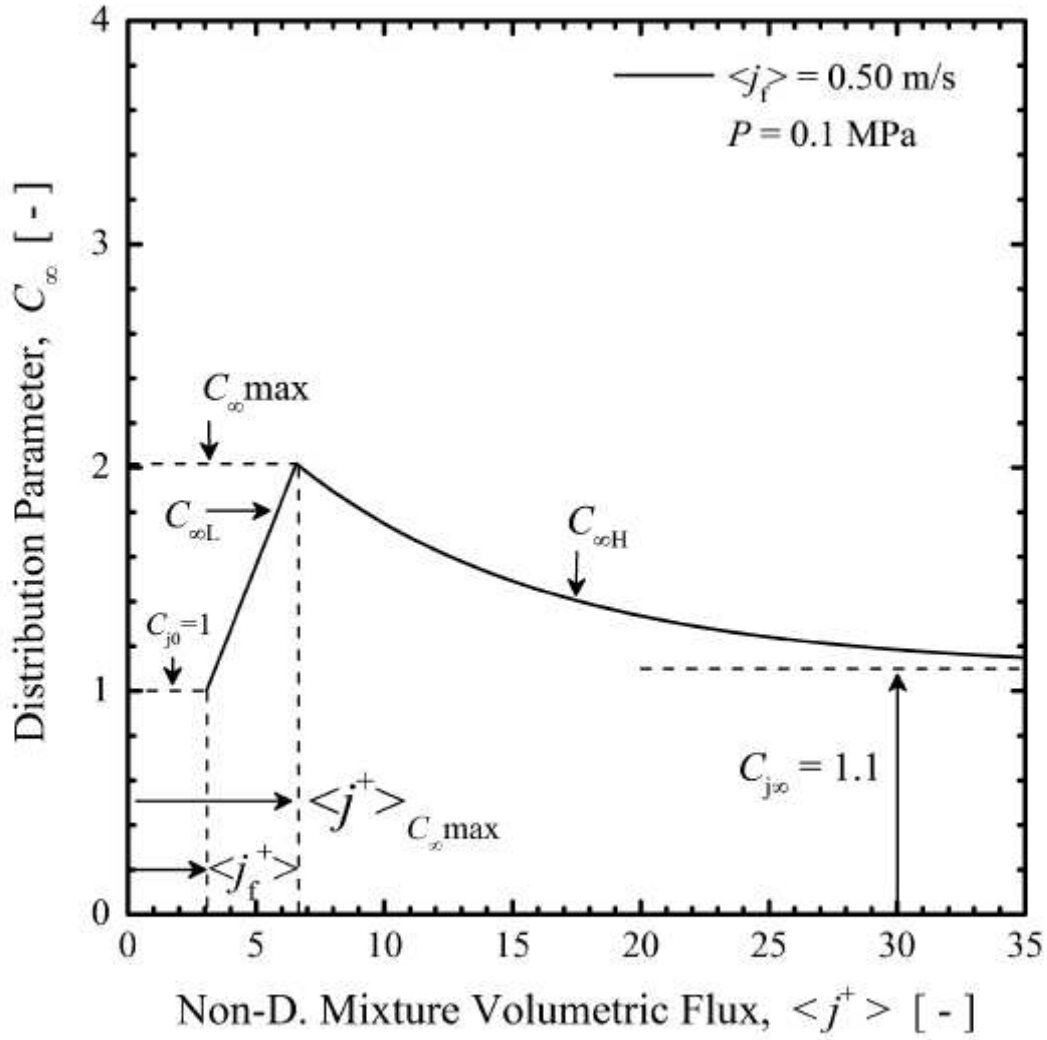

Figure 2-5 Schematic diagram of distribution parameter behavior and definitions of key parameters used in distribution parameter model [2-47].

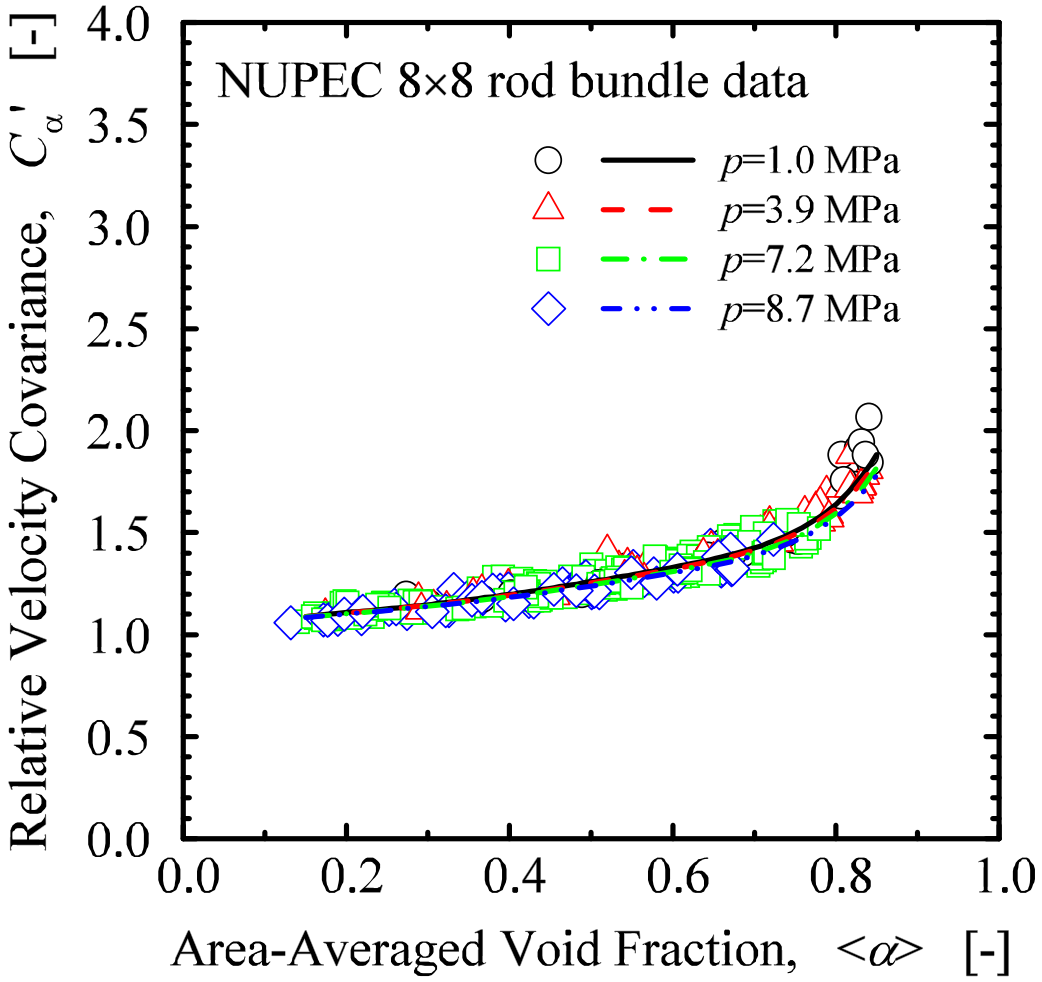

Figure 2-6 Comparison of Ozaki and Hibiki's correlation with relative velocity covariance measured in vertical 8×8 rod bundle [2-44].

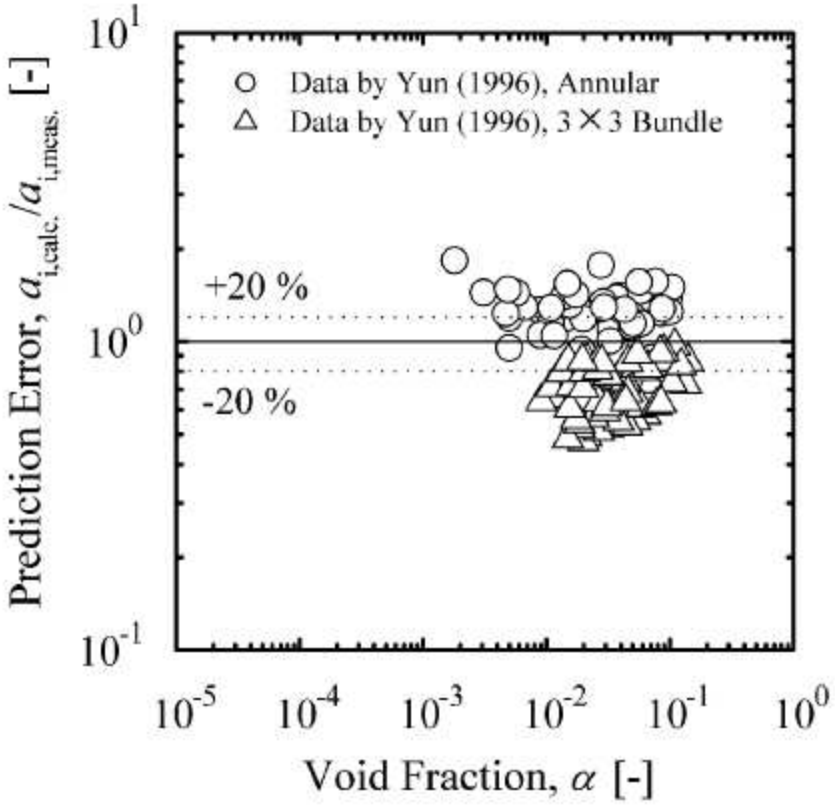

Figure 2-7 Comparison of Hibiki et al.'s correlation with data taken in vertical 3×3 rod bundle [2-55].

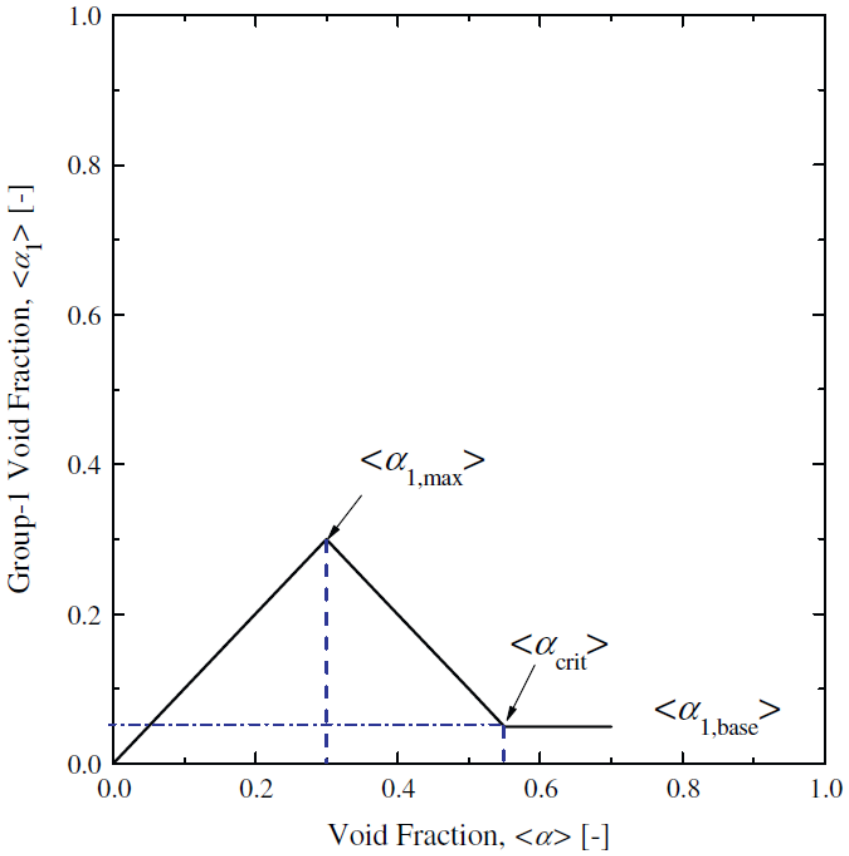

Figure 2-8 Schematic diagram of group-1 void fraction behavior and definitions of key parameters used in group-1 void fraction model [2-56].

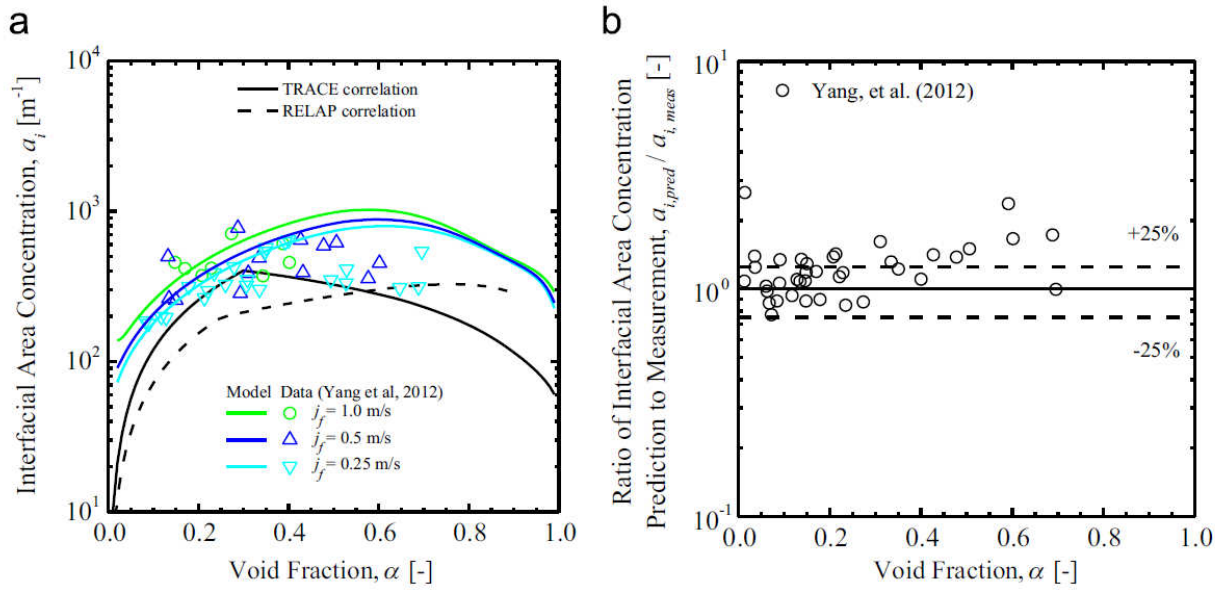

Fig. 17. Comparison of model with rod bundle data.

Figure 2-9 Comparison of Schlegel and Hibiki's correlation with data taken in vertical 8×8 rod bundle [2-48].

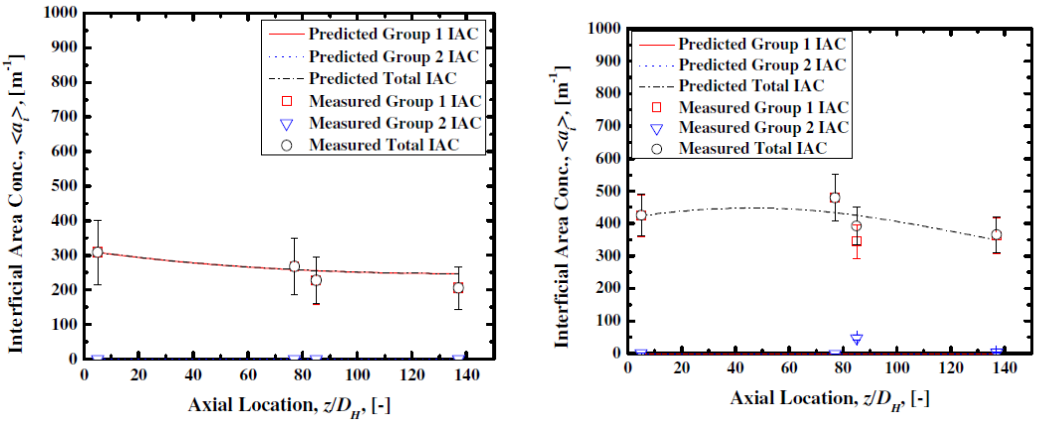

Figure 2-10 Comparison of interfacial area concentration calculated by interfacial area transport equation with adiabatic air-water two-phase flow data taken in 8×8 rod bundle [2-57].

(a) $\langle j_f \rangle$=0.59 m/s, $\langle j_g \rangle$=0.1 m/s, (b) $\langle j_f \rangle$=1.05 m/s, $\langle j_g \rangle$=0.37 m/s

Table 2-1 Existing flow regime maps of upward two-phase flow observed in vertical rod bundles.

Investigators	Flow Type	Geometry			Working Fluids	Identified Flow Regimes	Flow Regime Identification Method
		P_0/D_0 [mm]	# of rods [-]	Length [m]			
Venkateswararao et al. [2-9]	Adiabatic	17.5/12.7	24	1.83	Air-Water	B,F,S,C,A	Visual Observation
Mizutani et al. [2-10]	Adiabatic	16/12	4×4	1.90	Air-Water	B,BC,C,CA,A	Visual Observation
Paranjape et al. [2-11]	Adiabatic	16.7/12.7	8×8	3.00	Air-Water	B,CB,CT,C	Neural Network with Void Fraction Signal
Zhou et al. [2-12]	Boiling	15/10	3×3	1.33	Steam-Water	B,BC,C,A	Visual Observation
Liu et al. [2-13]	Adiabatic	12.6/9.5	5×5	1.52	Air-Water	DB,B,CB,CT,C	Visual Observation
Lee et al. [2-14]	Adiabatic	19/14	3×3	1.00	Air-Water	B,CB,S,C	Visual Observation

DB: Dispersed Bubbly, B: Bubbly, F: Froth, S: Slug, CB: Cap Bubbly, CT: Cap Turbulent, BC: Bubbly Churn, C: Churn,

CA: Churn Annular, A: Annular

Table 2-2 Existing void fraction database obtained in vertical rod bundles.

Experimental Facility	Length (m)	Rods (Heated)	D_H (mm)	D_e (mm)	Axial Power Distribution	ΔT_{sub} (K)	P (MPa)	G (kg/m^{2}s)	q'' (kW/m^2)	Measurement Technique	Ref.
PERICLES (1985)	3.7	357 (357)	9.5	11	Chopped cosine	20/60	0.3-0.6	21-48	11-40	DP transducers	[2-20]
NEPTUN (1988)	1.7	37 (37)	10.7	4	Chopped cosine	0.5/3	0.4	42/91	5/10	DP transducers	[2-21]
BWR 4×4 (1990)	3.7	16 (16)	12.3	12	Uniform	0	0.5/1	833/1390	350-743	X-ray tomography	[2-22]
BWR 8×8	3.7	64 or 61 (62 or 60)	12.3	13	Uniform /Chopped cosine /Bottom peaked	9-12	1-8.6	280-2000	225-3377	X-ray tomography	[2-23, 2-24, 2-25, 2-26]
LSTF (1990)	3.7	1104(1008)	9.5	13	Chopped cosine	0	1/7.3/15	2.2-84	5-45	DP transducers	[2-27]
TPTF (1994)	3.7	32(24)	9.5	10	Uniform	5-35	3/6.9/11.8	11-189	9-170	γ radiation and DP transducer	[2-28, 2-29]
THTF (1982)	3.7	64(60)	9.5	11	Uniform	46-118	3.9-8.1	3.1-29	11-74	DP transducers	[2-30]
Yun (2008)	1.7	9(9)	18.4	8.2	Uniform	3.5-11	0.12	250-522	25-185	Conductivity probe, Pitot tube	[2-31]
Yang (2012)	3.1	64(0)	10.3	16	N/A	N/A	0.1/0.3	90-1400	0(adiabatic)	Conductivity probe	[2-32]
Chen (2012)	3	64(0)	12.7	14.8	N/A	N/A	0.1	Pool	0(adiabatic)	Impedance meter	[2-33]
Lee (2017)	1	9(0)	14	18.83	N/A	N/A	0.1	100-1500	0(adiabatic)	Impedance meter	[2-14]
Katono (2017)	3.7	25(0)	10	12 / 8	N/A	N/A	5/7/7.5	75-500	0(adiabatic)	X-ray tomography	[2-34]
Liu (2017)	1.5	25(0)	9.5	10.3	N/A	N/A	0.1	500-3000	0(adiabatic)	Conductivity probe	[2-35]

Table 2-3 Interfacial area correlation developed by Ozar et al. [2-56].

Parameter	Recommended formulation
Total interfacial area concentration	$\langle a_i \rangle = \langle a_{i1} \rangle + \langle a_{i2} \rangle$
Group-1 (small bubbles) interfacial area concentration	$\langle a_{i1} \rangle = \frac{6\langle \alpha_{gs} \rangle}{D_{Sm1}} \frac{1-\langle \alpha \rangle}{1-\langle \alpha_{gs} \rangle}$
Group-2 (slug/churn bubbles) interfacial area concentration	$\langle a_{i2} \rangle = \frac{4.5 C_{ct}}{D_H} \frac{\langle \alpha \rangle - \langle \alpha_{gs} \rangle}{1-\langle \alpha_{gs} \rangle}$
Void fraction of small bubbles in liquid slug	$1-\langle a_{gs} \rangle = \frac{1-\langle \alpha \rangle}{1-\langle \alpha \rangle - \langle \alpha_1 \rangle}$
Sauter mean diameter for Group-1 bubbles	$N_{DSm1} = 1.99 N_{Lo}^{-0.335} N_{Re_b}^{-0.239}$ or $N_{DSm1} = 1.63 N_{Lo}^{-0.335} \langle \alpha \rangle^{0.170} N_{Re_b}^{-0.239} N_\rho^{0.138}$ $N_{DSm1} = \frac{D_{Sm1}}{Lo}, \quad N_{Lo} = \frac{Lo}{D_H}, \quad N_\rho = \frac{\rho_f}{\rho_g}, \quad N_\rho = \frac{\langle \varepsilon \rangle^{1/3} Lo^{4/3}}{\nu_f}$
Turbulence dissipation	$\langle \varepsilon \rangle = \langle \varepsilon_{BI} \rangle \left\{ 1 - \exp\left(-A N_{Re_f} \right) \right\} + \langle \varepsilon_{sh} \rangle \exp\left(-A N_{Re_f} \right)$ $\langle \varepsilon_{BI} \rangle = g \langle j_g \rangle, \quad \langle \varepsilon_{sh} \rangle = \frac{\langle j \rangle}{\rho_m} \left(-\frac{dP}{dz} \right)_F, \quad \rho_m = \rho_g \langle \alpha \rangle + \rho_f \left(1 - \langle \alpha \rangle \right), \quad A = 0.0005839$
Group-1 void fraction	$\langle \alpha_1 \rangle = \begin{cases} \langle \alpha \rangle & \langle \alpha \rangle \le \langle \alpha_{1,max} \rangle \\ \langle \alpha_{1,max} \rangle + \left(\frac{\langle \alpha_{1,max} \rangle - \langle \alpha_{1,base} \rangle}{\langle \alpha_{1,max} \rangle - \langle \alpha_{crit} \rangle} \right) \left(\langle \alpha \rangle - \langle \alpha_{1,max} \rangle \right) & \langle \alpha_{1,max} \rangle < \langle \alpha \rangle \le \langle \alpha_{crit} \rangle \\ \langle \alpha_{1,base} \rangle & \langle \alpha_{crit} \rangle < \langle \alpha \rangle \end{cases}$
Transition void fraction	$\langle \alpha_{1,\max} \rangle = \begin{cases} 0.235 + 0.011 \langle j_f^* \rangle & \langle j_f^* \rangle \le 6.1 \\ 0.325 - 0.004 \langle j_f^* \rangle & \langle j_f^* \rangle > 6.1 \end{cases}$
Critical void fraction	$\langle \alpha_{crit} \rangle = \begin{cases} 0.511 + 0.006 \langle j_f^* \rangle & \langle j_f^* \rangle \le 6.1 \\ 0.645 - 0.015 \langle j_f^* \rangle & \langle j_f^* \rangle > 6.1 \end{cases}$
Asymptotic value of void fraction	$\langle \alpha_{1,base} \rangle = \begin{cases} 0.099 - 0.009 \langle j_f^* \rangle & \langle j_f^* \rangle \le 6.1 \\ 0.05 & \langle j_f^* \rangle > 6.1 \end{cases}$

Table 2-4 Interfacial area correlation developed by Schlegel and Hibiki [2-48].

Parameter	Recommended formulation
Total interfacial area concentration	$\langle a_i \rangle = \langle a_{i1} \rangle + \langle a_{i2} \rangle$
Group-1 (small bubbles) interfacial area concentration	$\langle a_{i1} \rangle = \frac{6\langle \alpha_1 \rangle}{D_{Sm1}}$
Group-2 (slug/churn bubbles) interfacial area concentration	$\langle a_{i2} \rangle = \frac{6\langle \alpha_2 \rangle}{D_{Sm2}}$
Sauter mean diameter for Group-1 bubbles	$N_{DSm1} = \frac{D_{Sm,1}}{D_{Sm,2}} = \frac{C_2\alpha_1\left[1.13C_1\alpha_1^{2/3}\alpha_2 N_{vr} + 0.238\left(1.39(1-\alpha_2)^{2/3} + \frac{\sqrt{2}(1-\alpha_1)^{7/4}}{3.0(1-\alpha_2)^{1/2}} - 1\right)\right]}{\left[2.44C_1(1-\alpha)N_{vr} + 0.00362N_{We}^{-2/5}\left(\frac{\rho_f}{\rho_g}\right)\right]}$
	$N_{vr} = \frac{\langle \varepsilon \rangle^{1/3} Lo^{1/3}}{v_{r2}}, \quad N_{We} = \frac{\rho_f v_{r2}^2 D_H}{\sigma}, \quad C_1 = 0.120, \quad C_2 = 2.30$
Sauter mean diameter for Group-2 bubbles	$N_{D_{Sm2}} = \frac{D_{Sm2}}{D_H} = \frac{C_3 N_{We}^{-1}}{0.238N_{vr}(1+\alpha_1\alpha_2-\alpha) + 0.996\alpha_1\left(1.39(1-\alpha_2)^{2/3} + \frac{\sqrt{2}(1-\alpha_1)^{7/4}}{3.0(1-\alpha_2)^{1/2}} - 1\right)}$
	$C_3 = 8.55$
Turbulence dissipation	$\langle \varepsilon \rangle = \langle \varepsilon_{sh} \rangle + \langle \varepsilon_{BI} \rangle \approx \frac{0.316}{Re_m^{0.25}} \frac{v_m^3}{2D_H} + \langle j_g \rangle g$
	$N_{Re_m} = \frac{\rho_m v_m D_H}{\mu_f} \frac{1}{1-\langle \alpha \rangle}, \quad \rho_m = \rho_g \langle \alpha \rangle + \rho_f (1 - \langle \alpha \rangle), \quad v_m = \frac{\rho_g \langle j_g \rangle + \rho_f \langle j_f \rangle}{\rho_m}$
Group-1 void fraction	$\langle \alpha_1 \rangle = \langle \alpha_{gs} \rangle \frac{1-\langle \alpha \rangle}{1-\langle \alpha_{gs} \rangle}$
	$\langle \alpha_{gs} \rangle = \min\left\{\langle \alpha \rangle \quad , \quad 0.63\tanh\left(0.00145N_{Re_c}\langle \alpha \rangle\right)\right\}$
Group-2 void fraction	$\langle \alpha_2 \rangle = 1 - \langle \alpha_1 \rangle$

References

[2-1] Chuang, T.J., Hibiki, T., Vertical upward two-phase flow CFD using interfacial area transport equation. Progress in Nuclear Energy 85 (2015) 415-427.

[2-2] Vaidheeswaran, T., Hibiki, T., Bubble induced turbulence modeling for vertical bubbly flows. International Journal of Heat and Mass Transfer 115 (2017) 741-752.

[2-3] Chuang, T.J., Hibiki, T., Interfacial forces used in two-phase flow numerical simulation. International Journal of Heat and Mass Transfer 113 (2017) 741-754.

[2-4] Lin, C.H., Hibiki, T., Databases of interfacial area concentration in gas –liquid two-phase flow. Progress in Nuclear Energy 74 (2014) 91-102.

[2-5] Ishii, M., Hibiki, T., Thermo-fluid dynamics of two-phase flow. 2nd ed. Springer, New York, 2010.

[2-6] Atomic Energy Society of Japan (AESJ), Numerical analysis of two-phase flow. Thermal-hydraulic Division (THD), Asakura Publishing Company, 1993.

[2-7] Griffiths, M. J., Schlegel, J. P., Hibiki, T., Ishii, M., Kinoshita, I., Yoshida, Y., Phenomena identification and ranking table for thermal-hydraulic phenomena during a small-break LOCA with loss of high pressure injection. Progress in Nuclear Energy 73 (2014) 51-63.

[2-8] Shen, X., Schlegel, J., Chen, S.W., Rassame, S., Griffiths, M.J., Hibiki, T., Ishii, M., Flow characteristics and void fraction prediction in large diameter pipes. Frontiers and Progress in Multiphase Flow, Springer, Chapter 2 (2014) 55-103.

[2-9] Venkateswararao, P., Semiat, R., Dukler, A.E., Flow pattern transition for gas-liquid flow in a vertical rod bundle. International Journal of Multiphase Flow 8 (1982) 509-524.

[2-10] Mizutani, Y., Tomiyama, A., Hosokawa, S., Sou, A., Kudo, Y., Mishima, K., Two-phase flow patterns in a four rod bundle, Journal of Nuclear Science and Technology 44 (2007) 894-901.

[2-11] Paranjape, S., Chen, S.W., Hibiki, T., Ishii, M., Flow regime identification under adiabatic upward two-phase flow in a vertical rod bundle geometry. Journal of Fluids Engineering 133 (2011) 091302.

[2-12] Zhou, Y., Hou, Y., Li, H., Sun, B., Yang, D., Flow pattern map and multi-scale entropy analysis in 3×3 rod bundle channel. Annuls of Nuclear Energy 80 (2015) 144-150.

[2-13] Liu, H., Ren, Q., Pan, L., Hibiki, T., Zhou, W., Ye, T., Experimental study of flow regime map in 5×5 rod bundle. Proceedings of ICONE 25, July 2-6 2017, Shanghai, ICONE25-67307, 2017.

[2-14] Lee, J. W., Kim, H. S., Lee, J. Y., Euh, D. J., Kim, J. R., An experimental study on measuring volumetric void fraction using impedance meter in 3×3 rod bundle consisting of metal filter,

Proc. 17th International Topical Meeting on Nuclear Reactor Thermal Hydraulics, Xi'an, Shaanxi, China, Spt. 3-8 2017, Paper No. 2017036, 2017.

[2-15] Liu, H., Hibiki, T., Flow regime transition criteria for upward two-phase flow in vertical rod bundles. International Journal of Heat and Mass Transfer 108 (2017) 423-433.

[2-16] Ozaki, T., Hibiki, T., Drift-flux model for rod bundle geometry. Progress in Nuclear Energy 83 (2015) 229-247.

[2-17] Hibiki, T., Ishii, M., One-dimensional drift-flux model for two-phase flow in a large diameter pipe. International Journal of Heat and Mass Transfer 46 (2003) 1773-1990.

[2-18] Zuber, N., Findlay, J.A., Average volumetric concentration in two-phase flow systems. Journal of Heat Transfer 87 (1965) 453-468.

[2-19] Brooks, C.S., Hibiki, T., Ishii, M., Interfacial drag force in one-dimensional two-fluid model. Progress in Nuclear Energy 61 (2012) 57-68.

[2-20] Deruaz, R., Clement, P, Veteau, J.M., Study of two-dimensional effects in the core of a light water reactor during the ECC's phase following a loss of coolant accident, EUR 10076 EN, Grenoble, Commissariat a 1'Energie Atimique, Centre d'Etude Nucleaires de Grenoble, Service des Transferts Thermiques, 1985.

[2-21] Dreier, J., Analytis, G., Chawla, R., NEPTUN-III reflooding and boil-off experiments with an LWHCR fuel bundle simulator: experimental results and initial core assessment efforts. Nuclear Technology 80 (1988) 99-108.

[2-22] Mitsutake, T., Morooka, S., Suzuki, K., Tsunoyama, S., Yoshimura, K., Void fraction estimation within rod bundle based on three-fluid model and comparison with X-ray CT void data. Nuclear Engineering and Design 120 (1990) 203-212.

[2-23] Morooka, S., Inoue, A., Oishi, M., Aoki, T., Nagaoka, K., Yoshida, H., In-bundle void measurement of BWR fuel assembly by X-ray CT scanner. Proceedings of ICONE-1, Nov. 4-7 1991, Tokyo, Paper no. 38, 1991.

[2-24] Inoue, A., Kurosu, T., Aoki, T., Yagi, M., Void fraction distribution in BWR fuel assembly and evaluation of subchannel code. Journal of Nuclear Science and Technology 32 (1995) 629-640.

[2-25] Nuclear Power Engineering Test Center, Report on proving test on reliability for BWR fuel bundles (void fraction tests in BWR fuel bundles – support document). NUPEC, Tokyo, 1992.

[2-26] Nuclear Power Engineering Corporation, Report on proving test on reliability for BWR fuel bundles (Supplement) (void fraction tests for high burnup fuel bundle – Overall evaluation). NUPEC, Tokyo, 1993.

[2-27] Anoda, Y., Kukita, Y., Tasaka, K., Void fraction distribution in rod bundle under high pressure

conditions. Proceedings of ASME Winter Annual Meeting, Nov. 25-30 1990, Dallas, ASME. Advances in Gas-Liquid Flows, 1990.

[2-28] Kumamaru, H., Kondo, M., Murata, H., Kukita, Y., Void-fraction distribution under high-pressure boil-off conditions in rod bundle geometry. Nuclear Engineering and Design 150 (1994) 95-105.

[2-29] Kondo, M., Kumamaru, H., Murata, H., Anoda, Y., Kukita, Y., Core void fraction distribution under high-temperature high-pressure boil-off conditions: experimental study with two-phase flow test facility (TPTF), JAERI-M 93-200, JAERI, 1993.

[2-30] Anklam, T.M., Miller, R.F., Void fraction under high pressure, low flow conditions in rod bundle geometry. Nuclear Engineering and Design 75 (1983) 99-108.

[2-31] Yun, B.J., Park, G.C., Julia, J.E., Hibiki, T., Flow structure of sub-cooled boiling water flow in a sub-channel of 3×3 rod bundles. Journal of Nuclear Science and Technology 45 (2008) 402-422.

[2-32] Yang, X., Schlegel, J.P., Liu, Y., Paranjape, S., Hibiki, T., Ishii, M., Measurement and modeling of two-phase flow parameters in scaled 8×8 BWR rod bundle. International Journal of Heat and Fluid Flow 34 (2012) 85-97.

[2-33] Chen, S.W., Liu, Y., Hibiki, T., Ishii, M., Yoshida, Y., Kinoshita, I., Murase, M., Mishima, K., Experimental study of air-water two-phase flow in a 8×8 rod bundle under pool condition for one-dimensional drift-flux analysis. International Journal of Heat and Fluid Flow 33 (2012) 168-181.

[2-34] Katono, K., Fujimoto, K., Nagoyoshi, T., Aoyama, G., Nagasawa, Y., Arai, T., Experimental study of void fraction distribution in a rod bundle at conditions of low flow rate and wide pressure range using X-ray CT images, Proc. 17th International Topical Meeting on Nuclear Reactor Thermal Hydraulics, Xi'an, Shaanxi, China, Spt. 3-8 2017, Paper No. 19811, 2017.

[2-35] Liu, H., Pan, L., Ren, Q., Hibiki, T., Zhou, W., Li, S., Some characteristics of interfacial area transport for air-water two-phase flow in 5×5 rod bundles. Proc. 17th International Topical Meeting on Nuclear Reactor Thermal Hydraulics, Xi'an, Shaanxi, China, Spt. 3-8, Paper No. 20932, 2017.

[2-36] Ozaki, T., Suzuki, R., Mashiko, H., Hibiki, T., Development of drift-flux model based on 8 × 8 BWR rod bundle geometry experiments under prototypic temperature and pressure conditions. Journal of Nuclear Science and Technology 50 (2013) 563-580.

[2-37] Bestion, D., The physical closure laws in the CATHARE code. Nuclear Engineering and Design 124 (1990) 229-245.

[2-38] Chexal, B., Lellouche, G., The Chexal-Lellouche void fraction correlation for generalized applications. NSAC-139, 1991.

[2-39] Inoue, A., Kurose, T., Yagi, M., Morooka, S, Hoshide, A., Ishizuka, T., Yoshimura, K., In-bundle void measurement of a BWR design void correlation. Proceedings of the ASME/JSME Nuclear Engineering Conference , 1993 March 21-24, San Francisco, 39-45, 1993.

[2-40] Maier, D., Coddington,P., Review of wide range void correlations against and extensive data base of rod bundle void measurements. Proceedings of ICONE-5, 1997 March 26-30, Nice, Paper no. 2434, 1997.

[2-41] Julia, J.E., Hibiki, T., Ishii, M., Yun, B.J., Park, G.C., Drift-flux model in a sub-channel of rod bundle geometry. Interfacial Journal of Heat and Mass Transfer 52 (2009) 3032-3041.

[2-42] Ishii, M., One-dimensional drift-flux model and constitutive equations for relative motion between phases in various two-phase flow regimes. ANL-77-47, USA (1977).

[2-43] Kataoka, I., Ishii, M., Drift-flux model for large diameter pipe and new correlation for pool void fraction. International Journal of Heat and Mass Transfer 30 (1987) 1927-1939.

[2-44] Ozaki, T., Hibiki, T., Modeling of distribution parameter, void fraction covariance and relative velocity covariance for upward steam-water boiling flow in vertical rod bundle. Journal of Nuclear Science and Technology 55 (2018) 386-399.

[2-45] Hibiki, T., Situ, R., Mi, Y., Ishii, M., Modeling of bubble-layer thickness for formulation of one-dimensional interfacial area transport equation in subcooled boiling two-phase flow. International Journal of Heat and Mass Transfer 46 (2003) 1409-1423.

[2-46] Liu, H., Pan, L. M., Hibiki, T., Ren, Q. Y., Zhou, W. X., Li, S. S., One-dimensional interfacial area transport for bubbly two-phase flow in vertical 5×5 rod bundle. International Journal of Heat and Fluid Flow (under review).

[2-47] Clark, C., Griffiths, M., Chen, S.W., Hibiki, T., Ishii, M., Ozaki, T., Kinoshita, I., Yoshida, Y., Drift-flux correlation for rod bundle geometries. International Journal of Heat and Fluid Flow 48 (2014) 1-14.

[2-48] Schlegel, J.P., Hibiki, T., A correlation for interfacial area concentration in high void fraction flows in large diameter channels. Chemical Engineering Science 31 (2015) 172-186.

[2-49] Kinoshita, I., Torige, T., Schlegel, J. P., Hibiki, T., Development of a new drift flux model for rod bundle geometries at low flow and pressure conditions (1) New drift flux model development and validation. Proceedings of 2017 Annual Meeting of Atomic Energy Society of Japan, Mar. 27-29 2017, Kanagawa, 1K14, 2017.

[2-50] Brooks, C.S., Liu, Y., Hibiki, T., Ishii, M., Effect of void fraction covariance on relative velocity in gas-dispersed two-phase flow. Progress in Nuclear Energy 70 (2014) 209-220.

[2-51] Ozaki T., Hibiki, T., Miwa, S, Mori, M., Development of one-dimensional two-fluid model with consideration of void fraction covariance effect. Journal of Nuclear Science and Technology (under review)

[2-52] Hibiki, T., Ishii, M., One-group interfacial area transport of bubbly flows in vertical round tubes. International Journal of Heat and Mass Transfer 43 (2000) 2711-2726.

[2-53] Hibiki, T., Ishii, M., Two-group interfacial area transport equations at bubbly-to-slug flow transition. Nuclear Engineering and Design 202 (2000) 39-76.

[2-54] Hibiki, T., Ishii, M., Interfacial area concentration of bubbly flow systems, Chemical Engineering Science 57 (2002) 3967-3977.

[2-55] Hibiki, T., Lee, T.H., Lee, J.Y., Ishii, M., Interfacial area concentration in boiling bubbly flow systems. Chemical Engineering Science 61 (2006) 7979-7990.

[2-56] Ozar, B., Dixit, A., Chen, S.W., Hibiki, T., Ishii, M., Interfacial area concentration in gas-liquid bubbly to churn-turbulent flow regime. International Journal of Heat and Fluid Flow 38 (2012) 168-179.

[2-57] Yang, X., Schlegel, J.P., Liu, Y., Paranjape, S., Hibiki, T., Ishii, M., Bajorek, S., Ireland, A., Prediction of interfacial area transport in a scaled 8×8 BWR rod bundle. Nuclear Engineering and Design 310 (2016) 638-647.

[2-58] Sun, X., Kim, S., Ishii, M., Beus, S.G., Modeling of bubble coalescence and disintegration in confined upward two-phase flow. Nuclear Engineering and Design 230 (2004) 3-26.

[2-59] U.S.NRC, TRACE/V5.0 Theory Manual; Field Equations, Solutions Methods, and Physical Models, US NRC, Washington (DC) (2008).

[2-60] Information System Laboratories (ISL), RELAP5/MOD3.3 Code Manual Volume IV: Models and Correlations. NUREG/CR-5535/Rev 1-Vol. IV, US NRC, Washington (DC) (2001).

[2-61] Borkowski, J.A., Wade, N.L., TRAC-BF1/MOD1 Models and Correlations. NUREG/CR-4391/EGG-2680R4, US NRC, Washington (DC) (1992).

[2-62] Churchill, S.W., Friction factor equations spans all fluid-flow regimes. Chemical Engineering (1977) 91-92.

[2-63] Zigrang, D.J., Sylvester, N.D., A review of explicit friction factor equations. Journal of Energy Resources Technology 107 (1985). 280-283.

[2-64] Pfann, J., A new description of liquid metal heat transfer in closed conduits. Nuclear Engineering and Design 41 (1977) 149-163.

[2-65] Levy, S., Forced convection subcooled boiling prediction of vapor volumetric fraction. International Journal of Heat and Mass Transfer 10 (1967) 951-965.

[2-66] Haaland, S.E., Simple and explicit formulas for the friction factor in turbulent pipe flow. Journal of Fluids Engineering 105 (1983) 89-90.

[2-67] Lockhart, R.W., Martinell, R.C., Proposed correlation of data for isothermal two-phase, two-component flow in pipes. Chemical Engineering Progress 45 (1949) 39-48.

[2-68] Chisholm, D., A theoretical basis for the Lockhart-Martinelli correlation for two-phase flow. International Journal of Heat and Mass Transfer 10 (1967) 1767-1778.

[2-69] Chaxton, K.T., Collier, J.G., Ward, A., HTFS correlation for two-phase pressure drop and void fraction in tubes. AERE-R7162, 1972.

[2-70] Hancox, W.T., Nicoll, W.B., Prediction of time dependent diabatic two-phase water flows. Progress in Heat and Mass Transfer 6 (1972) 119-135.

3. Effect of Void Fraction Covariance on Two-Fluid Model Based Code Calculation in Pipe Flow

3.1 Introduction

In order to evaluate the safety of nuclear power plants that possess highly complicated and large-scaled systems, it is essential to utilize numerical simulation codes. Accidents in nuclear power plants can cause severe public hazards, and may lead to serious social and economic consequences. Hence, careful safety evaluation must be conducted using proper simulation method at the design stage of the plant. Also, those in charge of safety regulatory must consider the validity of the simulation methods upon their decision-making process. A method to evaluate the validity of numerical simulation is standardized in V&V (Verification and Validation) guideline [3-1, 3-2, 3-3]. According to the guideline, thorough understandings of the uncertainties arise by the (1) lack of knowledge, (2) lack of experimental database for model development, and (3) approximation for shortening iteration time, are crucial when numerically obtained results are compared to the exact solution.

Gas-liquid two-phase flow phenomena in nuclear reactor are highly linked to the safety of nuclear power plants in terms of the plant's thermal power, fuel cooling, pressure loss, flow profiles within reactor core, flow induced vibration characteristics, and so on. Hence, accurate two-phase flow simulation is indispensable for conducting safety evaluation of nuclear power plants. Advanced thermal-hydraulics codes such as TRACE [3-4], RELAP5 [3-5], and TRAC-BF1 [3-6] utilize interfacial drag term in the momentum equation to represent the interfacial momentum transfer between two phases. Interfacial drag term is the most important interfacial transfer term that governs velocity fields of two-phases, and it highly influences the void fraction prediction. Void fraction being one of the most important parameters to conduct plant's safety evaluation, it is typically categorized as the high ranked parameter in phenomena identification and ranking table (PIRT) for many associated evaluation events [3-7].

In general, safety evaluation of nuclear power plants is conducted by treating coolant flow within the reactor core and piping systems as one-dimensional flow, as is the case for the safety codes including TRACE [3-4], RELAP5 [3-5], and TRAC-BF1 [3-6]. Capability of three-dimensional CFD technique to simulate two-phase flow phenomena is still immature due to the high computational cost, and lack of experimental database to perform benchmarking at local-level. Hence, it is still not a practical approach to conduct plant-level three-dimensional thermal-hydraulic analysis, despite of the recent advancement in computational methodologies. In typical safety

analysis codes, one-dimensional two-fluid model is utilized. However, the interfacial drag term, which represents the interfacial momentum transfer between two-phases, is typically given as the area-averaged quantity, and such area-averaged approximation may influence the void fraction calculation results.

In order to eliminate the influence of area-averaged approximation, various works have been undertaken with the advancement of two-phase flow simulation capability. Covariance of the mixture volumetric flux and phase fraction profiles was defined as the distribution parameter for the general expression of drift-flux model, and its relationship with respect to area-averaged void fraction was established [3-8]. The area-averaged void fraction can be obtained from the distribution parameter, but it is highly dependent on channel geometry and flow conditions. Hence, various works have been undertaken to develop the constitutive equations for the distribution parameter [3-9, 3-10, 3-11, 3-12]. Additionally, Ishii and Mishima [3-13] utilized the distribution parameter to develop area-averaged relative velocity model, and contributed to the advancement of one-dimensional two-phase flow codes. However, Ishii and Mishima [3-13] derived the area-averaged relative velocity term without considering the covariance of void fraction distribution (spatial auto-correlation of void fraction). Hence, utilization of the Ishii and Mishima's model alone will not address the dependency of void fraction covariance on the local relative velocity expression. Recent advancement on measurement technique enables one to conduct local time-averaged void fraction measurement [3-14, 3-15, 3-16, 3-17, 3-18, 3-19], and the constitutive equations on void fraction covariance were developed based on such experimental database. Brooks et al. [3-20] developed a covariance model based on the void fraction database obtained in adiabatic and boiling experiments performed in circular pipe. Hibiki and Ozaki [3-21] proposed the covariance model for subcooled boiling flow. By combining the model with the Brooks et al [3-20]'s, Hibiki and Ozaki [3-21] extended their work to develop a new model that is applicable for entire dispersed bubbly flow regime. Hibiki and Ozaki [3-21] clarified the relationship between the interfacial drag term of one-dimensional two-fluid model and covariance term, and formulated the interfacial drag term with covariance effect that can be embedded on system analysis codes such as RELAP5 and TRACE.

In this study, constitutive equations for covariance proposed by Hibiki and Ozaki [3-21] were included in the one-dimensional two-fluid code, and the effect of covariance on circular round tube was evaluated. Based on the analysis, proper treatment of the interfacial drag term and formulation of the momentum equation in two-fluid model were considered. The interfacial drag term with covariance effect proposed by Hibiki and Ozaki [3-21] is comprehensive enough to conduct

quantitative evaluation using one-dimensional numerical code. On the other hand, in the original form of momentum equation, uniform void fraction distribution is assumed, and it is uniformly distributed to each phase to calculate wall shear force, and viscous and turbulent shear stress. This may create discrepancy against the interfacial drag term calculated with covariance. In this chapter, section 3.2 discusses on the inclusion of interfacial drag term with covariance in two-fluid model, and section 3.3 discusses on the methodology of one-dimensional safety code analysis and the calculation domain nodalization. Section 3.4 discusses on the cause of a discrepancy in void fraction calculations obtained by the use of covariance and traditional drift-flux model, and propose a new momentum equation formulation to resolve such issue.

3.2 Interfacial drag term for one-dimensional two-fluid model

3.2.1 Derivation of the interfacial drag term

In order to evaluate two-phase velocity fields using two-fluid model, proper usage of constitutive relation for the interfacial momentum transfer, especially the interfacial drag term, is indispensable. In one-dimensional two-fluid model, interfacial drag term must be supplied as an area-averaged quantity over the flow channel of interest. Also, interfacial drag term should be expressed as a function of relative velocity due to its high dependency. The interfacial drag term also has an effect to suppress numerical instabilities. Based on above considerations, modeling of the interfacial drag term for one-dimensional two-fluid model will be discussed in this section.

As was mentioned in Brooks et al. [3-22], and Hibiki and Ozaki [3-21], area averaged interfacial drag force term used in one-dimensional two fluid model is expressed as follows:

$$\left\langle M_{ig}^{D} \right\rangle = -\left\langle C_i \right\rangle \left| \left\langle v_r \right\rangle \right| \left\langle v_r \right\rangle . \tag{3-1}$$

Here, M_{ig}^{D} , C_i and v_r are the interfacial drag force term, drag coefficient and relative velocity, respectively. The $\langle\ \rangle$ symbol indicates the area-averaging over the flow cross section. The area-averaged drag coefficient can be formulated as follows:

$$\left\langle C_i \right\rangle = \frac{\left\langle \alpha \right\rangle \left(1 - C_\alpha \left\langle \alpha \right\rangle\right)^3 \Delta\rho g}{\left\langle\left\langle v_{gj} \right\rangle\right\rangle^2} \tag{3-2}$$

Here, α , $\Delta\rho$, g , and $\left\langle\left\langle v_{gj} \right\rangle\right\rangle$ are void fraction, density difference between the two phases,

gravitational acceleration, and void fraction-weighted mean drift velocity, respectively. C_α is the covariance in void fraction distribution arise by the area-averaging, which is defined as follows:

$$C_\alpha \equiv \frac{\langle \alpha^2 \rangle}{\langle \alpha \rangle \langle \alpha \rangle} \tag{3-3}$$

Under a steady state condition, the interfacial drag force acting on bubbles are balanced with the buoyancy force as shown in Eq. (3-4).

$$\left\langle M_{ig}^D \right\rangle = -\left\langle \alpha \left(1-\alpha\right) \right\rangle \Delta\rho g = -\left\langle \alpha \right\rangle \left(1 - C_\alpha \left\langle \alpha \right\rangle\right) \Delta\rho g \tag{3-4}$$

Substituting Eq. (3-4) into Eq. (3-1) yields the drag coefficient given by Eq. (3-2). Additionally, area-averaged relative velocity can be expressed as a function of distribution parameter (C_0) and the covariance C_α defined in Eq. (3-3) as follows [3-20, 3-22]:

$$\left\langle v_r \right\rangle = \frac{1-\langle \alpha \rangle}{1 - C_\alpha \langle \alpha \rangle} \left(\frac{1 - C_0 \langle \alpha \rangle}{1 - \langle \alpha \rangle} \left\langle \left\langle v_g \right\rangle \right\rangle - C_0 \left\langle \left\langle v_f \right\rangle \right\rangle \right) \tag{3-5}$$

Here, v_g and v_f are, respectively, the gas velocity and liquid velocity. By substituting Eqs. (3-2) and (3-5) into Eq. (3-1), one obtains an expression for interfacial drag as follows:

$$\left\langle M_{ig}^D \right\rangle = -\frac{1}{C'_\alpha} \frac{\langle \alpha \rangle \left(1 - \langle \alpha \rangle\right)^3 \Delta\rho g}{\left\langle \left\langle v_{gj} \right\rangle \right\rangle^2} \times \left(\frac{1 - C_0 \langle \alpha \rangle}{1 - \langle \alpha \rangle} \left\langle \left\langle v_g \right\rangle \right\rangle - C_0 \left\langle \left\langle v_f \right\rangle \right\rangle \right) \left| \left(\frac{1 - C_0 \langle \alpha \rangle}{1 - \langle \alpha \rangle} \left\langle \left\langle v_g \right\rangle \right\rangle - C_0 \left\langle \left\langle v_f \right\rangle \right\rangle \right) \right| \tag{3-6}$$

Here, C'_α means relative velocity covariance (represents the effect of covariance C_α on area-averaged relative velocity) and is defined as shown in Eq. (3-7).

$$C'_\alpha \equiv \frac{1-\langle \alpha \rangle}{1 - C_\alpha \langle \alpha \rangle} \tag{3-7}$$

As was shown in Eq. (3-7), in one-dimensional two-fluid model, constitutive equations for

distribution parameter (C_0), drift velocity ($\left\langle\left\langle v_{gj} \right\rangle\right\rangle$), and covariance (C'_{α}) are the necessary terms to obtain area-averaged interfacial drag.

3.2.2 Constitutive equations for distribution parameter and drift velocity

Constitutive equations for distribution parameter and drift velocity utilized in TRAC-BF1 code [3-6] are tabulated in Table 1. For the distribution parameter, Rouhani's equation [3-23] is utilized in TRAC-BF1. However, for the distribution parameter in circular round tube, the generalized form proposed by Ishii [3-9] is widely utilized, which is shown in Eq. (3-8).

$$C_0 = 1.2 - 0.2\sqrt{\frac{\rho_g}{\rho_f}} \tag{3-8}$$

Here, ρ_g and ρ_f are the density of gas phase and liquid phase, respectively. Difference in distribution parameter value using Rouhani [3-23] and Ishii [3-9]'s equations is shown in Fig. 3-1. Rouhani [3-23] considered the dependence of mass velocity and channel size on the distribution parameter but the distribution parameter takes very high value as the channel size increases. TRAC-BF1 code implements the limiting value of the distribution parameter being 1.33. On the other hand, Ishii [3-9] assumed negligible dependence of Reynolds number on the distribution parameter and modeled the distribution parameter with the density ratio, see Eq. (3-8).

For constitutive equations for drift velocity, modified Zuber and Findlay [3-8]'s model based on Wilson's upward bubbly flow data [3-24] is utilized. However, for churn flow in standard pipe size, Ishii's drift velocity expression is widely utilized [3-9].

$$V_{gj}^{+} = \sqrt{2} \tag{3-9}$$

Here, V_{gj}^{+} is defined as,

$$V_{gj}^{+} = \frac{\left\langle\left\langle v_{gj} \right\rangle\right\rangle}{\left(\frac{\Delta\rho g\sigma}{\rho_f^2}\right)^{1/4}} \tag{3-10}$$

and σ represents the surface tension.

For large diameter pipe, Hibiki and Ishii [3-25]'s model, which considered the secondary flow due to the presence of bubbles within flow channel, can be utilized.

$$V_{gj}^{+} = V_{gj,B}^{+} \exp\left(-1.39\left\langle j_g^{+}\right\rangle\right) + V_{gj,P}^{+}\left\{1 - \exp\left(-1.39\left\langle j_g^{+}\right\rangle\right)\right\} \tag{3-11}$$

Here, $j_g^{+} = j_g / (\Delta\rho g\sigma / \rho_f^2)^{0.25}$ and $V_{gj,B}^{+}$ is the drift velocity for bubbly flow defined by Ishii [3-8].

$$V_{gj,B}^{+} = \sqrt{2}\left(1 - \left\langle \alpha \right\rangle\right)^{1.75} \tag{3-12}$$

$V_{gj,P}^{+}$ is the drift velocity under pool condition proposed by Kataoka and Ishii [3-10], and it is expressed as shown in Eq. (3-13) for the low viscosity fluid, such as water.

$$V_{gj,P}^{+} = \begin{cases} 0.0019\left(D_h^{+}\right)^{0.809}\left(\dfrac{\rho_g}{\rho_f}\right)^{-0.157} N_{\mu f}^{-0.562} & \text{for} \quad D_h^{+} \le 30 \\ 0.030\left(\dfrac{\rho_g}{\rho_f}\right)^{-0.157} N_{\mu f}^{-0.562} & \text{for} \quad D_h^{+} \ge 30 \end{cases} \tag{3-13}$$

D_h^{+} and $N_{\mu f}$ are the non-dimensional hydraulic diameter and viscosity number, respectively.

$$D_h^{+} = \frac{D_h}{\sqrt{\dfrac{\sigma}{\Delta\rho g}}} \tag{3-14}$$

$$N_{\mu f} = \frac{\mu_f}{\left(\rho_f \sigma \sqrt{\dfrac{\sigma}{\Delta\rho g}}\right)^{1/2}} \tag{3-15}$$

Here, D_h and μ_f are the hydraulic diameter and liquid viscosity, respectively.

Note that covariance is not considered in the original TRAC-BF1 code, such that, it is assumed to be one.

$$C_\alpha = C'_\alpha = 1 \tag{3-16}$$

Hibiki and Ozaki [3-21] extended the work of Brooks et al. [3-20] using Garnier's void fraction distribution data [3-14] under subcooled boiling condition and proposed following expressions for covariance. Brooks et al. [3-20] developed the constitutive equations for covariance term using the database obtained in 0.1 ~ 0.603 MPa pressure conditions. Additionally, the database developed by Garnier utilizes Freon as a working fluid, which simulates prototypic condition of PWR at 15 MPa.

$$C_\alpha = \begin{cases} \max\left(C_{\alpha,SB}, C_{\alpha,BB}\right) & \text{for} \quad \left\langle\alpha\right\rangle \le \left\langle\alpha_{crit}\right\rangle - 0.01 \\ \dfrac{1 - C_\alpha\left(\left\langle\alpha_{crit}\right\rangle - 0.01\right)}{1 - \left(\left\langle\alpha_{crit}\right\rangle - 0.01\right)}\left(\left\langle\alpha\right\rangle - 1\right) + 1 & \text{for} \quad \left\langle\alpha\right\rangle > \left\langle\alpha_{crit}\right\rangle - 0.01 \end{cases} \tag{3-17}$$

$$C'_\alpha = \begin{cases} \max\left(C'_{\alpha,SB}, C'_{\alpha,BB}\right) & \text{for} \quad \left\langle\alpha\right\rangle \le \left\langle\alpha_{crit}\right\rangle - 0.01 \\ \dfrac{1 - C'_\alpha\left(\left\langle\alpha_{crit}\right\rangle - 0.01\right)}{1 - \left(\left\langle\alpha_{crit}\right\rangle - 0.01\right)}\left(\left\langle\alpha\right\rangle - 1\right) + 1 & \text{for} \quad \left\langle\alpha\right\rangle > \left\langle\alpha_{crit}\right\rangle - 0.01 \end{cases} \tag{3-18}$$

Here,

$$C_{\alpha,SB} = \frac{1}{\left\langle\alpha\right\rangle}\frac{\alpha_W^2}{2\alpha_W - \left\langle\alpha\right\rangle} \tag{3-19}$$

$$C'_{\alpha,SB} = \frac{1-\langle\alpha\rangle}{1-\frac{\alpha_W^2}{2\alpha_W-\langle\alpha\rangle}} \tag{3-20}$$

$$C_{\alpha,BB} = 1.16 - 0.16\sqrt{\frac{\rho_g}{\rho_f}} \tag{3-21}$$

$$C'_{\alpha,BB} = \frac{1-\langle\alpha\rangle}{1-\left(1.16-0.16\sqrt{\frac{\rho_g}{\rho_f}}\right)\langle\alpha\rangle} \tag{3-22}$$

$$\alpha_W = \left[\left(\frac{9}{2}\right)\left\{\frac{1-\left(1.2-0.2\sqrt{\frac{\rho_g}{\rho_f}}\right)\left(1-e^{-18\langle\alpha\rangle}\right)}{\left(1.2-0.2\sqrt{\frac{\rho_g}{\rho_f}}\right)\left(1-e^{-18\langle\alpha\rangle}\right)}\right\}+1\right]\langle\alpha\rangle \tag{3-23}$$

$$\langle\alpha_{crit}\rangle = \frac{1}{C_\alpha} \tag{3-24}$$

Figure 3-2 shows the dependency of void fraction and relative velocity covariances on area-averaged void fraction using Eqs. (3-17) and (3-18). Analytically, $C_\alpha = 1/\langle\alpha\rangle$ is obtained under the separated flow model, where uniform distributions are assumed in liquid film and gas core. As a result, $C_\alpha' \to \infty$ is obtained. Additionally, available experimental data shows the increase in relative velocity covariance with respect to area-averaged void fraction [3-20]. Considering the interfacial drag model in annular flow regime, covariance shouldn't be considered beyond the separated flow regime. For the transition from dispersed flow to separated flow, constitutive

equations (3-17) and (3-18) from Hibiki and Ozaki [3-21] are given to properly define the transition using the system analysis code. As can be seen from Fig. 3-2, influence of covariance becomes significantly large near the transition to annular flow regime. From Eq. (3-6), interfacial drag term becomes smaller when neglecting the presence of covariance.

3.3 Evaluation of void fraction in circular pipe using TRAC-BF1 code

To understand the effect of void fraction distribution covariance on area-averaged void fraction, TRAC-BF1 code was utilized to simulate upward two-phase flow through circular tube. TRAC-BF1, similar to TRACE and RELAP5 codes, is the thermal-hydraulic analysis code, which utilizes mass, momentum, and energy equations for both gas and liquid phases with interfacial transfer terms. These codes have been utilized in nuclear industry for number of years to assess the safety of nuclear power plant. In these safety analysis codes, covariance introduced in section 3.2 is not considered. As can be seen from the relationship between relative velocity covariance and Eq. (3-6) shown in Fig. 3-2, introducing covariance highly affects the interfacial drag term. Especially for high void fraction condition, effect of the covariance on interfacial drag term is relatively large, hence, it is essential to examine the characteristics of system analysis codes when the covariance term is introduced.

The computational domain is shown in Fig. 3-3, which comprised of main pipe simulated by 50 cells of primary arm of TEE component. Inner diameter was set to 25 mm for medium size pipe, and 250 mm for large diameter at adiabatic condition. Additionally, FILL components were utilized for both liquid-phase and gas-phase inlets, and gas-phase inlet was placed at the second cell counting from the bottom. The outlet pressure boundary condition was controlled by using BREAK component connected to the outlet of the TEE component.

Four models tabulated in Table 3-2 were utilized to calculate interfacial drag term in TRAC-BF1 code, and influences of the distribution parameter and covariance were evaluated.

For the steady-state analysis, outlet pressure boundary at BREAK component and inlet flow conditions at FILL component were kept constant. For the transient analysis, unsteady inlet and boundary conditions were utilized. By conducting these two analyses, calculated results of void fraction values in circular round tube were evaluated.

For the outlet boundary condition, 7 MPa, which is the BWR's normal operation condition, was applied. It is confirmed that covariance term does not show pressure dependency for the ranges of 1 to 9 MPa [3-26]. Here, 7 MPa was selected for the analysis condition. Inlet superficial gas

velocity ($\langle j_g \rangle$) was evaluated using drift flux model by supplying targeted void fraction value ($\langle \alpha \rangle_{target}$) and superficial liquid velocity value ($\langle j_f \rangle$) using following drift-flux model formulation.

$$\langle j_g \rangle = \frac{\left(C_0 \langle j_f \rangle + \langle \langle v_{gj} \rangle \rangle \right) \langle \alpha \rangle_{target}}{1 - C_0 \langle \alpha \rangle_{target}} \tag{3-25}$$

Here, recommended models tabulated in Table 3-1 were utilized for distribution parameter and drift velocity. Unlike drift-flux model, it is not guaranteed that area-averaged void fraction calculation matches with $\langle \alpha \rangle_{target}$ value in TRAC-BF1 code. However, for steady and fully developed conditions, it is expected that calculated void fraction matches with $\langle \alpha \rangle_{target}$ value, since interfacial drag term is calculated using distribution parameter and drift velocity in TRAC-BF1 code. In section 3.4, comparison of the analysis results and $\langle \alpha \rangle_{target}$ is done, and well-posedness of constitutive equations and governing equations due to the inclusion of covariance term is considered.

3.4 Results and Discussions

3.4.1 Steady-State Conditions

For the current analysis, change in TEE component's void fraction values in axial direction was investigated for both medium (25 mm ID) and large (250 mm ID) diameter pipes using four conditions tabulated in Table 3-2. Figures 3-4 and 3-5 depict the results of the test cases with targeted void fraction values of 0.70 and 0.50 for medium diameter pipe. As can be seen from the figures, liquid superficial velocities were set to 0.5, 1.0, and 2.0 m/s, respectively. Figures 3-6 and 3-7 depict the results for the cases with large diameter pipe with targeted void fraction values of 0.70 and 0.50.

From the trends observed in Figs 3-4 through 3-7, noticeable difference in area-averaged void fraction values can be confirmed using different constitutive relations of drift-flux model. In particular, high sensitivity on void fraction values by the constitutive equations of distribution parameter and interfacial drag term can be confirmed. The distribution parameter directly relates the

area-averaged relative velocity and two-phase velocities, hence, its sensitivity on void fraction calculation is also high for the TRAC-BF1 calculation.

As is depicted in Fig. 3-1, since Rouhani's distribution parameter model is dependent on flow rate, distribution parameter tends to become smaller as the flow rate increases. As a result, area-averaged void fraction tends to be higher compared to the low flow rate cases. In addition, Rouhani's model is also dependent on pipe diameter, and as can be seen from the comparison of Figs. 3-4 and 3-6, and Figs. 3-5 and 3-7, area-averaged void fraction for large diameter pipe tends to become smaller than medium diameter pipe due to the increase in the distribution parameter.

From the covariance model shown in Fig. 3-2 and the interfacial drag defined in Eq. (3-6), for the area-averaged void fraction below the annular flow transition, inclusion of covariance term largely affects the calculation results for the high area-averaged void fraction conditions. It can be confirmed from the comparison of Figs. 3-4 and 3-5 (medium diameter pipe), and Figs. 3-6 and 3-7 (large diameter pipe) that larger covariance effect is confirmed for the analysis case of void fraction 0.70 than that of 0.50.

Furthermore, it can be also confirmed from Figs. 3-4 through 3-7 that the effect of covariance becomes large for the conditions with low flow rate. Figures 3-8 and 3-9 depict the ratio between calculated and targeted void fraction values plotted with mixture volumetric flux. As can be seen from the figures, effect of the covariance term is not noticeable, but inclusion it underestimates the void fraction values at the low flow rate conditions. The current simulation condition was set to steady-state without phase-change, and theoretically, void fraction calculated by TRAC-BF1 code with recommended models should match with drift-flux model. The discrepancy of void fraction values between the models with and without covariance may be caused by introducing the interfacial drag term which may have affected the code accuracy of TRAC-BF1 models.

3.4.2 Effect of covariance on drift velocity term

In case of utilizing drift velocity constitutive equations in multi particle system, which is derived based on the terminal velocity of bubbles in an infinite medium, in a strict sense, covariance must be considered. Drift velocity for churn flow, for instance, is defined as follows [3-8]:

$$v_{gj} = \sqrt{2}\left(\frac{\Delta\rho g\sigma}{\rho_f^2}\right)^{0.25}\left(1-\alpha\right)^{0.25} \tag{3-26}$$

Then, its one-dimensional form can be expressed as,

$$\left\langle\left\langle v_{gj}\right\rangle\right\rangle \equiv \frac{\left\langle \alpha v_{gj}\right\rangle}{\left\langle \alpha \right\rangle} = \sqrt{2}\left(\frac{\Delta\rho g\sigma}{\rho_f^2}\right)^{0.25}\left(1-\left\langle \alpha \right\rangle\right)^{0.25} C_{\alpha}'' \tag{3-27}$$

Here, C_{α}'' term is defined as follows:

$$C_{\alpha}'' \equiv \frac{\left\langle \alpha\left(1-\alpha\right)^{0.25}\right\rangle}{\left\langle \alpha \right\rangle\left(1-\left\langle \alpha \right\rangle\right)^{0.25}} \tag{3-28}$$

As shown in Fig. 3-10, Eq. (3-28) can be numerically calculated by assuming the presence of the following power-law void fraction spatial distribution.

$$\frac{\alpha}{\alpha_0} = 1-\left(\frac{r}{R_w}\right)^n \tag{3-29}$$

where α_0, r and R_w are, respectively, the value of α at center, radial distance and the radius of a pipe. Eq. (3-29) represents the approximate void fraction profile which can be utilized for dispersed flow regime. *n* is the exponent for the void fraction profile ranging from 2 to 7. In Fig. 3-10, the result was obtained based on $n=2$, but the sensitivity of *n* on Eq. (3-28) is found to be very small.

From the results of Fig. 3-10, covariance term defined in Eq. (3-28) can be approximated as a following functional form.

$$C_{\alpha}'' = 1+0.8807\left\langle \alpha \right\rangle^{2.263} \tag{3-30}$$

Here, utilizing the drift velocity with covariance defined in Eq. (3-27), and non-dimensional drift velocity defined in Eqs. (3-9) and (3-10), $\left\langle\left\langle v_{gj}^{*}\right\rangle\right\rangle$ can be newly defined as follows:

$$\left\langle\left\langle v_{gj}^{*}\right\rangle\right\rangle = \left(1-\left\langle \alpha \right\rangle\right)^{0.25}\left(1+0.8807\left\langle \alpha \right\rangle^{2.263}\right). \tag{3-31}$$

Figure 3-11 shows the calculated results of Eq. (3-31) with respect to area-averaged void fraction.

As can be seen, drift velocity can be approximated as $\left\langle\left\langle v_{gj}^{*}\right\rangle\right\rangle \simeq 1$,until it reaches churn flow regime. Hence, Eqs. (3-9) and (3-10) can be utilized as drift velocity for churn flow regime without considering covariance. For the constitutive equation for large diameter pipe proposed by Kataoka and Ishii [3-10], covariance is already included in the model since the model is based on the area-averaged experimental database.

3.4.3 Momentum equation in one-dimensional two-fluid model

Steady-state area-averaged momentum equation for gas phase without phase-change is expressed as follows:

$$-\left\langle\alpha\right\rangle\frac{dp}{dz}+\left\langle\alpha\right\rangle\left\langle M_{\tau g}\right\rangle-\frac{4\alpha_{w}\tau_{gw}}{D_{h}}-\left\langle\alpha\right\rangle\rho_{g}g+\left\langle M_{ig}^{D}\right\rangle=0 \tag{3-32}$$

Here, p, z, $M_{\tau g}$, α_w, τ_{gw} are respectively, pressure, position in axial direction, viscous and turbulent shear stress, void fraction at the wall, and wall shear stress.

In TRAC-BF-1 code, distribution of phase fraction for the pressure drop term due to wall shear stress F_w is performed by calculating the area-averaged volume fraction for each phase, based on the assumption of uniform void fraction distribution. With this regard, Eq. (3-32) can be expressed as follows.

$$-\left\langle\alpha\right\rangle\frac{dp}{dz}-\left\langle\alpha\right\rangle F_{w}+\phi_{g}-\left\langle\alpha\right\rangle\rho_{g}g+\left\langle M_{ig}^{D}\right\rangle=0 \tag{3-33}$$

Here, ϕ_g is expressed as follows:

$$\phi_{g}\equiv\left\langle\alpha\right\rangle F_{w}-\left\langle\alpha\right\rangle\left\langle M_{\tau g}\right\rangle-\frac{4\alpha_{w}\tau_{gw}}{D_{h}} \tag{3-34}$$

Likewise, momentum equation for liquid phase can be expressed as follows:

$$-\left(1-\left\langle\alpha\right\rangle\right)\frac{dp}{dz}-\left(1-\left\langle\alpha\right\rangle\right)F_{w}+\phi_{f}-\left(1-\left\langle\alpha\right\rangle\right)\rho_{f}g+\left\langle M_{if}^{D}\right\rangle=0 \tag{3-35}$$

$$\phi_{f}\equiv\left(1-\left\langle\alpha\right\rangle\right)F_{w}-\left(1-\left\langle\alpha\right\rangle\right)\left\langle M_{\tau f}\right\rangle-\frac{4\left(1-\alpha_{w}\right)\tau_{fw}}{D} \tag{3-36}$$

Solving for the pressure gradient of two phase mixture by summing Eqs. (3-33) and (3-35), one obtains following expression:

$$\frac{dp}{dz} = -F_w + \left(\phi_g + \phi_f\right) - \rho_m g \tag{3-37}$$

where, ρ_m is mixture density defined by $\left\langle \alpha \right\rangle \rho_g + \left(1 - \left\langle \alpha \right\rangle\right)\rho_f$.

Two-phase pressure drop can be explained by the contributions of friction, acceleration, and gravity. When the flow area remains same, accelerational pressure drop can be considered negligible. Hence, by only considering the effects due to gravitational and frictional pressure drop, Eq. (3-37) is deduced as follows:

$$\phi_g + \phi_f = 0 \tag{3-38}$$

Substituting Eq. (3-37) into Eq. (3-33), and utilizing interfacial drag term defined in Eq. (3-4), one obtains

$$\left(1 - \left\langle \alpha \right\rangle\right)\phi_g - \left\langle \alpha \right\rangle \phi_f = \left\langle \alpha \right\rangle^2 \left(1 - C_\alpha\right)\Delta\rho g, \tag{3-39}$$

and based on the relationship defined in Eq. (3-38), the following should hold.

$$\phi_g = -\phi_f = \left\langle \alpha \right\rangle^2 \left(1 - C_\alpha\right)\Delta\rho g \tag{3-40}$$

The variables ϕ_g and ϕ_f, as defined in Eqs. (3-34) and (3-36), represent the momentum sources obtained by subtracting (1) void fraction-weighted stress tensor in axial direction and (2) wall shear stress, from the loss due to void fraction-weighted wall frictional pressure drop.

In other words, Eq. (3-40) shows that the magnitude of the difference between exact solution and the momentum equation obtained based on the uniform void fraction distribution on wall-friction term can be expressed in terms of void fraction covariance.

By eliminating the pressure gradient term from the momentum equation of two-fluid model defined in Eqs. (3-33) and (3-35), one obtains follows:

$$\left\langle M_{ig}^{D}\right\rangle + \phi_g = \phi_s \tag{3-41}$$

Here, ϕ_s is defined as,

$$\phi_s \equiv -\langle\alpha\rangle\left(1-\langle\alpha\rangle\right)\Delta\rho g\,. \tag{3-42}$$

Figure 3-12 shows the calculation results of $\left\langle M_{ig}^{D}\right\rangle$, ϕ_g and ϕ_s obtained from Eqs. (3-6), (3-40) and (3-42), respectively. As was shown in subsection 3.4.1, effect of the covariance becomes larger at high void fraction and low flow velocity conditions. Thus, void fraction and liquid superficial velocity values of 0.7 and 0.01 m/s were selected for the analysis. The source terms are plotted with respect to area averaged void fraction along with the interfacial drag without considering covariance. When covariance is not considered in the calculation, $C_\alpha = 1$ is assumed, which results in $\phi_g = 0$. Hence, momentum equation is solved when interfacial drag term is equal to ϕ_g. This is equivalent to saying that the intersection (point *A*) between momentum source terms $\left\langle M_{ig}^{D}\right\rangle$ and ϕ_s on Fig. 3-12 is the solution, and void fraction value 0.7 matches with the target void fraction value obtained using drift-flux model.

When covariance is considered, $\phi_g = 0$ is utilized to solve momentum equation, and the intersection (point B) satisfying Eq. (3-41) is equal to void fraction 0.68. As can be seen from Fig. 3-8, 0.68 is equivalent to the void fraction value obtained by the TRAC-BF1 calculation with covariance. The difference in void fraction with respect to the target void fraction of 0.7 is small (0.02), important point here is that utilization of interfacial drag term with covariance consideration on conventional momentum equation loses rigorousness of the formulations. The discrepancy between calculated and targeted void fraction values arise from the fact that covariance is not considered in the momentum equation utilized in TRAC-BF1 code. Such discrepancy can be eliminated by utilizing Eq. (3-40), instead.

Figure 3-12 shows the plot of the summation of $\left\langle M_{ig}^{D}\right\rangle$ calculated with covariance and ϕ_g obtained by Eq. (3-40) with respect to area-averaged void fraction. As can be seen from the plot,

when the momentum equation is utilized with covariance, the void fraction value that satisfy Eq. (3-41) is intersected at the point *A*, which is equivalent to the target void fraction value 0.70.

In summary, following conclusions were obtained for the steady-state analysis of one-dimensional two-fluid model analysis, where momentum equation and interfacial drag term with consideration of void fraction were taken into consideration:

- It is recommended to utilize ϕ_g defined in Eq. (3-40) for momentum equation, when considering the covariance effect in the interfacial drag term.
- In the case where covariance is not considered in the interfacial drag term, $\phi_g = 0$ holds, and it shouldn't be considered in momentum equation as well.
- In the steady-state analysis, almost identical calculation results can be obtained for both the models with and without covariance.

3.4.4 Transient Conditions

It was shown in the previous section that for steady-state analysis, effect of covariance on interfacial drag term can be cancelled out by ϕ_g and ϕ_f terms, which arise by the area-averaging of momentum equation. In the transient condition, however, difference in interfacial drag term may influence the interfacial drag term since it is given by the phasic velocity of both phases through coupling of gas and liquid phase momentum equations. In the current analysis, effect of covariance on void fraction in transient case scenario was evaluated. Time-dependent inlet liquid velocity was given using the same computational model as the steady-state case.

For including covariance effect in interfacial drag term in transient analysis, usage of ϕ_g and ϕ_f terms were considered based on the momentum equation defined in Eqs. (3-33) and (3-35). Therefore, inclusion of covariance would not affect the calculation results obtained under steady-state domain.

For the boundary conditions, in order to effectively assess the influence of covariance on void fraction after the transient period, void fraction and liquid superficial velocity values were set to 0.70 and 0.01 m/s, respectively. By utilizing drift-flux model with these values, gas superficial velocity was set to 0.67 m/s. For the initial conditions prior and posterior to the transient period, area-averaged void fraction was set to 0.20, which resulted in gas and liquid superficial velocity values as 0.67 and 2.1 m/s, respectively. During the transient period, liquid superficial velocity was changed linearly in the time period of 5 to 6 seconds, as depicted in Fig. 3-13. Pressure and temperature were set to constant.

Figure 3-14 shows the change in area-averaged void fraction with respect to time for the cell number 10, 25, and 40 of the TEE component (counting from upstream) in Fig. 3-3. Prior to the transient period, it can be confirmed that the covariance effect is negligibly small. During the transient period, inclusion of covariance leads to the larger overshoot in void fraction value.

It can be seen from the interfacial drag term defined in Eq. (3-6), covariance affects the magnitude of velocity coupling of two-phase through relative velocity term. As can be seen from Fig. 3-2, the relative velocity covariance value is always greater than or equal to 1 ($C'_{\alpha} \geq 1$) . This suggests that the inclusion of covariance tends to weaken the velocity coupling.

The variables ϕ_g and ϕ_f, included in momentum equation to consider covariance effect, are not directly related to two-phase velocity fields, and they do not compensate the decrease in velocity coupling when covariance is included in the interfacial drag term.

It is expected that the oscillatory behaviors observed in the transient void fraction values in Fig. 3-14 resulted from the decrease in two-phase coupling that was enhanced with inclusion of covariance. It can be said that the effect of covariance on void fraction may not be so large for the transient case as well, but for the reactor safety analysis, slight difference in void fraction will affect the parameters such as reactor stability, thermal power output and so on. In case of the stability analysis, the stability damping ratio plays as evaluation criteria to assess the reactor condition. Thus, as is presented in the current study, appropriate treatment of covariance term is significant for the reactor safety analysis.

3.5 Conclusions

In this study, effect of drift flux parameters and covariance on the interfacial drag term appear in one-dimensional two-fluid model was investigated using TRAC-BF1 code.

One of the most significant interfacial terms, interfacial drag term, is a function of relative velocity which is directly linked to the phasic velocity calculation. Hence, accurate prediction of the interfacial drag term is crucial to perform correct area-averaged volume fraction calculation.

Recently, Hibiki and Ozaki [3-21] developed a rigorous interfacial drag model for one-dimensional two-fluid model, which takes into consideration of the void fraction covariance on drag coefficient and relative velocity. Such considerations were never addressed in previously reported models.

In this study, the model developed by Hibiki and Ozaki [3-21] was embedded into TRAC-BF1. By using the code, effect of the model on the calculated void fraction results was analyzed and the following conclusions summarize major findings:

- Large covariance is observed at high void fraction region such as bulk boiling region. It has an effect to reduce the interfacial drag term by half , at void fraction 0.80. Sensitivity towards the area-averaged void fraction calculated by the TRAC-BF1 code was found to be small.
- Interfacial drag term is one of the most important source terms to evaluate void fraction. Inclusion of covariance greatly reduced interfacial drag at high void fraction region. Considering the fact that the analysis code is utilized for the nuclear power plant's safety evaluation, the difference in interfacial drag term should not be neglected, but for the current sensitivity analysis, it was shown that the term is not highly sensitive to the area-averaged void fraction values. As was presented, it is important to confirm the validity of the conventional formulations without considering covariance term. On the other hand, result of the present work urges code users to be cautious on the fact that the conventional formulations are not rigorous by overestimating the interfacial drag term.
- By comparing the void fraction calculation results based on drift-flux model and TRAC-BF1 calculation, under estimation of void fraction was observed for the case with covariance. Inclusion of covariance in interfacial drag term creates deviation related to covariance through the distribution of stresses due to wall friction on two-phases.
- By modelling this deviation and including it in momentum equation, it is possible to obtain rigorous model, void fraction calculation results are identical to the ones calculated without covariance, and ones calculated by drift-flux model.
- When covariance is included in interfacial drag term, covariance of the momentum equation's source term deviation should be considered as well.
- When utilizing drift velocity constitutive relation obtained by the force balance between buoyancy and drag forces of multi-particle system, covariance due to area-averaging operation should be considered. However, it was confirmed that for the drift velocity correlation in churn-turbulent flow in small diameter pipe, effect of the covariance was found to be negligible.
- By conducting transient analysis using the TRAC-BF1 code with covariance, calculated void fraction trend was comparable to the results without covariance. For the model with covariance, oscillatory behavior in void fraction output was seen due to the decrease in phase velocity coupling in interfacial drag term.

Typical one-dimensional two-fluid model analysis utilizes momentum equation without considering the void fraction covariance. The interfacial drag term is obtained by expressing the area-averaged quantity of drift-flux parameters. However, this procedure ignores the relative velocity and buoyancy covariance, hence, effect of covariance is not adequately considered. In addition, covariance is considered for the drift velocity correlation proposed by Kataoka and Ishii [3-10]'s drift velocity correlation, effect of the covariance on the correlations proposed by Ishii [3-9] has not been discussed. As can be seen, there hasn't been any standardized treatment on the covariance on one-dimensional two-fluid model.

In this study, Hibiki and Ozaki [3-21] model was adopted to the modeling of interfacial drag term including covariance effect, which hasn't been adequately considered in traditional approach. From the analysis conducted, (1) effect of covariance on drift velocity models, (2) covariance effect on momentum equation, were evaluated and comprehensive model that can include covariance effect was proposed.

The physical phenomena within nuclear reactor core are highly complex. Thus, considering the important role of reactor safety analysis, development of the rigorous formulation for two-phase flow analysis is crucial. In this study, it was confirmed that the effect of covariance on area-averaged void fraction was small. However, for the transient case, difference in dynamic behavior of void fraction may affect the reactor power output as well as the stability evaluation. This study provided complete constitutive formulation with covariance term for one-dimensional two-phase flow analysis, and compare to the conventional set of governing equations, more rigorous and accurate evaluations of two-phase flow are now possible.

Table 3-1 Distribution Parameter and Drift Velocity Implemented in Original TRAC-BF1 and recommended model.

	Distribution Parameter, C_0	**Drift Velocity,** V_{gj}^+
Original TRAC-BF1	$C_{0,R} = C_\infty - \left(C_\infty - 1\right)\sqrt{\frac{\rho_g}{\rho_f}}$ $C_\infty = 1 + 0.2\left(\frac{\rho_f}{G}\sqrt{gD_h}\right)^{0.5}$ $C_0 = \min\left(1.33, C_{0,R}\right)$	$V_{gj}^+ = 1.53 + A\left(1 - F_\alpha\right)$ $A \equiv 0.73\left(D_h^+\right)^{0.121}\left(\frac{\Delta\rho}{\rho_g}\right)^{0.203}\left\langle j_g^{+}\right\rangle^{0.635} - C_0\left\langle j_g^+\right\rangle$ $F_\alpha \equiv \frac{\left\langle\alpha\right\rangle - 0.3}{\alpha_{tran} - 0.3}$ $\alpha_{tran} \equiv \left(1 + 4\sqrt{\frac{\rho_g}{\rho_f}}\right)\frac{1}{C_0} - 4\sqrt{\frac{\rho_g}{\rho_f}} - 0.15$
Recommended Model	$C_0 = C_\infty - \left(C_\infty - 1\right)\sqrt{\frac{\rho_g}{\rho_f}}$ $C_\infty = 1.2$	$V_{gj}^+ = \sqrt{2}$ for Medium Diameter Pipe $V_{gj}^+ = V_{gj,B}^+ \exp\left(-1.39\left\langle j_g^+\right\rangle\right) + V_{gj,P}^+\left\{1 - \exp\left(-1.39\left\langle j_g^+\right\rangle\right)\right\}$ for Large Diameter Pipe

Table 3-2 Evaluation cases implemented in TRAC-BF1 code and corresponding constitutive models

Model (Case Name)	**Distribution Parameter Model** **Drift Velocity Model**[*1]	**Covariance Model**
Original w/o Cov	Original TRAC-BF1	Not Applied
Original + Cov	Original TRAC-BF1	Hibiki and Ozaki [3-21]
Ishii w/o Cov	Recommended Model	Not Applied
Ishii + Cov	Recommended Model	Hibiki and Ozaki [3-21]

*1 : “Original TRAC-BF1” and “Recommended Model” are corresponding to the models shown in Table 3-1

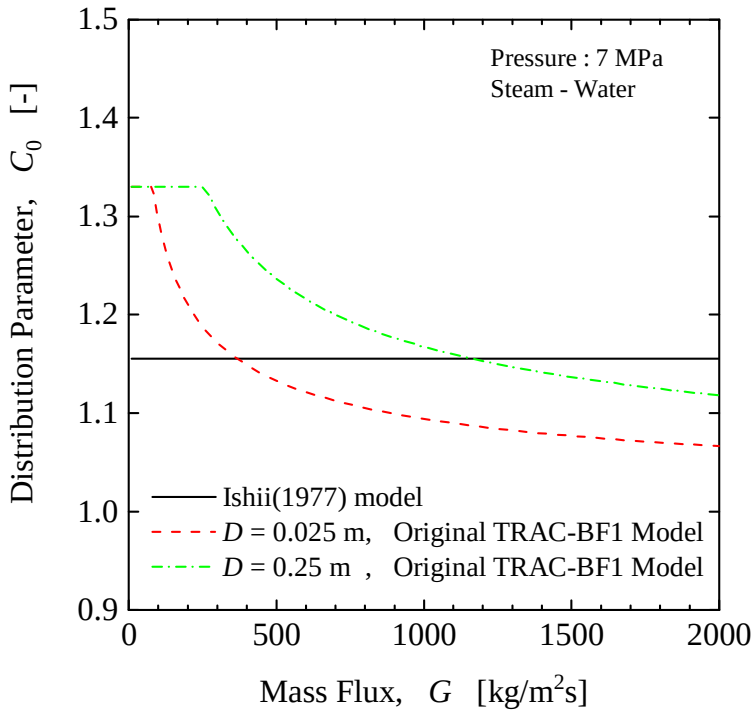

Figure 3-1 Comparison of distribution parameter model between Ishii [3-9] model and original TRAC-BF1 model [3-23].

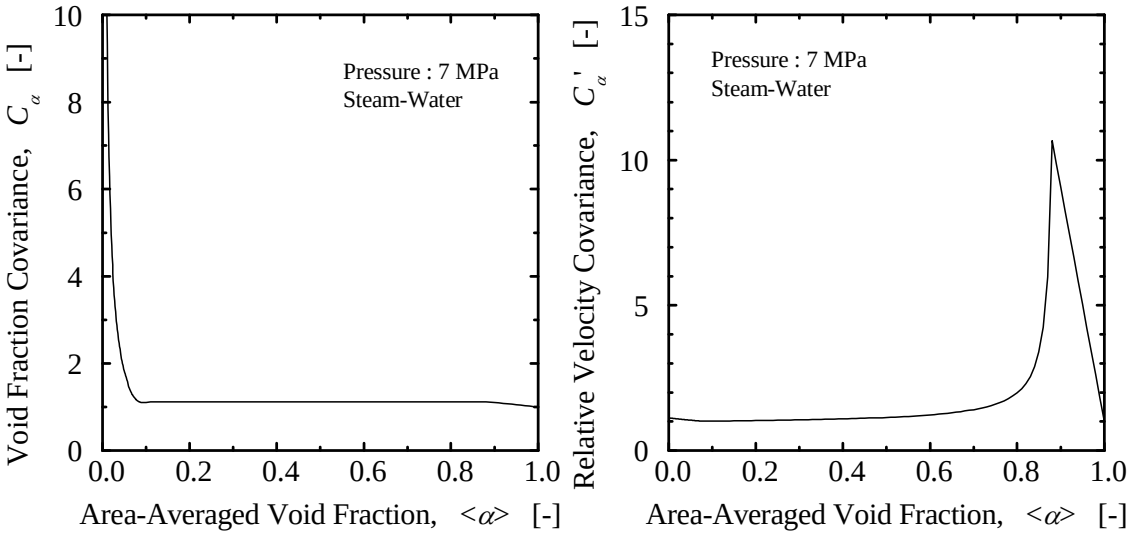

Figure 3-2 Void fraction covariance and relative velocity covariance calculated by Hibiki and Ozaki [3-21] model at pressure of 7 MPa.

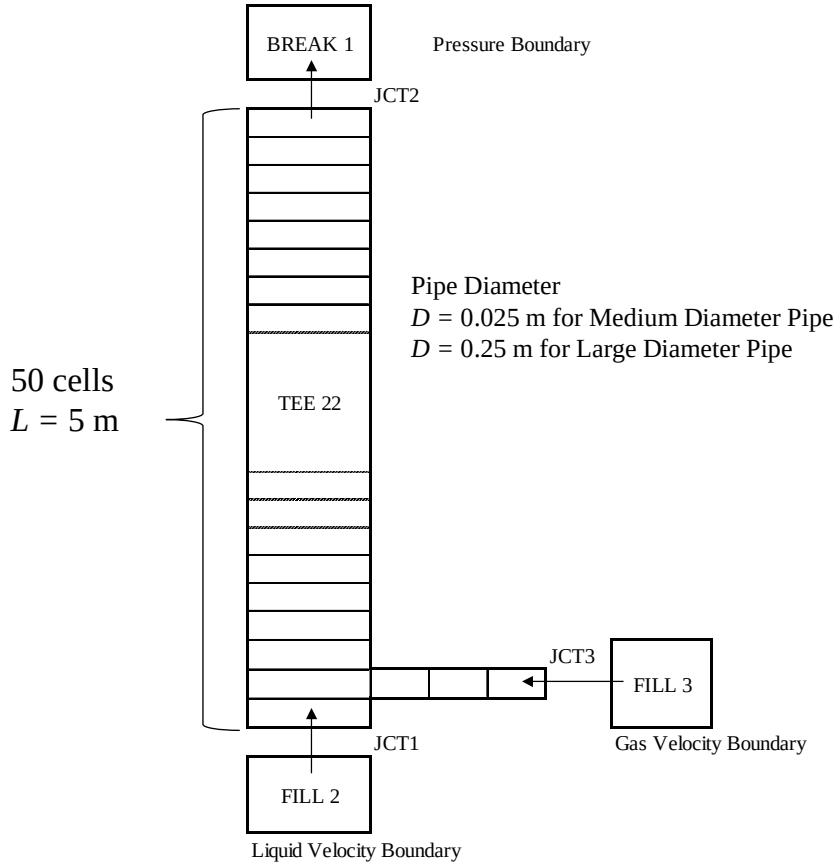

Figure 3-3 Calculation model and nodalization of TRAC-BF1 for pipe under two-phase flow.

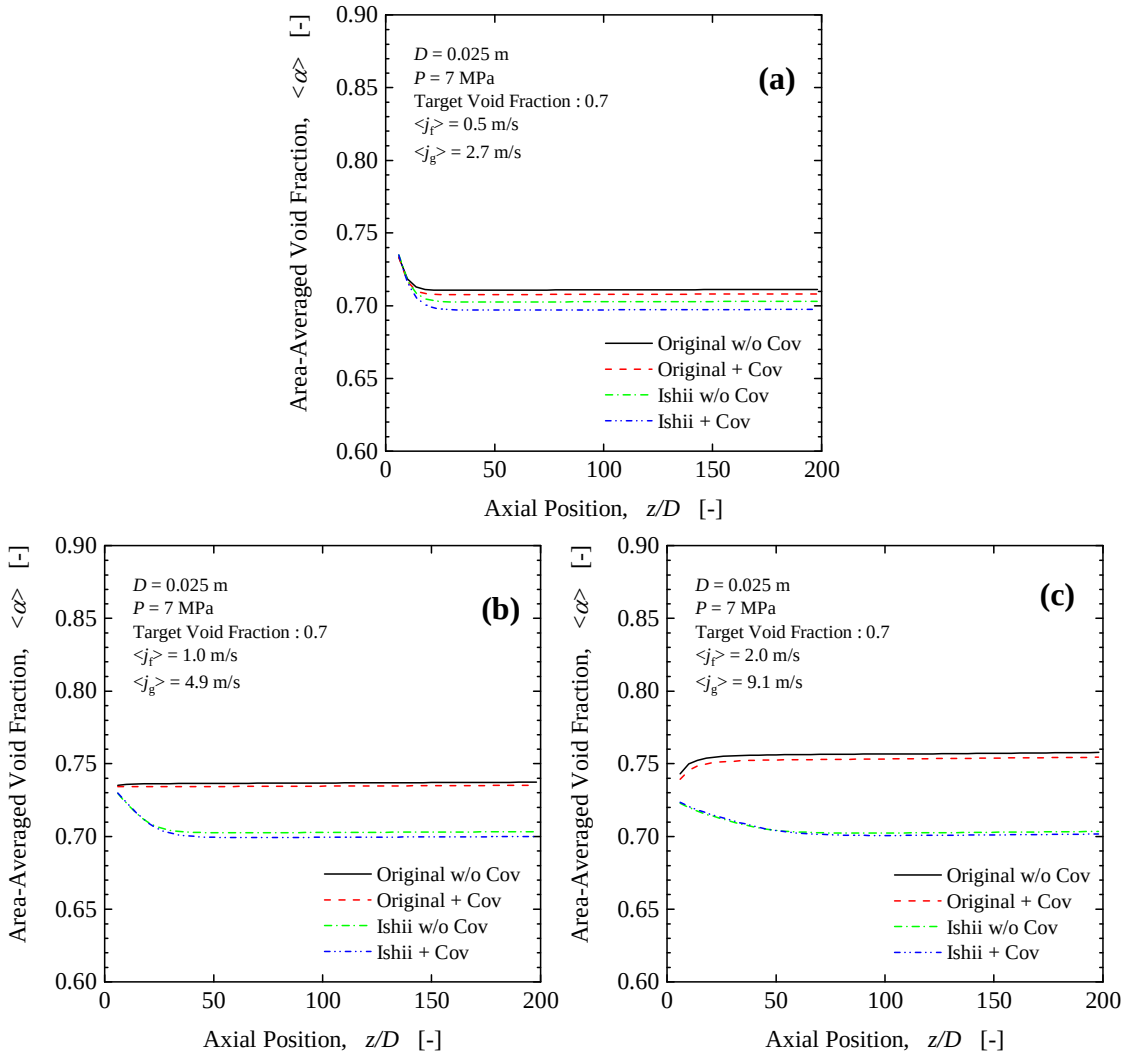

Figure 3-4 Comparisons of axial void fraction profiles for each calculation cases with medium diameter pipe at targeted void fraction of 0.7 and liquid superficial velocity of (a) 0.5 m/s, (b) 1.0 m/s and (c) 2.0 m/s.

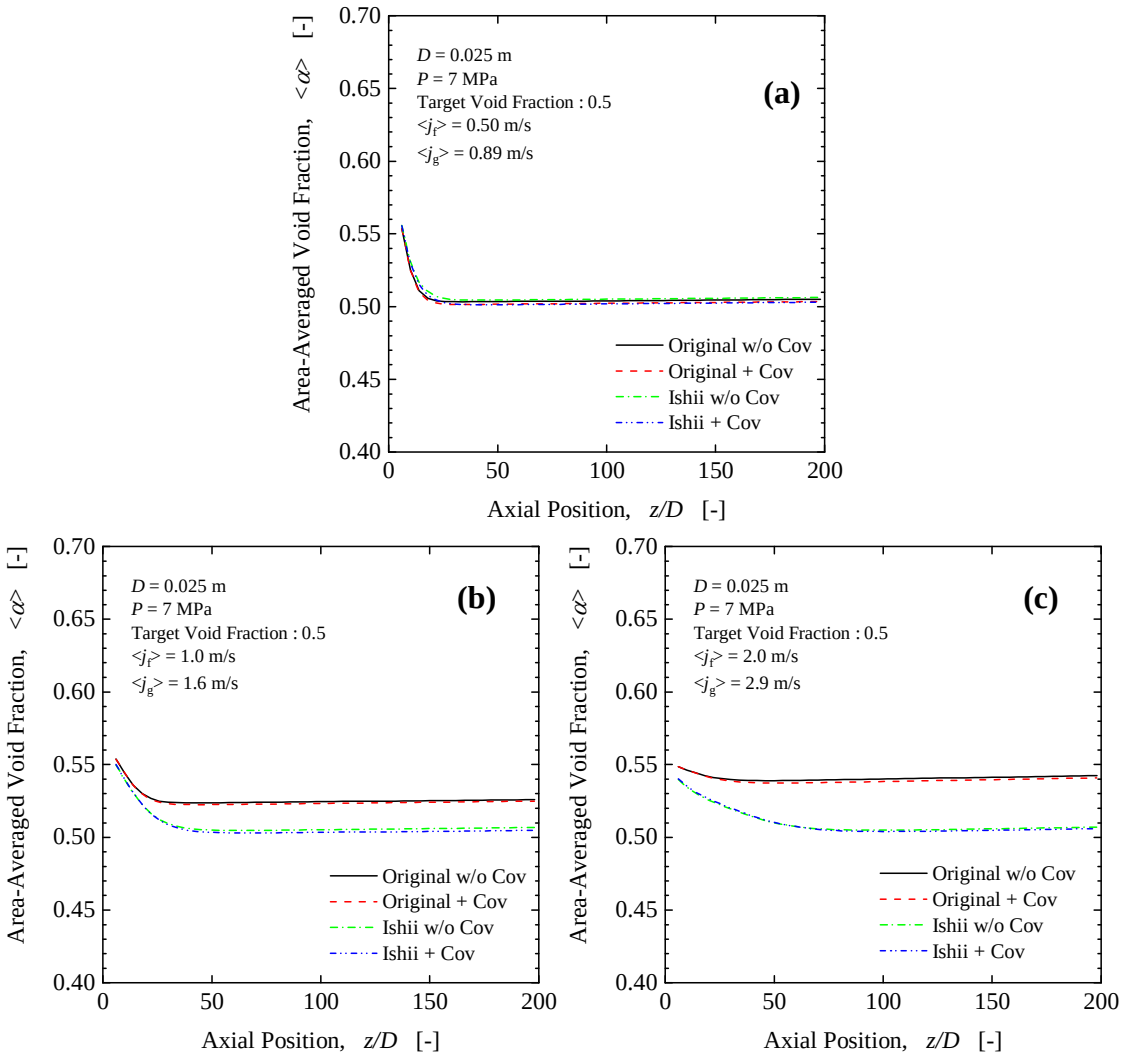

Figure 3-5 Comparisons of axial void fraction profiles for each calculation cases with medium diameter pipe at targeted void fraction of 0.5 and liquid superficial velocity of (a) 0.5 m/s, (b) 1.0 m/s and (c) 2.0 m/s.

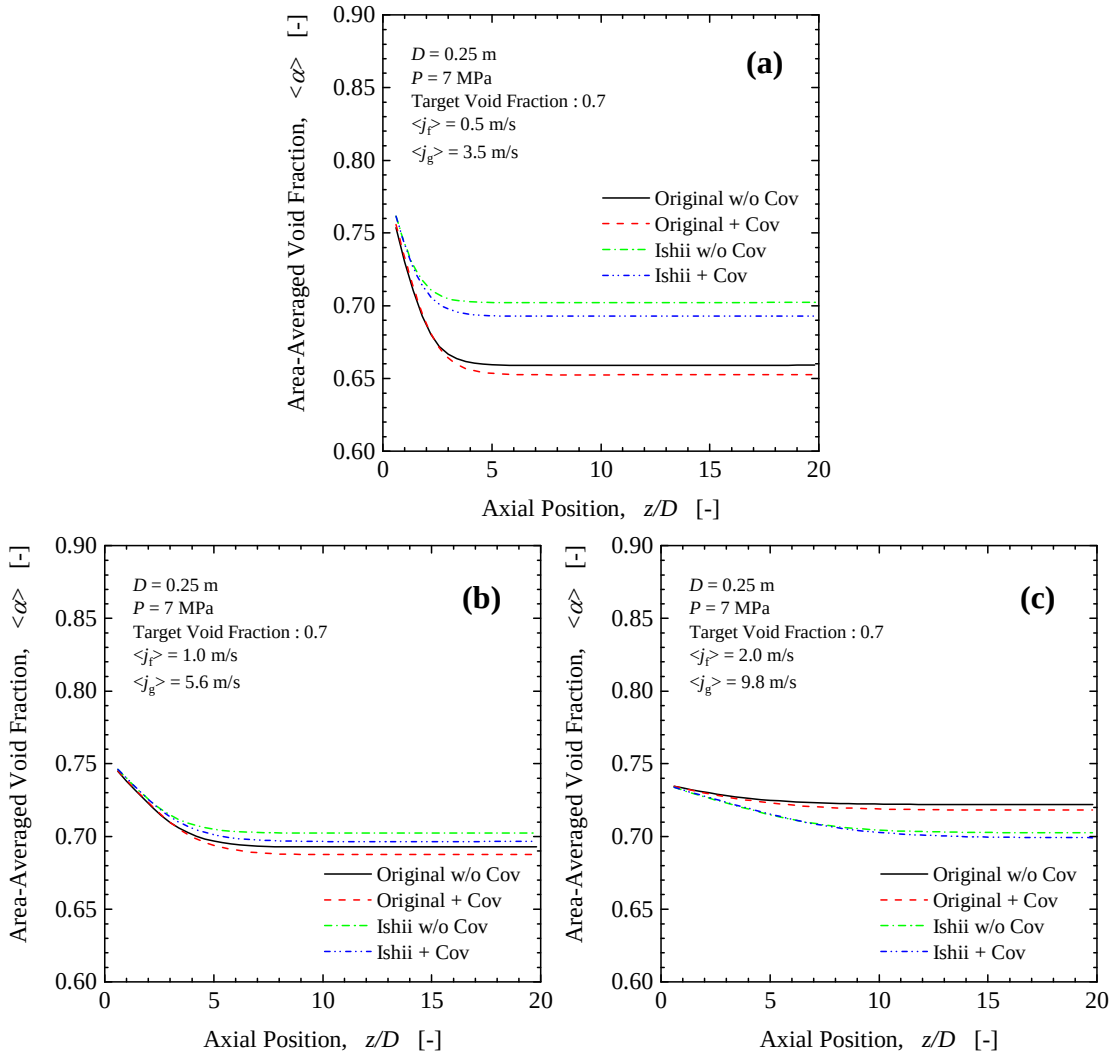

Figure 3-6 Comparisons of axial void fraction profiles for each calculation cases with large diameter pipe at targeted void fraction of 0.7 and liquid superficial velocity of (a) 0.5 m/s, (b) 1.0 m/s and (c) 2.0 m/s.

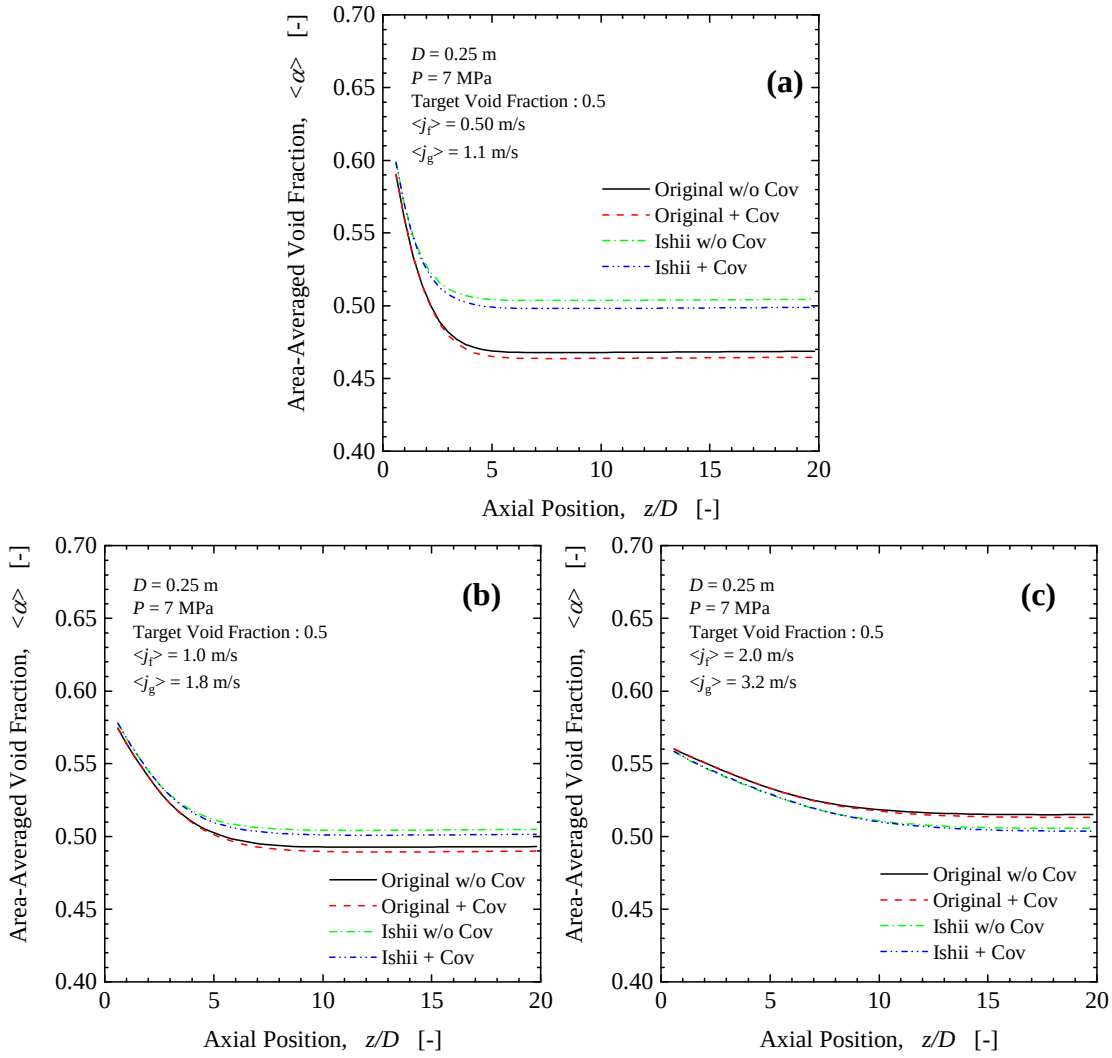

Figure 3-7 Comparisons of axial void fraction profiles for each calculation cases with large diameter pipe at targeted void fraction of 0.5 and liquid superficial velocity of (a) 0.5 m/s, (b) 1.0 m/s and (c) 2.0 m/s.

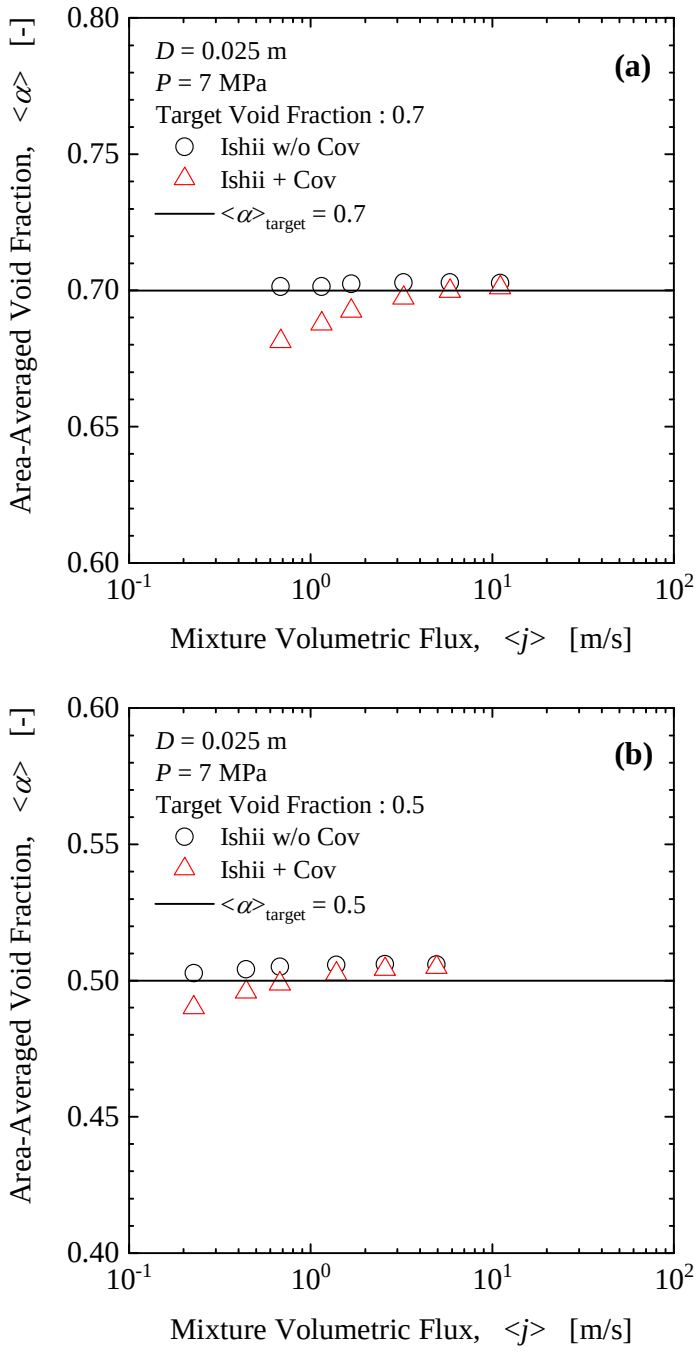

Figure 3-8 Comparisons between calculated void fractions at z/D = 178 and targeted void fraction of (a) 0.7 and (b) 0.5 with mixture volumetric flux at medium diameter pipe.

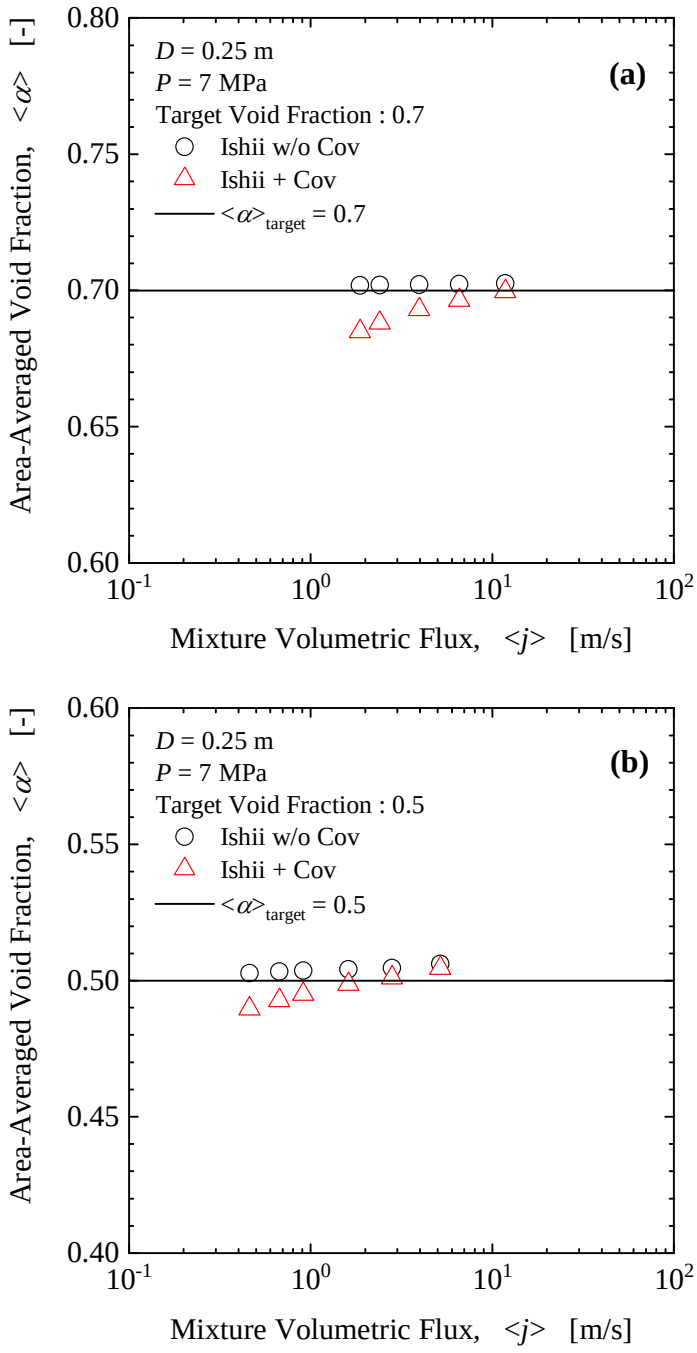

Figure 3-9 Comparisons between calculated void fractions at z/D = 17.8 and targeted void fraction of (a) 0.7 and (b) 0.5 with mixture volumetric flux at large diameter pipe.

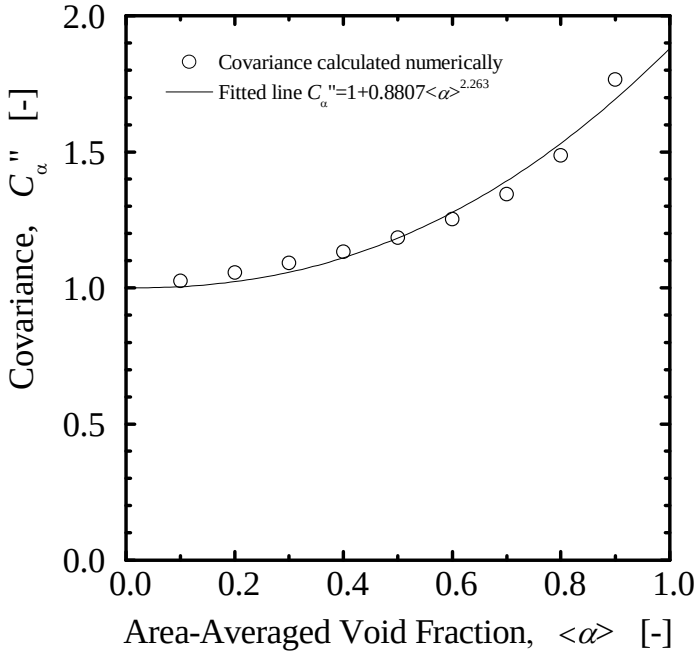

Figure 3-10 Covariance factor with respect to area-averaged void fraction

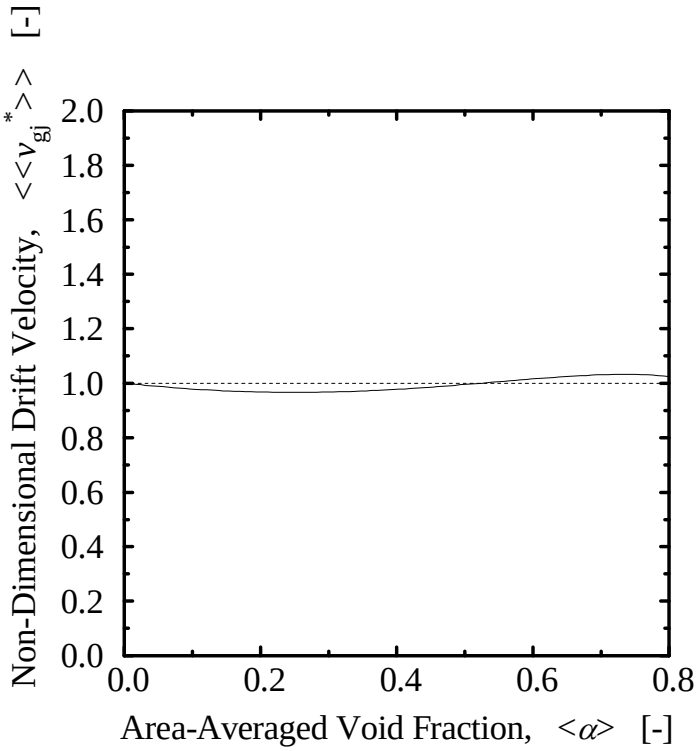

Figure 3-11 Non-dimensional drift velocity for churn flow with area-averaged void fraction.

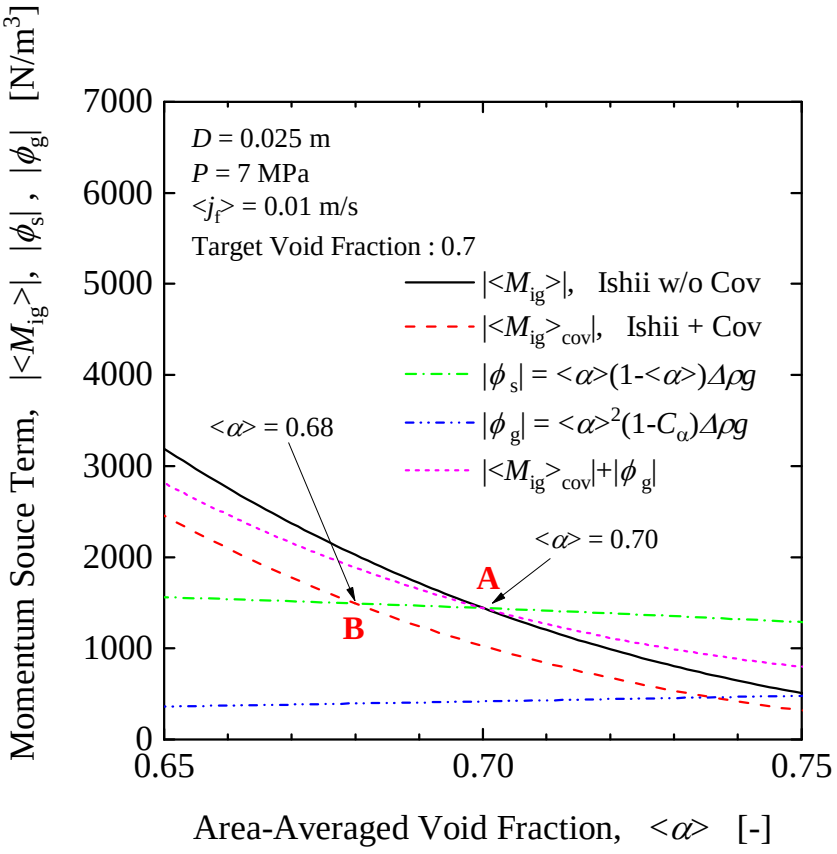

Figure 3-12 Momentum source terms with void fraction and evaluation of balancing points to satisfy steady state momentum equations.

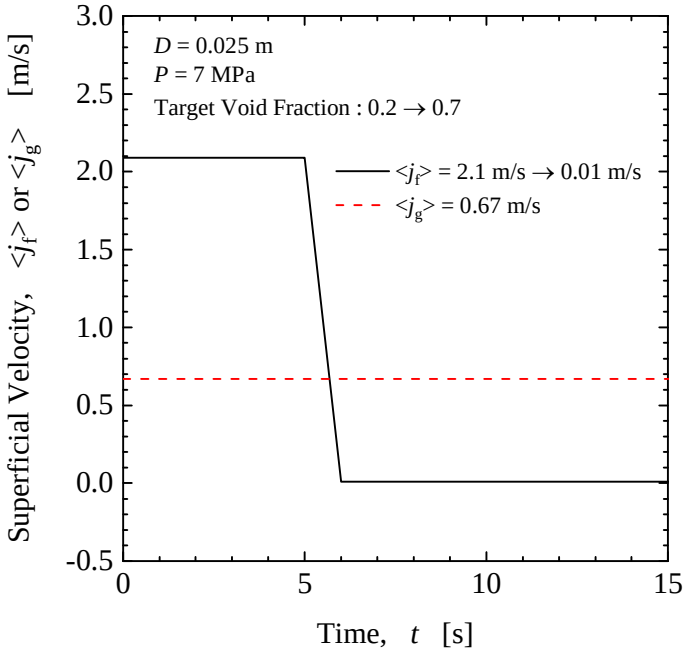

Figure 3-13 Inlet flow boundary conditions for transient calculation case.

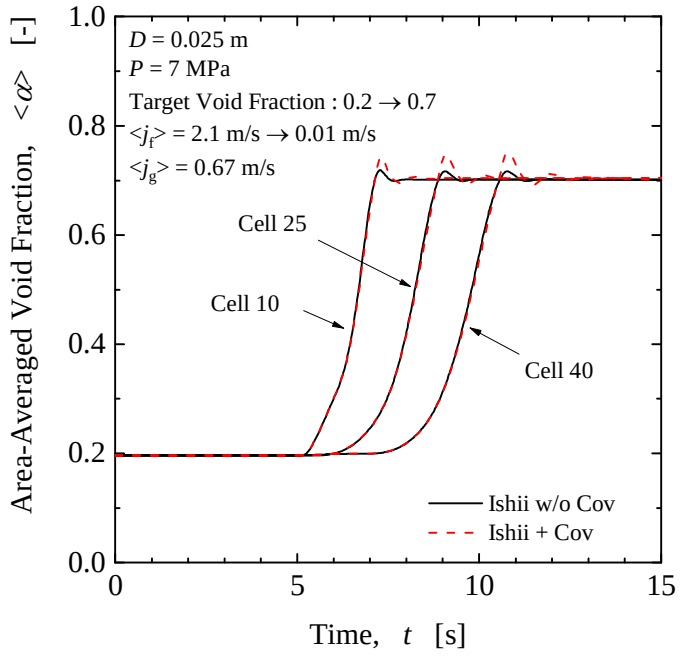

Figure 3-14 Comparisons of area averaged void fraction trend between models with covariance and without covariance for transient calculation case.

References

[3-1] Boyack B, Duffey R, Griffith P, Lellouche G, Levy S, Rohatgi U, Wilson G, Wulff W, Zuber N., Quantifying reactor safety margins: Application of code scaling, applicability, and uncertainty evaluation methodology to a large-break, loss-of-coolant accident. NUREG/CR-5249/EGG-2552. US NRC, Washington (DC) (1989).

[3-2] Atomic Energy Society of Japan (AESJ), Standard method for safety evaluation using best estimate code based on uncertainty and scaling analyses with statistical approach. Atomic Energy Society of Japan, Tokyo, (2008). (in Japanese)

[3-3] Atomic Energy Society of Japan (AESJ), Guideline for credibility assessment of nuclear simulations : 2015. Atomic Energy Society of Japan, Tokyo (2015). (in Japanese)

[3-4] U.S.NRC, TRACE/V5.0 Theory Manual; Field Equations, Solutions Methods, and Physical Models. US NRC, Washington (DC) (2008).

[3-5] Information System Laboratories (ISL), RELAP5/MOD3.3 Code Manual Volume IV: Models and Correlations. NUREG/CR-5535/Rev 1-Vol. IV. US NRC, Washington (DC) (2001).

[3-6] Borkowski JA., Wade NL., TRAC-BF1/MOD1 Models and Correlations. NUREG/CR-4391/EGG-2680R4. US NRC, Washington (DC) (1992).

[3-7] Griffiths MJ, Schlegel JP, Hibiki T, Ishii M. Kinoshita I, Yoshida Y., Phenomena identification and ranking table for thermal-hydraulic phenomena during a small-break LOCA with loss of high pressure injection. Progress in Nuclear Energy 73, 51-63 (2014).

[3-8] Zuber, N., Findlay, J.A., Average volumetric concentration in two-phase flow system. Journal of Heat Transfer 87, 453-468 (1965).

[3-9] Ishii M., One-dimensional drift-flux model and constitutive equations for relative motion between phases in various two-phase flow regimes. ANL-77-47. Argonne National Laboratory, Argonne (IL) (1977).

[3-10] Kataoka I, Ishii M., Drift flux model for large diameter pipe and new correlation for void fraction. International Journal of Heat and Mass Transfer 30, 1927-1939 (1987).

[3-11] Hibiki T., Ishii M., One dimensional drift-flux model and constitutive equations for relative motion between phases in various two-phase flow regimes. International Journal of Heat and Mass Transfer 46, 4935-4948 (2003).

[3-12] Ozaki T., Hibiki T., Drift-flux model for rod bundle geometry. Progress in Nuclear Energy 83, 229-247 (2015).

[3-13] Ishii M., Mishima K., Two-fluid model and hydrodynamic constitutive relations, Nuclear Engineering and Design 82, 107-126 (1984).

[3-14] Garnier, J., Manon, E., Cubizolles, G., Local measurements on flow boiling of refrigerant 12 in a vertical tube. Multiphase Science and Technology 13, 1-111 (2001).

[3-15] Roy, R., Kang, S., Zarate, J., Laporta, A., Turbulent subcooled boiling flow in – Experiments and simulations. Journal of Heat Transfer 124, 73-93 (2002).

[3-16] Situ, R., Hibiki, T., Sun, X., Mi, Y., Ishii, M., Flow structure of subcooled boiling flow in an internally heated annulus. International Journal of Heat and Mass Transfer 47, 5351-5364 (2004).

[3-17] Lee, T., Situ, R., Hibiki, T., Park, H., Ishii, M., Mori, M., Axial developments of interfacial area and void concentration profiles in subcooled boiling flow of water. International Journal of Heat and Mass Transfer 52, 473-487 (2009).

[3-18] Yun, B., Bae, B, Euh, D., Park, G., Song, C., Characteristics of the local bubble parameters of a subcooled boiling flow in an annulus. Nuclear Engineering and Design 240, 2295-2303 (2010).

[3-19] Ozar, B., Brooks, C.S., Hibiki, T., Ishii, M., Interfacial area transport of vertical upward steam-water two-phase flow in an annular channel at elevated pressures. International Journal of Heat and Mass Transfer 57, 504-518 (2013).

[3-20] Brooks C.S., Liu Y., Hibiki T., Ishii M., Effect of void fraction covariance on relative velocity in gas-dispersed two-phase flow. Progress in Nuclear Energy 70, 209-220 (2014).

[3-21] Hibiki T., Ozaki, T., Modeling of void fraction covariance and relative velocity covariance for upward boiling flow in vertical pipe. International Journal of Heat and Mass Transfer 112, 620-629 (2017).

[3-22] Brooks C.S., Ozar B., Hibiki T., Ishii M., Two-group drift-flux model in boiling flow. International Journal of Heat and Mass Transfer 55, 6121-6129 (2012).

[3-23] Rouhani S.Z., Modified correlation for void and pressure drop. AB Atomenergi, Sweden. Internal Report AE-RTV 841 (1969).

[3-24] Wilson J.F., Grenda R.J., Patterson J.P., The velocity of rising steam in a bubbling two-phase mixture. ANS Transactions 5(1), 151-152 (1961).

[3-25] Hibiki T., Ishii M., One-dimensional drift-flux model for two-phase flow in a large diameter pipe. International Journal of Heat and Mass Transfer 46, 1773-1790 (2003).

[3-26] Ozaki T., Hibiki T., Modeling of distribution parameter, void fraction covariance and relative velocity covariance for upward steam-water boiling flow in vertical rod bundle. Journal of Nuclear Science and Technology 55, 386-399 (2018).

4. Development of One-Dimensional Two-Fluid Model with Consideration of Void Fraction Covariance Effect

4.1 Introduction

In order to perform best-estimate safety evaluation for nuclear power plants, guidelines such as CSAU [4-1], V&V [4-2, 4-3], and EMDAP [4-4] have been proposed to require (1) proper model selection, (2) reliability of the models, and (3) quantification of the model uncertainties utilized in numerical simulation codes [4-5]. Since coolant water also acts as a neutron moderator in the light-water reactor (LWR), to properly evaluate the safety of nuclear reactor, it is essential to develop thermal-hydraulic calculation models that were validated under the guidelines such as V&V.

In general, prediction of void fraction is categorized as one of the most important factors for the safety evaluation of nuclear reactors at variety of scenarios and conditions. Especially for boiling-water reactor (BWR), two-phase flow behavior highly influences critical plant parameters such as core thermal power output, coolant pressure, core flow rate distribution, and so on. For example, significant parameters for the reactor safety evaluation such as Minimum Critical Power Ratio (MCPR), maximum pressure value at pressure-boundary, Maximum Linear Heat Generation Rate (MLHGR), two-phase water level, and core stability damping ratio, are highly sensitive to void fraction, and they are categorized as High-Rank in Phenomena Identification Ranking and Table (PIRT).

In the two-fluid model utilized in one-dimensional system analysis code, momentum equation for each phase govern the phase velocity fields and they highly influence the void fraction prediction. Among the constitutive relations necessary for momentum equation closure, interfacial drag term is high sensitivity towards void fraction prediction. For the safety evaluation code for nuclear power plants such as TRACE [4-6], RELAP5 [4-7] and TRAC-BF1[4-8], interfacial drag term proposed by Anderson and Chu [4-9] relates interfacial drag term with drift-flux parameters such as distribution parameter and drift velocity. In other words, interfacial drag expression is obtained by adapting the similar concept to the drift-flux model, which takes into consideration of velocity distribution and void fraction distribution. Distribution parameter is defined based on spatial distribution of flow velocity and void fraction, and it is mainly influenced by the flow channel geometry. Ishii [4-10] developed the distribution parameter model for circular and rectangular channels, but for thermal-hydraulic analysis of reactor fuel assembly, the proper constitutive relation for rod bundle geometry is necessary. Ozaki and Hibiki [4-11, 4-12] developed the drift-flux model for one-dimensional two-fluid model code based on the void fraction

experimental database obtained at prototypic rod bundle geometry at actual range of operation condition. Hence, for drift-flux parameters, a reasonable prediction for core thermal-hydraulics should be possible by utilizing this model.

Interfacial drag term is derived from the force balance with respect to buoyancy force. However, to embed the term into one-dimensional system analysis code, covariance term due to void fraction distribution is necessary [4-13, 4-14]. In traditional one-dimensional two-fluid model approach, covariance term is completely ignored in the area-averaged relative velocity term, as was presented by Ishii and Mishima [4-15]. Brooks et al. [4-14] pointed out that the area-averaged relative velocity without the covariance, namely, Ishii and Mishima's formulation, may underestimate the area-averaged relative velocity considerably. Due to the necessity of accurate modeling for area-averaged relative velocity, Hibiki and Ozaki [4-16] developed the covariance model applicable for one-dimensional two-fluid model code based on the void fraction measurement data obtained at pipe flow under the scaled pressure condition based on prototypic PWR condition. Ozaki and Hibiki [4-17] also developed the covariance model based on the void fraction distribution measurement within prototypic rod bundle geometry. By merging the interfacial drag term with covariance effect into the one-dimensional two-fluid model, it is expected that more accurate and rigorous thermal-hydraulic analysis will be possible. However, the effect of the developed covariance models on thermal-hydraulic parameters such as void fraction has not been tested using a code.

As was shown, necessary constitutive relations for nuclear thermal-hydraulic simulation have been developed by various authors. In this chapter, (1) modeling and modification of the momentum equation necessary for embedding new constitutive relations (related to void fraction covariance model proposed by Ozaki and Hibiki[4-17]) into one-dimensional two-fluid model, (2) comparison on code simulation results between models with and without covariance effect, and (3) evaluation of code performance in steady-state and transient conditions will be the main scope. It should be noted here that the covariance term is expected to affect the interfacial drag force, which may influence the damping of sudden flow parameter change.

4.2 Momentum Equation in One-dimensional Two-fluid Model

Thermal-hydraulics in rod bundle geometry has been a challenging issue due to its geometrical complexity, difficulty in obtaining local constitutive formulations and validating the obtained experimental database. Hence, the problem has been treated as one-dimensional flow using area-averaged models and constitutive relations. For the numerical simulation in large-scale

and complex flow geometry, it is necessary to conduct efficient calculation by optimizing the computational cost. Hence, the one-dimensional momentum equation utilized in system analysis code is obtained by area-averaging local momentum equation, and is given as follows [4-18]:

$$\left\langle \alpha_k \right\rangle \rho_k \frac{\partial \left\langle\left\langle v_k \right\rangle\right\rangle}{\partial t} + \left\langle \alpha_k \right\rangle \rho_k \left\langle\left\langle v_k \right\rangle\right\rangle \frac{\partial \left\langle\left\langle v_k \right\rangle\right\rangle}{\partial z} = - \left\langle \alpha_k \right\rangle \frac{\partial p}{\partial z} + \left\langle \alpha_k \right\rangle \left\langle M_{\tau k} \right\rangle - \left\langle \alpha_k \right\rangle \rho_k g + \left\langle M_{ik} \right\rangle - \frac{4\alpha_{kw}\tau_{kw}}{D_h} \tag{4-1}$$

Here, subscript *k* denotes gas or liquid phase, and α_k, ρ_k, v_k, t, z, p, $M_{\tau k}$, g, M_{ik}, τ_{kw}, α_{kw} and D_h, respectively, are the *k*-th phase void fraction, density, velocity, time, axial position, pressure, viscous and turbulent shear stress, gravitational acceleration, interfacial drag, wall shear stress, void fraction near the wall, and hydraulic diameter. The symbols $\left\langle \ \right\rangle$ and $\left\langle\left\langle \ \right\rangle\right\rangle$ are the area-averaging and void-weighted averaging operators.

4.2.1 Closure Relations Considering Void Fraction Distribution

In order to close Eq. (4-1), constitutive relations are necessary for viscous and turbulent shear stress, interfacial drag and wall shear stress terms, respectively. Interfacial drag is obtained by the force balance with respect to buoyancy force, as shown in Eq. (4-2).

$$M_{ig} = -M_{if} = -\alpha_g \alpha_f \Delta\rho g \tag{4-2}$$

By area-averaging Eq. (4-2), one obtains

$$\left\langle M_{ig} \right\rangle = -\left\langle M_{if} \right\rangle = -\left\langle \alpha_g \right\rangle \left(1 - C_\alpha \left\langle \alpha_g \right\rangle\right) \Delta\rho g \tag{4-3}$$

Here, C_α is the covariance arose by area averaging void fraction, and is defined as shown in Eq. (4-4).

$$C_\alpha \equiv \frac{\left\langle \alpha_g^2 \right\rangle}{\left\langle \alpha_g \right\rangle \left\langle \alpha_g \right\rangle} \tag{4-4}$$

The interfacial drag term is alternatively expressed in terms of the relative velocity between two-phases (v_r), as shown in Eq. (4-5).

$$M_{ig} = -M_{if} = -C_i \left| v_r \right| v_r \tag{4-5}$$

Here, C_i is the drag coefficient. Assuming uniform relative velocity profile across the flow channel, one obtains

$$\left\langle M_{ig} \right\rangle = -\left\langle C_i \right\rangle \left| \left\langle v_r \right\rangle \right| \left\langle v_r \right\rangle \tag{4-6}$$

From the relationship between Eqs. (4-3) and (4-6), the drag coefficient is formulated as shown in Eq. (4-7).

$$\left\langle C_i \right\rangle = \frac{\left\langle \alpha_g \right\rangle \left(1 - C_\alpha \left\langle \alpha_g \right\rangle\right) \Delta\rho g}{\left\langle v_r \right\rangle^2} \tag{4-7}$$

The area-averaged relative velocity term shown in the denominator of Eq. (4-7) can be re-expressed using drift velocity (v_{gj}) as follows[4-13, 4-14]:

$$\left\langle v_r \right\rangle = \frac{\left\langle\left\langle v_{gj} \right\rangle\right\rangle}{1 - C_\alpha \left\langle \alpha_g \right\rangle} \tag{4-8}$$

In addition, to express momentum coupling between two-phases, interfacial drag term should be related to relative velocity. Hence, the area-averaged relative velocity defined in Eq. (4-9) will be substituted into the momentum equation[4-13, 4-14].

$$\left\langle v_r \right\rangle = C'_\alpha \left(\frac{1 - C_0 \left\langle \alpha_g \right\rangle}{\left\langle \alpha_f \right\rangle} \left\langle\left\langle v_g \right\rangle\right\rangle - C_0 \left\langle\left\langle v_f \right\rangle\right\rangle \right) \tag{4-9}$$

$$C'_\alpha \equiv \frac{\left\langle \alpha_f \right\rangle}{1 - C_\alpha \left\langle \alpha_g \right\rangle} \tag{4-10}$$

Note that C_0 is the distribution parameter.

Substituting Eq. (4-8) into Eq. (4-7) leads to the expression of the drag coefficient as follows:

$$\left\langle C_i \right\rangle = \frac{\left\langle \alpha_g \right\rangle \left(1 - C_\alpha \left\langle \alpha_g \right\rangle\right)^3 \Delta\rho g}{\left\langle\left\langle v_{gj} \right\rangle\right\rangle^2} = \frac{1}{C'^3_\alpha} \frac{\left\langle \alpha_g \right\rangle \left\langle \alpha_f \right\rangle^3 \Delta\rho g}{\left\langle\left\langle v_{gj} \right\rangle\right\rangle^2} \tag{4-11}$$

Substituting the drag coefficient and Eq. (4-9) into Eq. (4-6), one obtains the expression for

area-averaged interfacial drag term as follows:

$$\left\langle M_{ig} \right\rangle = -\frac{1}{C_{\alpha}'} \frac{\left\langle \alpha_g \right\rangle \left\langle \alpha_f \right\rangle^3 \Delta\rho g}{\left\langle\left\langle v_{gj} \right\rangle\right\rangle^2} \times \left(\frac{1 - C_0 \left\langle \alpha_g \right\rangle}{\left\langle \alpha_f \right\rangle} \left\langle\left\langle v_g \right\rangle\right\rangle - C_0 \left\langle\left\langle v_f \right\rangle\right\rangle \right) \left| \left(\frac{1 - C_0 \left\langle \alpha_g \right\rangle}{\left\langle \alpha_f \right\rangle} \left\langle\left\langle v_g \right\rangle\right\rangle - C_0 \left\langle\left\langle v_f \right\rangle\right\rangle \right) \right| \tag{4-12}$$

Eq. (4-12) can be embedded into momentum equation along with the constitutive relations for distribution parameter, drift velocity, and covariance due to void fraction distribution.

Next, constitutive relations for viscous and turbulent shear stress will be discussed. Consider, non-accelerating steady-state two-phase flow condition, left-hand side of Eq. (4-1) becomes zero.

$$-\left\langle \alpha_g \right\rangle \frac{\partial p}{\partial z} + \left\langle \alpha_g \right\rangle \left\langle M_{\tau g} \right\rangle - \left\langle \alpha_g \right\rangle \rho_g g + \left\langle M_{ig} \right\rangle - \frac{4\alpha_{gw}\tau_{gw}}{D_h} = 0 \tag{4-13}$$

$$-\left\langle \alpha_f \right\rangle \frac{\partial p}{\partial z} + \left\langle \alpha_f \right\rangle \left\langle M_{\tau f} \right\rangle - \left\langle \alpha_f \right\rangle \rho_f g - \left\langle M_{ig} \right\rangle - \frac{4\alpha_{fw}\tau_{fw}}{D_h} = 0 \tag{4-14}$$

Summation of Eqs. (4-13) and (4-14) yields,

$$-\frac{\partial p}{\partial z} - \rho_m g + \left(\left\langle \alpha_g \right\rangle \left\langle M_{\tau g} \right\rangle - \frac{4\alpha_{gw}\tau_{gw}}{D_h} \right) + \left(\left\langle \alpha_f \right\rangle \left\langle M_{\tau f} \right\rangle - \frac{4\alpha_{fw}\tau_{fw}}{D_h} \right) = 0 \tag{4-15}$$

Here, mixture density is defined as $\rho_m = \left\langle \alpha_g \right\rangle \rho_g + \left\langle \alpha_f \right\rangle \rho_f$. The two-phase pressure drop ($\partial p / \partial z$) term is obtained by adding wall friction and gravitational components, and the accelerational term can be assumed to be negligible. Then, Eq. (4-16) can be obtained which accounts for the viscous and turbulent shear stress, and wall shear stress terms.

$$\left(\left\langle \alpha_g \right\rangle \left\langle M_{\tau g} \right\rangle - \frac{4\alpha_{gw}\tau_{gw}}{D_h} \right) + \left(\left\langle \alpha_f \right\rangle \left\langle M_{\tau f} \right\rangle - \frac{4\alpha_{fw}\tau_{fw}}{D_h} \right) = -F_w \tag{4-16}$$

Here, F_w accounts for the pressure drop component due to two-phase wall frictional loss, and typically, it is given by the constitutive relations of single-phase friction factor and two-phase multiplier. On the other hand, Eq. (4-17) is obtained by eliminating pressure gradient term in Eqs. (4-13) and (4-14).

$$\left\langle \alpha_f \right\rangle \left(\left\langle \alpha_g \right\rangle \left\langle M_{\tau g} \right\rangle - \frac{4\alpha_{gw}\tau_{gw}}{D_h} \right) - \left\langle \alpha_g \right\rangle \left(\left\langle \alpha_f \right\rangle \left\langle M_{\tau f} \right\rangle - \frac{4\alpha_{fw}\tau_{fw}}{D_h} \right) = \left\langle \alpha_g \right\rangle^2 \Delta\rho g \left(1 - C_\alpha\right) \tag{4-17}$$

Here, Eq. (4-3) was used for the interfacial drag term. Based on Eqs. (4-16) and (4-17), viscous and turbulent shear stress, and wall shear stress terms can be derived as shown in Eqs. (4-18) and (4-19).

$$\left(\left\langle \alpha_g \right\rangle \left\langle M_{\tau g} \right\rangle - \frac{4\alpha_{gw}\tau_{gw}}{D_h} \right) = -\left\langle \alpha_g \right\rangle F_w + \left\langle \alpha_g \right\rangle^2 \left(1 - C_\alpha\right) \Delta\rho g \tag{4-18}$$

$$\left(\left\langle \alpha_f \right\rangle \left\langle M_{\tau f} \right\rangle - \frac{4\alpha_{fw}\tau_{fw}}{D_h} \right) = -\left\langle \alpha_f \right\rangle F_w - \left\langle \alpha_g \right\rangle^2 \left(1 - C_\alpha\right) \Delta\rho g \tag{4-19}$$

Hence, closure relations for the momentum equation are completed by utilizing,

(1) Viscous and turbulent shear stress, and wall shear stress terms that are obtained by substituting Eqs. (4-18) and (4-19) into Eq. (4-1), and

(2) Interfacial drag term defined in Eqs. (4-12).

Constitutive correlations in the present study are detailed in subsection 4.3.1.1.

4.2.2 Closure Relations for Uniform Void Fraction Assumption

Area averaging the interfacial drag term defined in Eq.(4-2) assuming uniform void fraction distribution leads to the expression shown in Eq. (4-20).

$$\left\langle M_{ig} \right\rangle = -\left\langle M_{if} \right\rangle = -\left\langle \alpha_g \right\rangle \left\langle \alpha_f \right\rangle \Delta\rho g \tag{4-20}$$

As was shown in subsection 4.2.1, utilizing Eq. (4-6) for the relationship between interfacial drag and relative velocity, drag coefficient under uniform void profile assumption is derived as,

$$\left\langle C_i \right\rangle = \frac{\left\langle \alpha_g \right\rangle \left\langle \alpha_f \right\rangle \Delta\rho g}{\left\langle v_r \right\rangle^2} \tag{4-21}$$

In contrast to Eq. (4-8), the relationship between relative velocity and drift velocity is given as,

$$\left\langle v_r \right\rangle = \frac{\left\langle \left\langle v_{gj} \right\rangle \right\rangle}{\left\langle \alpha_f \right\rangle} \tag{4-22}$$

The relationship between relative velocity and field velocity, which corresponds to Eq. (4-9), is given as,

$$\left\langle v_r \right\rangle = \frac{1 - C_0 \left\langle \alpha_g \right\rangle}{\left\langle \alpha_f \right\rangle} \left\langle \left\langle v_g \right\rangle \right\rangle - C_0 \left\langle \left\langle v_f \right\rangle \right\rangle \tag{4-23}$$

Hence, for the uniform void profile assumption, area-averaged interfacial drag term defined in Eq. (4-12) can be expressed as,

$$\begin{aligned} \left\langle M_{ig} \right\rangle = & -\frac{\left\langle \alpha_g \right\rangle \left\langle \alpha_f \right\rangle^3 \Delta\rho g}{\left\langle \left\langle v_{gj} \right\rangle \right\rangle^2} \\ & \times \left| \frac{1 - C_0 \left\langle \alpha_g \right\rangle}{\left\langle \alpha_f \right\rangle} \left\langle \left\langle v_g \right\rangle \right\rangle - C_0 \left\langle \left\langle v_f \right\rangle \right\rangle \right| \left(\frac{1 - C_0 \left\langle \alpha_g \right\rangle}{\left\langle \alpha_f \right\rangle} \left\langle \left\langle v_g \right\rangle \right\rangle - C_0 \left\langle \left\langle v_f \right\rangle \right\rangle \right) \end{aligned} \tag{4-24}$$

As shown in Eq. (4-23), it is obtained by simplifying Eq. (4-9) with C_α=1 assumption. Similarly, C_0 should be ideally equal to 1 for the uniform void profile assumption, but as is the case for the simulation code, it is given by the constitutive relation. It is worthy of note that while emphasizing the importance of void profile distribution, setting $C_\alpha = 1$ largely contradicts the problem-solving approach and lacks consistency.

For viscous and turbulent stress terms, and wall shear stress term, Eq. (4-15) and (4-16) still hold for uniform void profile assumption with a non-accelerating steady-state condition. On the other hand, for Eq. (4-17), Eq. (4-25) is obtained by substituting interfacial drag term defined in Eq. (4-20).

$$\left\langle \alpha_f \right\rangle \left(\left\langle \alpha_g \right\rangle \left\langle M_{\tau g} \right\rangle - \frac{4\alpha_{gw}\tau_{gw}}{D_h} \right) - \left\langle \alpha_g \right\rangle \left(\left\langle \alpha_f \right\rangle \left\langle M_{\tau f} \right\rangle - \frac{4\alpha_{fw}\tau_{fw}}{D_h} \right) = 0 \tag{4-25}$$

Hence, for uniform void profile assumption, viscous and turbulent stresses and wall shear stress terms for gas and liquid phases are given as follows:

$$\left(\left\langle \alpha_g \right\rangle \left\langle M_{\tau g} \right\rangle - \frac{4\alpha_{gw}\tau_{gw}}{D_h} \right) = -\left\langle \alpha_g \right\rangle F_w \tag{4-26}$$

$$\left(\left\langle \alpha_f \right\rangle \left\langle M_{\tau f} \right\rangle - \frac{4\alpha_{fw}\tau_{fw}}{D_h} \right) = -\left\langle \alpha_f \right\rangle F_w \tag{4-27}$$

As was shown, uniform void profile assumption lacks consistency, since it still utilizes distribution parameter which put emphasis on the relative velocity and void fraction distributions.

It should be noted here that the interfacial drag force model is formulated by the drift-flux correlation developed under steady-state conditions. Since a bubbly in water reaches its terminal velocity within a few ten milliseconds[4-19], the steady-state assumption is acceptable for simulation slow transient phenomena. However, the applicability of the code with the interfacial drag force model for transient conditions should be validated.

4.3 Effect on Code Calculation due to Approximations

For one-dimensional system analysis code such as TRACE and TRAC-BF1, momentum equation derived under uniform void profile assumption (subsection 4.2.2) is commonly utilized, and the expression deviates from the rigorous and detailed formulation with void fraction covariance (subsection 4.2.1). In addition, void fraction covariance has an effect on area-averaged relative velocity term, but the current system analysis code still assumes uniform void distribution. When considering the effect of void distribution, it is necessary to supply covariance term. Due to the advancement of the instrumentations, such as conductivity probe for local void fraction measurement [4-20, 4-21, 4-22, 4-23, 4-24], void fraction distribution measurement using X-ray CT scanner [4-25], and so on, development of the covariance model for the void profile is now possible [4-13, 4-14, 4-16, 4-17]. For the safety assessment of the nuclear power plant, validity of the thermal-hydraulic simulation at reactor core region becomes crucial. Hence, in the following chapter, thermal-hydraulic analysis within fuel rod bundle using TRAC-BF1 code will be demonstrated to evaluate the effect on uniform void distribution assumption.

4.3.1 Code Model (Constitutive Relations) and Calculation Conditions

4.3.1.1 Constitutive relations

In order to close the momentum equation, it is necessary to supply constitutive relations for (1) distribution parameter, (2) drift velocity, and (3) void fraction covariance and wall frictional pressure loss, are necessary. In this chapter, appropriateness of fore mentioned constitutive relations that are related to void distribution will be assessed. They are tabulated in Table 4-1, and each category is summarized below:

(1) Distribution parameter model

The distribution parameter model proposed by Ozaki and Hibiki [4-11, 4-12] is utilized. This model was developed based on the void fraction database obtained at rod bundle geometry under prototypic BWR operation condition. Additionally, Ozaki and Hibiki [4-17]'s model was developed using bubble layer thickness model, which is applicable for subcooled flow boiling case. Hence, one of the advantages to use this model is that numerical discontinuity between subcooled and bulk boiling can be avoided.

(2) Drift velocity model

For the drift velocity model, Hibiki-Ishii model [4-26] is utilized. The model was developed based on the Ishii [4-10]'s drift velocity model under bubbly flow condition, and Kataoka and Ishii [4-27]'s model under pool and large-diameter pipe flow conditions. The model is applicable for rod bundle geometry [4-11, 4-12].

(3) Covariance model for void fraction distribution

Ozaki and Hibiki's model [4-17] is utilized for void fraction distribution covariance. Since covariance is affected by wall conditions as well as the distribution parameter, it is necessary to utilize model that was developed under void fraction database on rod bundle geometry. Ozaki and Hibiki [4-17] developed covariance model for bulk boiling condition based on the void fraction distribution database using X-ray CT scanner obtained at NUPEC's rod bundle geometry [4-25, 4-28, 4-29]. In addition, covariance model under subcooled boiling condition was also developed by adopting bubble-layer-thickness model, hence, it can cover wide range of void fraction under subcooled to bulk boiling conditions. The relationship between void fraction and covariance obtained using Ozakin and Hibiki [4-17] is depicted in Figure 4-1. As shown in the plot, the condition $C_{\alpha} \geq 1$ is satisfied for entire void fraction range, but at high void fraction value close to churn-annular flow transition region, covariance approaches to large value. Hence, it can be said that effect of void fraction distribution becomes noticeable at high void fraction region close to churn-annular flow transition region.

(4) Wall frictional pressure loss

The constitutive correlation based on Moody diagram[4-30] is used for calculating single-phase wall frictional pressure loss, whereas the constitutive correlation based on Martinelli-Nelson model[4-31] is adopted for calculating two-phase wall frictional pressure loss. It should be noted here that the pressure losses due to space grids is not considered in code calculations because reference void fraction is computed under hypothetical bundle without space grids.

4.3.1.2 Calculation condition

As can be seen from the derivations shown in the previous section, the interfacial drag model and calculated area-averaged void fraction value are highly related to one another. Hence, in this chapter, an effect of void distribution treatments (with and without covariance) on the area-averaged void fraction in rod bundle geometry is investigated.

Figure 4-2 shows the calculation domain used in the TRAC-BF1 analysis. As shown in the figure, CHAN component which utilizes constitutive relations for rod bundle geometry was used to simulate the 8 x 8 rod bundle two-phase flow. The overall length of CHAN component was set to 5 m and they were evenly divided into 50 cells. The upstream 2.4 m segment of CHAN component was set to uniform-heat generation cell, and two-phase flow condition was simulated with vapor generated via wall-heating. Note that the upstream component that acts as an inlet cell was set to an adiabatic condition. The downstream 25 cells with an overall length of 2.5 m were set to adiabatic condition, and steady-state two-phase flow condition without phase change was simulated.

The downstream of CHAN component was connected to BREAK component, which sets a pressure boundary value, and BWR's operation condition of 7 MPa was assigned. In addition, upstream of the CHAN component was connected to FILL component, which sets flow rate and temperature boundary value, and inlet subcooling was set to about 50 kJ/ kg. The thermal power output for the uniform heating section was calculated by solving for the corresponding void fraction value. By defining the void fraction value as $\left\langle \alpha_g \right\rangle_{target}$, exit flow quality at heating section $\left\langle x_f \right\rangle_{exit}$ can be calculated using drift-flux model [4-32] using following relation:

$$\left\langle \alpha_g \right\rangle_{target} = \frac{\left\langle x_f \right\rangle_{exit}}{C_0 \left[\left\langle x_f \right\rangle_{exit} + \left(1 - \left\langle x_f \right\rangle_{exit} \right) \frac{\rho_g}{\rho_f} \right] + \frac{\rho_g \left\langle \left\langle v_{gj} \right\rangle \right\rangle}{G}} \tag{4-28}$$

Here, *G* represents mass flux. If saturation condition was assumed at the exit of heating section, flow quality becomes identical to thermal equilibrium quality. Therefore, required heat generation value can be obtained from $\left\langle \alpha_g \right\rangle_{target}$ and inlet enthalpy value. As can be seen from Fig. 4-1, since covariance tends to be larger at high area-averaged void fraction region, $\left\langle \alpha_g \right\rangle_{target}$ was set to

high value and effect of void fraction covariance was investigated.

4.4 Results and Discussions

4.4.1 Steady-state Condition

For the steady-state analysis, void fraction calculation results for rod bundle geometry was obtained once by setting inlet and outlet boundary conditions and bundle power output value as constant. The target void fraction value was set to 0.8, and 9 inlet conditions with inlet flow rate ranging from 1.5 to 15 kg/s were considered. For the exit condition, the drift-flux model was utilized to obtain exit void fraction value equivalent to $\left\langle \alpha_g \right\rangle_{target}$. Inlet and outlet boundary conditions and bundle power output values are tabulated in Table 4-2.

Figure 4-3 shows the area-averaged void fraction calculated at the non-heated section with the inlet flow conditions of 5, 10, 15 kg/s (Run 7, 8, and 9). Calculation results of two cases, with uniform void fraction distribution (without covariance) and void fraction covariance (with covariance), are plotted in the figure.

As can be seen from the figure, area-averaged void fraction value tends to increase with vapor generation in the heated region. Due to the vapor generation and diffusion terms, the exit void fraction value at the heated region over estimated targeted void fraction value of 0.8, but it approaches to targeted void fraction value near the exit of rod bundle section. Such void fraction overestimation tends to be larger at downstream of heated region, but it quickly reaches to the targeted void fraction value in the case of low mass flow rate condition. On the other hand, at high mass flow rate condition, longer distance requires approaching targeted void fraction value because of large convection effect. In order to compare calculated results against targeted void fraction value, the relationship between area-averaged void fraction and mass flux was plotted in Fig. 4-4 for the downstream of heated-segment (cell #, 26, 35, 40, and 45). As can be seen from the plot, for both of void distribution treatments, calculation results obtained by the two-fluid model code is close to the targeted void fraction value obtained by the drift-flux model. Comparing the area-averaged void fraction values for both cases, a very small difference was confirmed (within 1%). For the case of void fraction covariance, void fraction overestimation at the exit of heated-region tends to be larger compared to the case with uniform void distribution. Summation of the source terms in right-hand-side of momentum equation matches for both cases, and interfacial drag term tends to be smaller for the void fraction covariance case, as shown in Eqs. (4-12) and (4-24). Hence, due to the weak binding of phase velocity for covariance case, additional distance is required to fully recover

the void fraction overestimation.

4.4.2. Transient Condition

As was shown in section 4.2, the case with void fraction covariance tends to weaken the momentum coupling between gas-liquid two phases. For non-accelerating steady-state condition, the results of two cases were found to be identical, as was shown in subsection 4.4.1. However, for a transient condition, a weakly coupled two-phase formulation may result in the difference in area-averaged void fraction calculation. For the transient condition, two-phase stability problem will be focused in the current study. It is well known that two-phase instability phenomenon arises when an external disturbance is added to the flow channel of constant hydraulic head [4-33]. As shown in Fig. 4-5, inlet boundary was changed to BREAK component, and both upstream and downstream pressure values were set to create a constant hydraulic-head condition. Under such boundary conditions, bundle power output of CHAN component was adjusted, and change in area-averaged void fraction and inlet flow rate with respect to time was assessed for the two cases. The upstream and downstream boundary conditions and initial conditions are tabulated in Table 4-3. Figure 4-6 depicts the rated power behavior with respect to time. Here, the differential pressure between upstream and downstream is adjusted to set 10 kg/s mass flow rate in an initial state. Also, since covariance term is highly dependent on void fraction value, several calculation cases with different initial void fraction condition were considered in this analysis. The ramp rate such as 1.4 times increase during the period from 1 to 3 seconds is determined to maximize the covariance effect on the void fraction in the code calculation.

Change in an area-averaged void fraction with respect to time at 45^{th} cell counting from the upstream of CHAN component is plotted in Fig. 4-7, and change in mass flow rate with respect to time at the 1^{st} cell from the upstream of CHAN component is plotted in Fig. 4-8, respectively. Initial void fraction and inlet flow rate were set to 0.7, and 10 kg/s, respectively and it is identical to the steady-state condition until the perturbation is added to the system. As shown in Fig. 4-6, bundle power perturbation is added after 1 sec, and void fraction and two-phase pressure drop within rod bundle tend to increase. This results in a decrease in inlet flow rate at constant differential pressure condition. Following the decrease in power output after 2 secs, void fraction tends to decrease. Similarly, inlet flow rate tends to increase, but it overshoots the initial condition, and oscillatory behavior is initiated. As shown in the figures, similar behaviors were observed for both cases with and without covariance, but the oscillation decays much faster for the uniform void distribution case. The drag coefficient for the case without the covariance is smaller than that for

the case with the covariance. The interfacial drag force stabilizes the oscillation. Therefore the smaller drag coefficient for the case without the covariance results in the larger amplitude and the longer period of the oscillation. In order to evaluate such oscillatory behaviors, damping ratio (DR) is now introduced for the analysis.

$$DR = \frac{X_{+4} - X_{steady}}{X_{+3} - X_{steady}} \tag{4-29}$$

Here, X is the parameter of interest, such as void fraction and/or inlet flow rate, and subscript +4, +3, and *steady* are the fourth positive peak, third positive peak, and steady-state condition, respectively. The time of positive second peaks, about 3.5 seconds shown in Figs. 4-7 and 4-8, are close to the time of the end of power perturbation, 3 seconds. Therefore, this external initial disturbance may affect the amplitude of the positive second peaks. Consequently, third and fourth peaks are selected for the representative peak values since these peaks are not affected by the initial disturbance.

Figure 4-9 shows the calculation results from the conditions shown in Table 4-3. For each condition, DR was obtained at given void fraction and inlet flow rate, and it was compared for both cases with and without covariance. The dumping behavior is affected by the magnitude of interfacial drag term expressed by Eq.(4-12). The drag term is inversely proportional to a relative velocity covariance, C'_{α} , whose dependency on void fraction is shown in Fig. 4-2. As can be seen from Fig. 4-9, DR value is underestimated at high void fraction region for uniform void distribution case, namely without covariance case. For the initial void fraction of 0.7, DR of without covariance case is underestimated around 8% compared to DR with covariance case. The ratio of DR almost linearly decreases as the decrease of the area-averaged initial void fraction. This tendency is in accordance with the trend of relative velocity covariance. The underestimation of DR for the case without covariance is thus expected to be less than about 3 % compared to DR with covariance case at the void fraction lower than 0.4. For the uniform void distribution case (without covariance case), underestimation of DR is caused by the excessive drag coefficient value which results in increased velocity coupling. For the case with covariance, the drag coefficient under more rigorous formulation is utilized as was shown in the previous section. Hence, for the transient two-phase flow analysis, the methodology suggested in this chapter is recommended.

4.5 Conclusions

In this chapter, the effect of void fraction covariance for momentum equation in the one-dimensional two-fluid model was discussed. For the system analysis code that utilizes one-dimensional two-fluid model, such as TRACE, RELAP5, and TRAC-BF1, interfacial drag term in momentum equation is given by the drift-flux parameters. Purpose of such approach is to include the void and flux distribution effect on the area-averaged one-dimensional model. However, uniform void fraction distribution is assumed by setting covariance as a unity for the source terms in momentum equation, which is not a consistent treatment. For the complete and rigorous formulation to assess void fraction distribution, the constitutive relation for void fraction covariance is essential. The covariance is affected by the phase distribution and flow channel geometry. Ozaki and Hibiki [4-17] developed covariance model applicable for BWR's rod bundle geometry. By embedding the model into the two-fluid model, a rigorous and complete set of momentum equation and constitutive relations with void distribution effect can be obtained. In this chapter, the difference in two cases, void distribution with and without covariance, was assessed using numerical simulation. For the steady-state analysis, the difference in these two cases can be summarized as follows:

- Vapor generation is almost non-existence at downstream of heated region, and the void fraction values for two cases match with the calculated results using drift-flux model. Hence, for under non-accelerating steady-state condition, both cases show same calculation results.
- At heated region, slightly larger void fraction value was obtained for the case with covariance. At the downstream of heated region, overestimation of void fraction value from the drift-flux model was seen for the case with covariance. This arises by the smaller drag coefficient for the case with covariance, which results in smaller momentum coupling between two phases compared to the uniform void distribution case.

Next, for the transient condition, external perturbation was added to evaluate the system stability, by setting the constant pressure values at inlet and outlet, and oscillatory behaviors for two cases were analyzed. Following results, which highlight the difference in two cases, were obtained.

- For the oscillatory behavior arose by the external perturbation, damping ratio is larger for the case with covariance compared to the uniform void distribution assumption. A decrease in momentum coupling between two phases is related to the system stability.
- Underestimation of the damping ratio for uniform void distribution case tends to increase with respect to void fraction value. At the initial void fraction of 0.7, damping ratio was

underestimated at around 8 %.

In this chapter, a new set of momentum equation and constitutive relations on interfacial drag term for the one-dimensional two-fluid model in rod bundle geometry was proposed. Traditional approach ignores the covariance effect, by treating it as a unity, but it still utilizes drift-flux parameters which consider distributions of void fraction and volumetric flux. Such approach for the void distribution treatment is highly inconsistent. The newly proposed equation set resolves such problem, and effect of void fraction distribution on momentum equation is rigorously treated. Hence, utilization of the present set of an equation is recommended for the system analysis code that utilizes one-dimensional two-fluid model.

Table 4-1 Constitutive equations implemented in TRAC-BF1 code.

Item	Model
Distribution Parameter, C_0	$C_0 = 1.1 - 0.1\sqrt{\frac{\rho_g}{\rho_f}}$, for bulk boiling condition $C_0 = \left(1.1 - 0.1\sqrt{\frac{\rho_g}{\rho_f}}\right)\left(1 - e^{-12.1\langle\alpha_g\rangle^{0.701}}\right)$, for subcooled boiling condition
Drift Velocity, $\left\langle\left\langle v_{gj}\right\rangle\right\rangle$	$\left\langle\left\langle V_{gj}^{+}\right\rangle\right\rangle = \left\langle\left\langle V_{gj,B}^{+}\right\rangle\right\rangle \exp\left(-1.39\left\langle j_g^{+}\right\rangle\right) + \left\langle\left\langle V_{gj,P}^{+}\right\rangle\right\rangle\left\{1 - \exp\left(-1.39\left\langle j_g^{+}\right\rangle\right)\right\}$ (Hibiki and Ishii, 2003) $\left\langle\left\langle V_{gj,B}^{+}\right\rangle\right\rangle = \sqrt{2}\left(1 - \langle\alpha\rangle\right)^{1.75}$ (Ishii, 1977) when $N_{\mu f} \le 2.25\times10^{-3}$ $\left\langle\left\langle V_{gj,P}^{+}\right\rangle\right\rangle = 0.0019\left(D_H^{+}\right)^{0.809}\left(\frac{\rho_g}{\rho_f}\right)^{-0.157} N_{\mu f}^{-0.562}$ for $D_H^{+} \le 30$ $\left\langle\left\langle V_{gj,P}^{+}\right\rangle\right\rangle = 0.030\left(\frac{\rho_g}{\rho_f}\right)^{-0.157} N_{\mu f}^{-0.562}$ for $D_H^{+} \ge 30$ when $N_{\mu f} \ge 2.25\times10^{-3}$ $\left\langle\left\langle V_{gj,P}^{+}\right\rangle\right\rangle = 0.92\left(\frac{\rho_g}{\rho_f}\right)^{-0.157}$ for $D_H^{+} \ge 30$ (Kataoka and Ishii, 1987) $\left\langle\left\langle V_{gj}^{+}\right\rangle\right\rangle = \frac{\left\langle\left\langle v_{gj}\right\rangle\right\rangle}{\left(\frac{\sigma g\Delta\rho}{\rho_f^2}\right)^{1/4}}$, $\left\langle j_g^{+}\right\rangle = \frac{\left\langle j_g\right\rangle}{\left(\frac{\sigma g\Delta\rho}{\rho_f^2}\right)^{1/4}}$, $D_H^{+} = \frac{D_H}{\sqrt{\frac{\sigma}{g\Delta\rho}}}$, $N_{\mu f} = \frac{\mu_f}{\left(\rho_f\sigma\sqrt{\frac{\sigma}{g\Delta\rho}}\right)^{1/2}}$
Void Fraction Covariance, C_α	$C_{\alpha,BB} = 1 + \left\{9.38\left(\left\langle\alpha_g\right\rangle - 0.5\right)^4 + 0.414\right\}\left\{1 - \left(\frac{\rho_g}{\rho_f}\right)^2\right\}\left\langle\alpha_f\right\rangle$ $C_{\alpha,SB} = \frac{0.190}{\left\langle\alpha_g\right\rangle^{0.855}}$ $C_\alpha\left(\left\langle\alpha_g\right\rangle\right) = \max\left(C_{\alpha,SB}, C_{\alpha,BB}\right)$ for $\left\langle\alpha_{crit}\right\rangle > \left\langle\alpha_g\right\rangle$ $C_\alpha\left(\left\langle\alpha_g\right\rangle\right) = \frac{1 - C_\alpha\left(\left\langle\alpha_{crit}\right\rangle\right)}{1 - \left\langle\alpha_{crit}\right\rangle}\left(\left\langle\alpha_g\right\rangle - 1\right) + 1$ for $\left\langle\alpha_{crit}\right\rangle \le \left\langle\alpha_g\right\rangle$ $\left\langle\alpha_{crit}\right\rangle = 0.84$

Table 4-2 Boundary conditions of inlet flow rate, outlet pressure and bundle power conditions for steady-state simulations.

Run No.	Inlet Mass Flow Rate [kg/s]	Mass Flux in bundle [kg/m^{2}s]	Outlet Pressure [MPa]	Bundle Power [MW]
1	1.5	154	7.0	1.5
2	2.0	205	7.0	1.7
3	2.5	256	7.0	1.9
4	3.0	308	7.0	2.1
5	3.5	359	7.0	2.3
6	4.0	410	7.0	2.5
7	5.0	513	7.0	2.9
8	10.0	1025	7.0	4.9
9	15.0	1538	7.0	6.9

Table 4-3 Pressure boundary conditions and initial power and void fraction conditions for transient simulations.

Run No.	Inlet Pressure [MPa]	Outlet Pressure [MPa]	Initial Bundle Power [MW]	Initial Targeted Outlet Void Fraction [-]
10	7.04	7.0	1.15	0.4
11	7.04	7.0	1.50	0.5
12	7.04	7.0	2.03	0.6
13	7.05	7.0	2.95	0.7

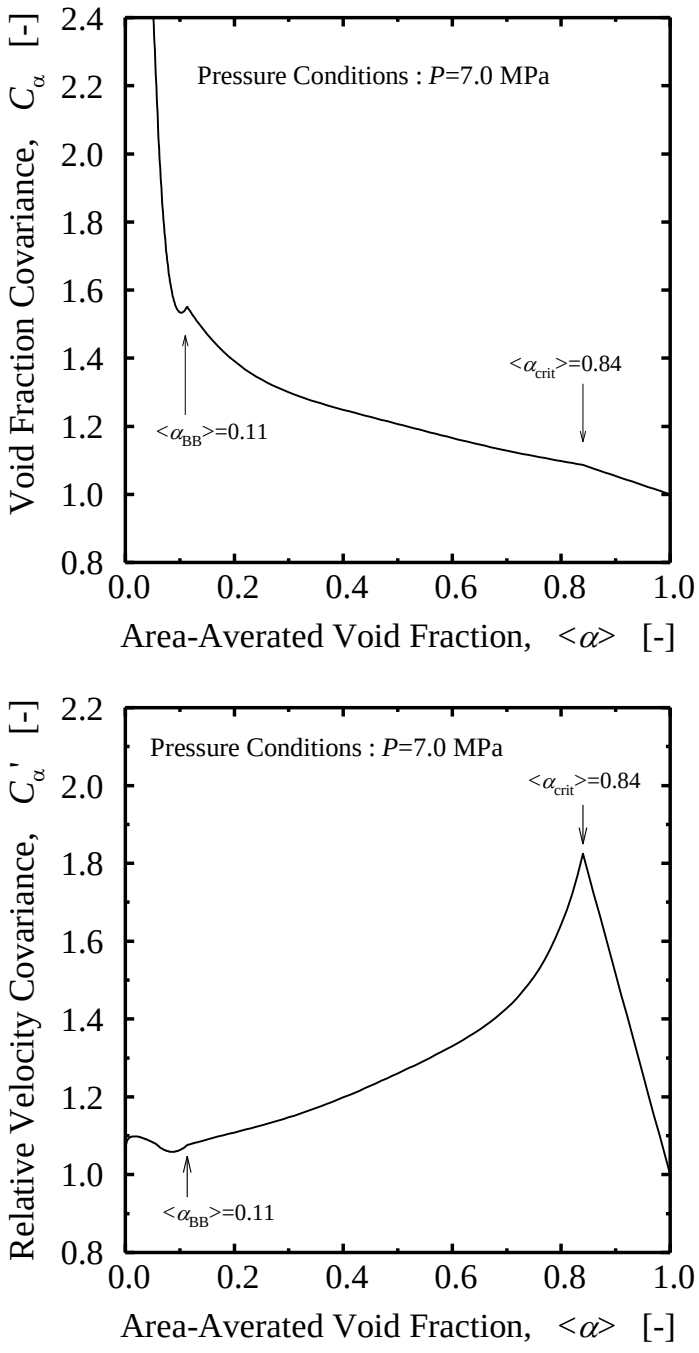

Figure 4-1 Void fraction covariance and relative velocity covariance calculated by Ozaki and Hibiki [4-17] model at a pressure of 7 MPa.

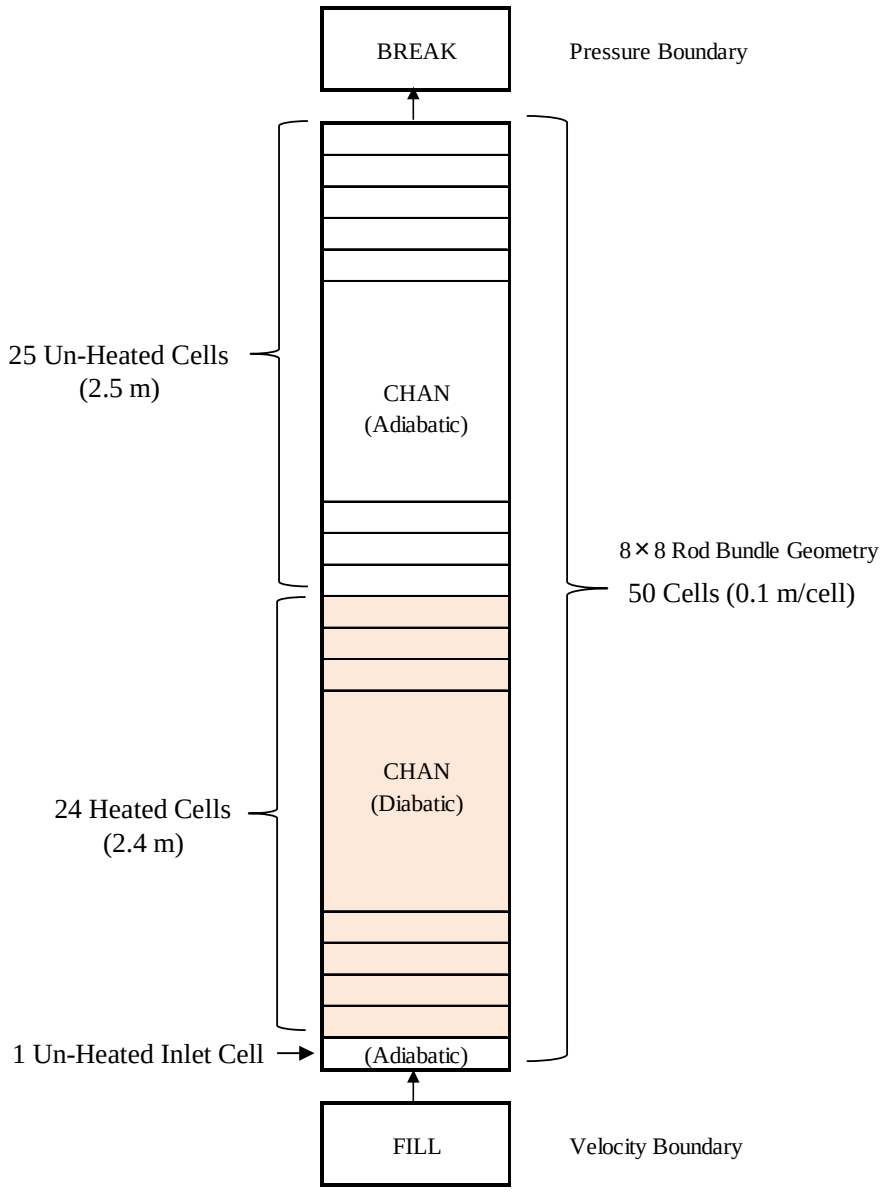

Figure 4-2 Calculation model and nodalization of TRAC-BF1 for rod bundle under two-phase flow (Steady state simulation case).

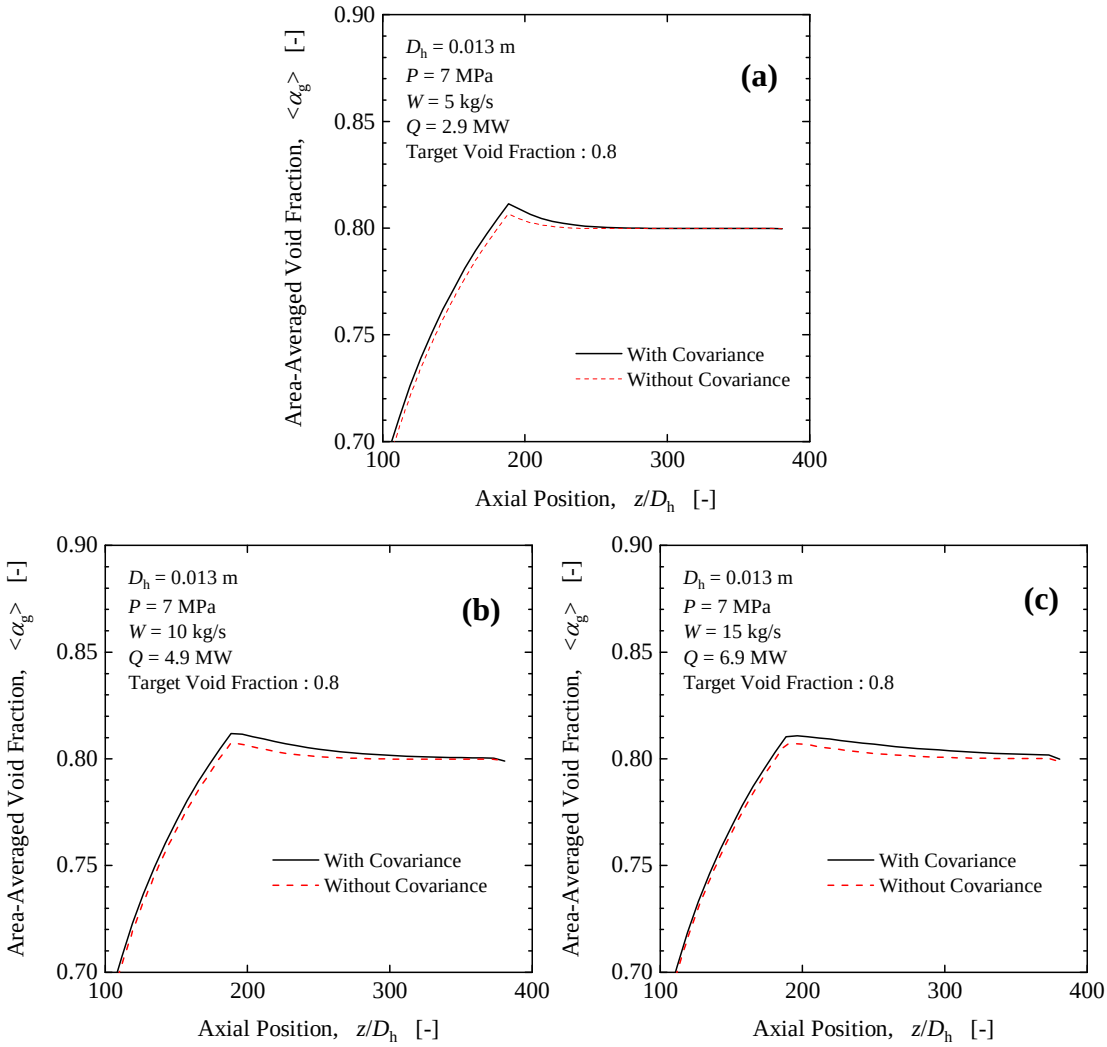

Figure 4-3 Comparisons of axial void fraction profiles for steady-state simulation cases at targeted void fraction of 0.8 and mass flow rate of (a) 5 kg/s, (b) 10 kg/s and (c) 15 kg/s.

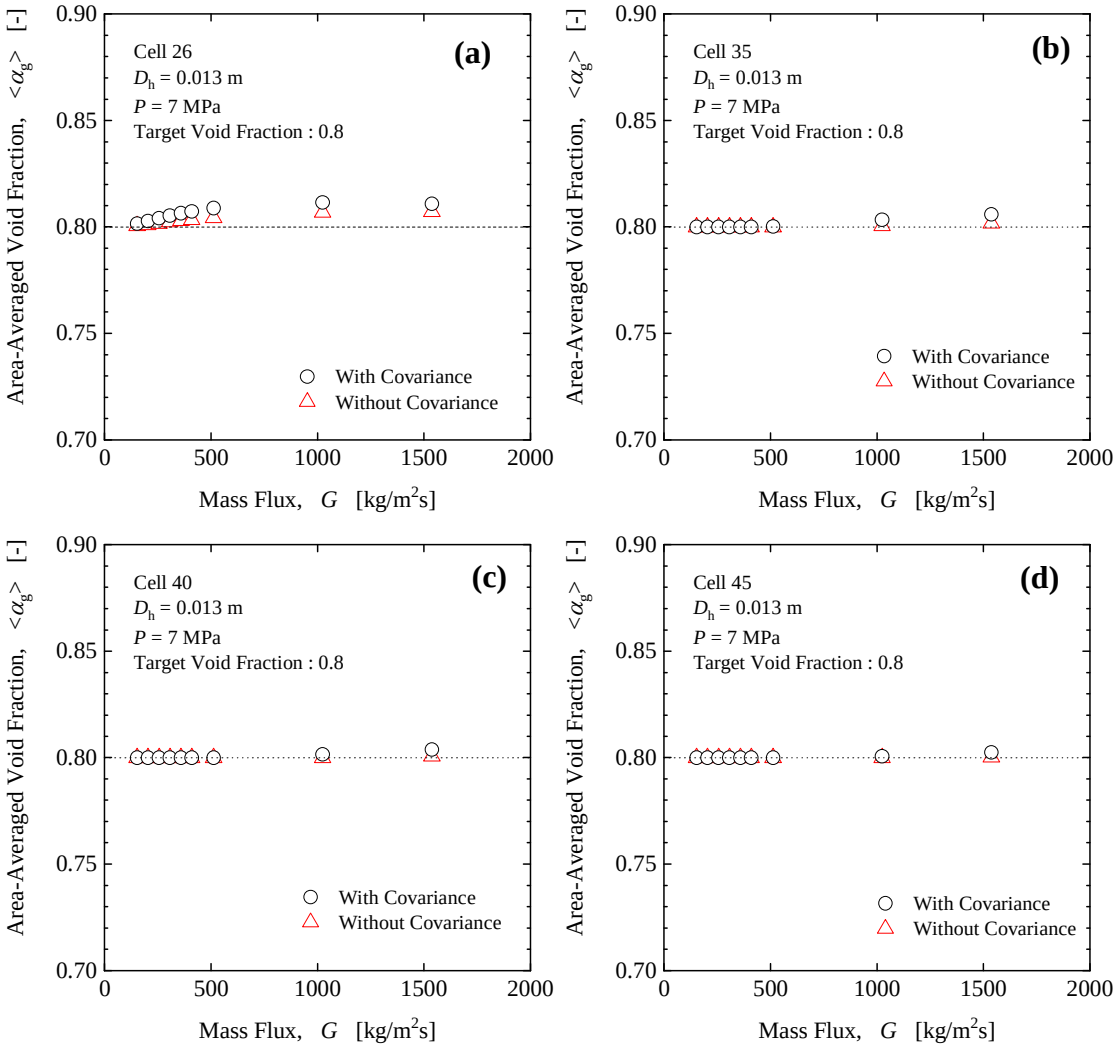

Figure 4-4 Comparisons of the void fraction at (a) 26th cell, (b) 35th cell, (c) 40th cell and (d) 45 th cell from the inlet of CHAN component with the conditions of mass flux.

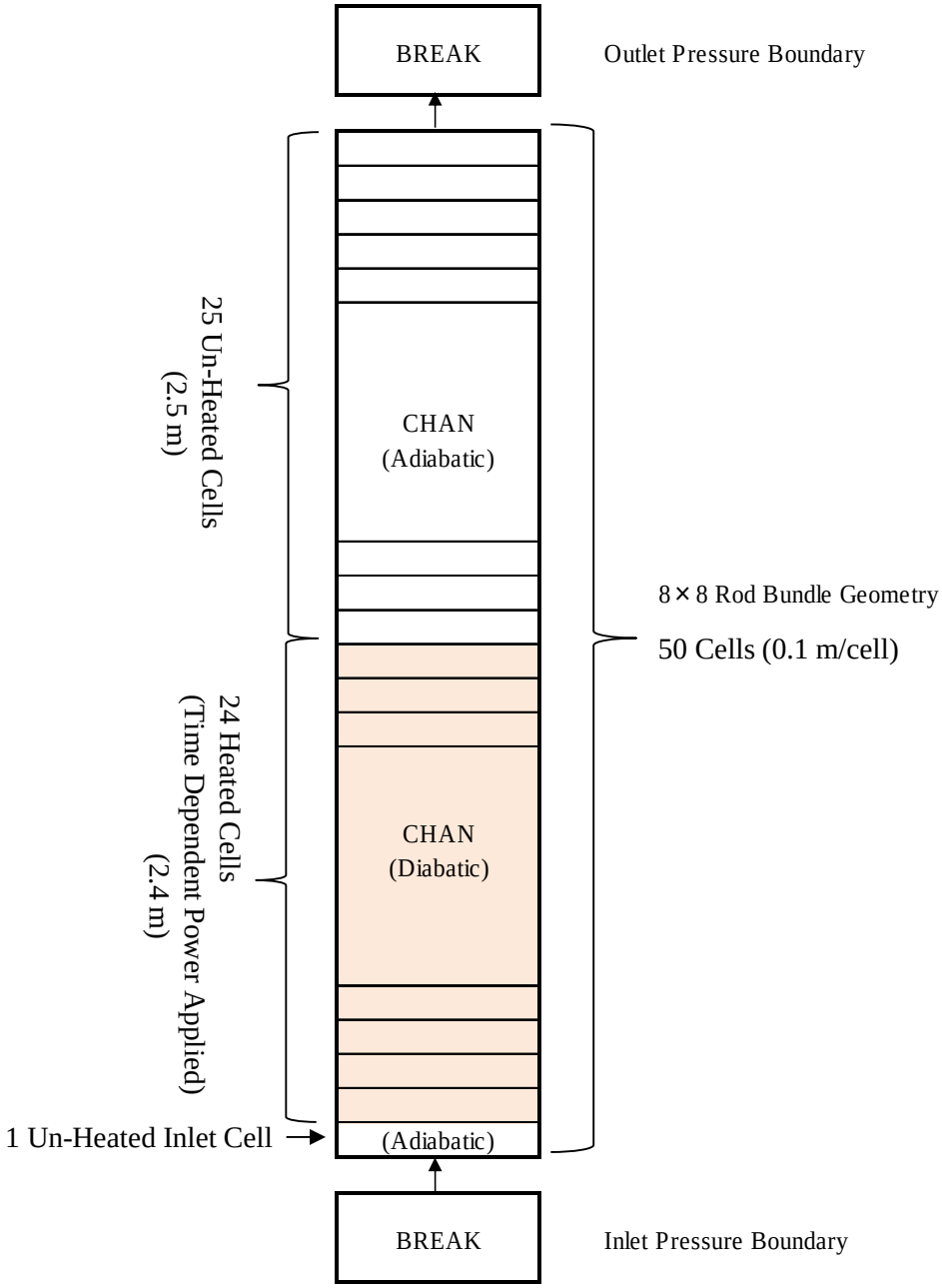

Figure 4-5 Calculation model and nodalization of TRAC-BF1 for rod bundle under two-phase flow (transient simulation case).

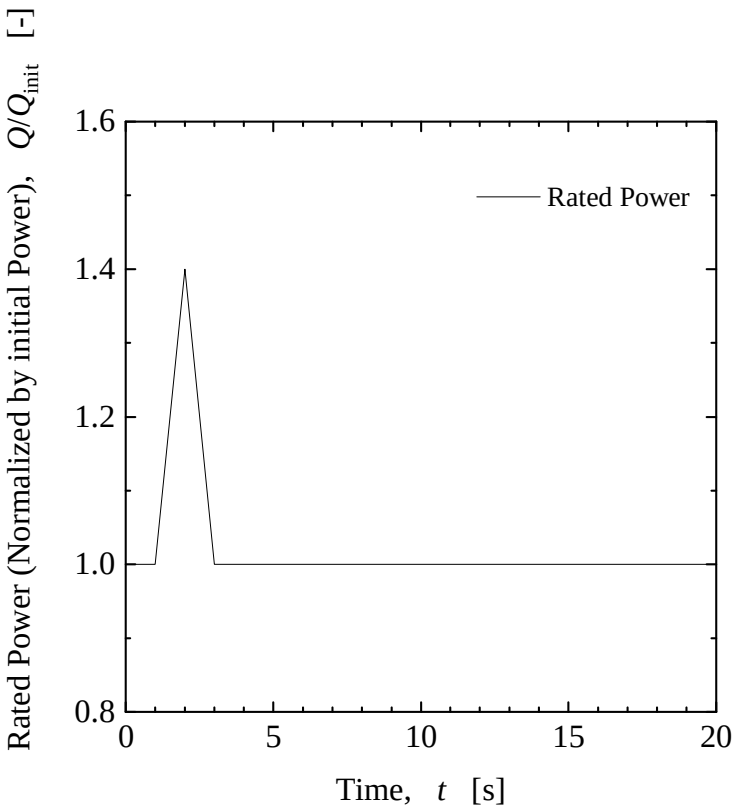

Figure 4-6 Bundle power perturbation applied for transient simulation case.

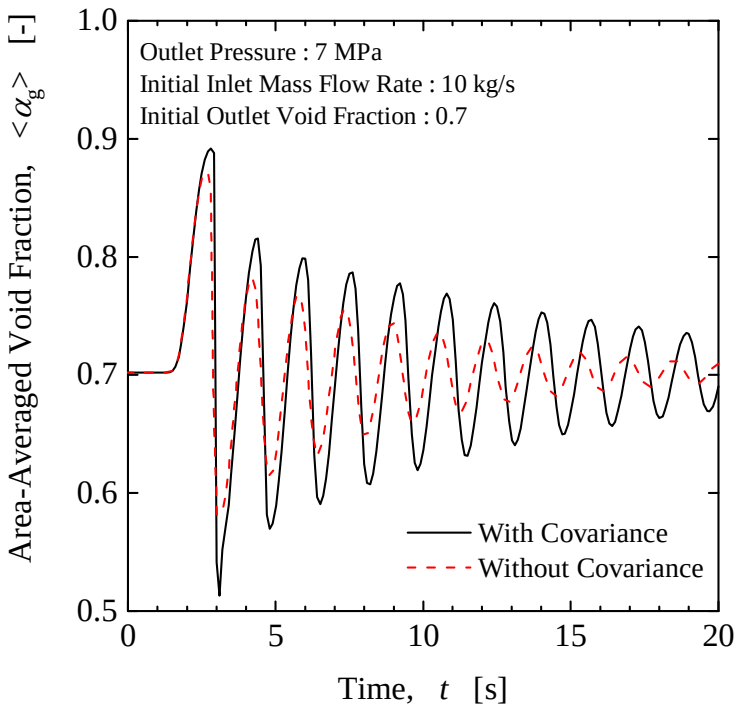

Figure 4-7 Comparison of area-averaged void fraction trend at the 45th cell from the inlet of CHAN component.

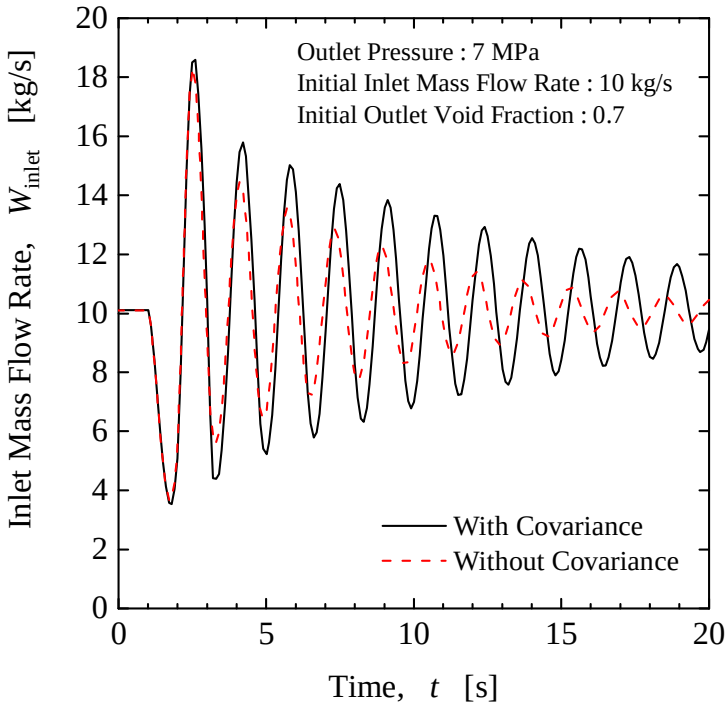

Figure 4-8 Comparison of inlet flow rate of CHAN component.

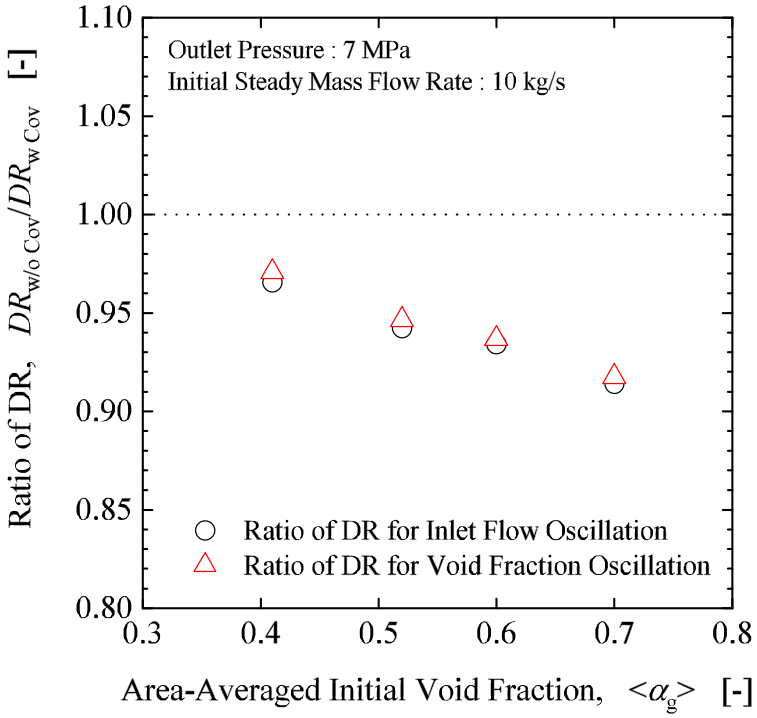

Figure 4-9 Comparisons of decay ratio for inlet flow rate and void fraction oscillation.

References

[4-1] Boyack B, Duffey R, Griffith P ,et al. Quantifying reactor safety margins: Application of code scaling, applicability, and uncertainty evaluation methodology to a large-break, loss-of-coolant accident. USA: US NRC; 1989. (NUREG/CR-5249/EGG-2552).

[4-2] American Society of Mechanical Engineers (ASME). Standard for verification and validation in computational fluid dynamics and heat transfer. New York: ASME; 2009. V&V 20-2009.

[4-3] Atomic Energy Society of Japan (AESJ). Guideline for credibility assessment of nuclear simulations: 2015. Tokyo: AESJ, 2016. AESJ-SC-A008:2015. Japanese.

[4-4] US Nuclear Regulation Committee (US NRC). Transient and accident analysis methods. Washington DC: US NRC, 2005. US NRC Regulatory Guide 1.203.

[4-5] Atomic Energy Society of Japan (AESJ). Standard method for safety evaluation using best estimate code based on uncertainty and scaling analyses with statistical approach: 2008. Tokyo: AESJ, 2009. AESJ-SC-S001:2008. Japanese.

[4-6] US Nuclear Regulation Committee (US NRC). TRACE/V5.0 Theory manual; Field equations, solutions methods, and physical models. Washington DC: US NRC; 2008.

[4-7] Information System Laboratories (ISL). RELAP5/MOD3.3 Code manual volume IV: Models and correlations. Washington DC: US NRC; 2001. (NUREG/CR-5535/Rev 1-Vol.IV).

[4-8] Borkowski JA., Wade NL. TRAC-BF1/MOD1 Models and correlations. Washington DC: US NRC; 1992. (NUREG/CR-4391/EGG-2680R4).

[4-9] Andersen JGM, Chu KH. BWR refill-reflood program constitutive correlations for shear and heat transfer for the BWR version of TRAC. Washington DC: US NRC; 1983. (NURG/CR-2134/GEAP-24940).

[4-10] Ishii M. One-dimensional drift-flux model and constitutive relations for relative motion between phases in various two-phase flow regimes. Argonne (IL): ANL; 1977. (ANL-77-47).

[4-11] Ozaki T, Suzuki R, Mashiko H, Hibiki T. Development of drift-flux model based on 8×8 BWR rod bundle geometry experiments under prototypic temperature and pressure conditions. Journal of Nuclear Science and Technology 2013;50:563-580.

[4-12] Ozaki T, Hibiki T. Drift-flux model for rod bundle geometry. Progress in Nuclear Energy 2015;83:229-247.

[4-13] Brooks CS, Ozar B, Hibiki T, et al. Two-group drift-flux model in boiling flow. International Journal of Heat and Mass Transfer 2012;55:6121-6129.

[4-14] Brooks CS, Liu Y, Hibiki T, et al. Effect of void fraction covariance on relative velocity in gas-dispersed two-phase flow. Progress in Nuclear Energy 2014;70:209-220.

[4-15] Ishii M, Mishima K. Two-fluid model and hydrodynamic constitutive relations. Nuclear Engineering and Design 1984;82:107-126.

[4-16] Hibiki T, Ozaki T. Modeling of distribution parameter, void fraction covariance and relative velocity covariance for upward steam-water boiling flow in vertical pipe. International Journal of Heat and Mass Transfer 2017;112:620-629.

[4-17] Ozaki T, Hibiki T. Modeling of distribution parameter, void fraction covariance and relative velocity covariance for upward steam-water boiling flow in vertical rod bundle. Journal of Nuclear Science and Technology (in print).

[4-18] Ishii M, Hibiki T. Thermo-fluid dynamics of two-phase flow. 2nd ed. New York: Springer; 2011.

[4-19] Tomiyama A, Kataoka, I, Fukuda, T, et al. Drag Coefficients of Bubbles : 2nd Report, Drag Coefficient for a Swarm of Bubbles and its Applicability to Transient Flow. Transactions of the Japan Society of Mechanical Engineers Series B 2008;61:2810-2817. Japanese.

[4-20] Garnier J, Manon E, Cubizolles G. Local measurements on flow boiling of refrigerant 12 in a vertical tube. Multiphase Science and Technology 2001;13:1-111.

[4-21] Roy R, Kang S, Zarate J, et al. Turbulent subcooled boiling flow in – Experiments and simulations. Journal of Heat and Mass Transfer 2002;124:73-93.

[4-22] Situ R, Hibiki T, Sun X, et al. Flow structure of subcooled boiling flow in an internally heated annulus. International Journal of Heat and Mass Transfer 2004;47:5351-5364.

[4-23] Lee T, Situ R, Hibiki T, et al. Axial developments of interfacial area and void concentration profiles in subcooled boiling flow of water. International Journal of Heat and Mass Transfer 2009;52:473-487.

[4-24] Yun B, Bae B, Euh D, et al. Characteristics of the local bubble parameters of a subcooled boiling flow in an annulus. Nuclear Engineering and Design 2010;240:2295-2303.

[4-25] Morooka S, Inoue A, Oishi M, et al. In-bundle void measurement of BWR fuel assembly by X-ray CT scanner. Proceedings of ICONE-1; 1991 November 4-7; Tokyo; Paper No.38.

[4-26] Hibiki T, Ishii M. One dimensional drift-flux model for two-phase flow in a large diameter pipe. International Journal of Heat and Mass Transfer 2003;46:1773-1790.

[4-27] Kataoka I, Ishii M. Drift flux model for large diameter pipe and new correlation for pool void fraction. International Journal of Heat and Mass Transfer 1987;30:1927-1939.

[4-28] Nuclear Power Engineering Test Center. Report on proving test on reliability for BWR fuel bundles (void fraction tests in BWR fuel bundles – support document). Tokyo: NUPEC; 1992. Japanese.

[4-29] Nuclear Power Engineering Corporation (NUPEC). Report on proving test on reliability for BWR fuel bundles (Supplement) (Void fraction tests for high burnup fuel bundle – Overall evaluation). Tokyo: NUPEC; 1993. Japanese.

[4-30] Moody LF. An Approximate Formula for Pipe Friction Factors. Trans ASME 1947;69:1005-1011.

[4-31] Martinelli RC, Nelson DB. Prediction of pressure drop during forced circulation boiling of water. Trans. ASME 1948;70:695-702.

[4-32] Zuber N, Findlay JA. Average volumetric concentration in two-phase flow systems. Journal of Heat Transfer 1965;87:453-468.

[4-33] Ruspini LC, Marcel CP, Clausse A. Two-phase flow instabilities: A review. International Journal of Heat and Mass Transfer 2014;71:521-548.

5. Code Performance with Improved Two-Group Interfacial Area Concentration for One-Dimensional Forced Convective Two-Phase Flow Simulation

5.1 Introduction

The implementation of the interfacial area transport equation (IATE) into a one-dimensional nuclear thermal-hydraulic system analysis code has been recommended to simulate dynamic nature of two-phase interfacial structure without flow regime transition criteria developed for steady-state, fully developed flow and to avoid compound errors in predicting an interfacial area concentration due to errors in flow regime identification method and a flow-regime-dependent correlation. Talley et al. [5-1] implemented one-group (or small distorted bubble group) interfacial area transport equation in a pilot code of TRACE (TRACE 4.291b) and compared TRACE-T (TRACE with the interfacial area transport equation) with TRACE-NT (TRACE without the interfacial area transport equation). TRACE-T calculated an interfacial drag force using a drag coefficient, whereas TRACE-NT calculated an interfacial drag force using a drift velocity (Andersen approach [5-2]). The comparison between TRACE-T and TRACE indicates no significant difference in predicted local pressure and void fraction between the codes. However, the comparison also shows that bubble velocity or gas velocity predicted by TRACE-NT is higher than that by TRACE-T. Talley et al. [5-1] explained that this difference was due to different closure relations to calculate the interfacial drag coefficient between the codes. It should be noted here that the gas velocity is also expressed by the ratio of superficial gas velocity to void fraction. The superficial gas velocity should be the same between the codes due to mass conservation and the calculated void fractions were the same between the codes. This indicates that the calculated gas velocity should be the same between the two codes. It is unclear why the difference in the calculated gas velocity between the codes exists. The bubble Sauter mean diameter for Run 2-7 is experimentally measured to be 2.4 mm [5-1] and the bubbles are considered in a distorted particle regime. However, Talley et al. [5-1] utilized the drag coefficient in a viscous regime and thus the drag coefficient used in TRACE-T is considered to be underestimated. Tally et al. [5-1] also used a correlation of the distribution parameter for a round pipe proposed by Ishii [5-3] and a correlation of drift velocity for a churn flow regime. Hibiki and Ishii [5-4] identified that the distribution parameter in a bubbly flow is lower than that calculated by Ishii's correlation due to wall peaking phenomena in a bubbly flow. The estimation of the distribution parameter significantly affects the predicted area-averaged relative velocity resulting in inaccurate code predictions. Tally et al. [5-1]

claimed the superiority of the interfacial area transport equation over a correlation based on the comparison between the code calculation and co-current downward bubbly flow data taken at the superficial gas velocity of 3.11 m/s. However, this argument may not be appropriate in the capacity of one-group interfacial area transport equation because the data contains group-2 (or large cap bubble group) bubbles at the test section inlet [5-5]. In addition, the interfacial area transport equation may not predict an accurate interfacial area concentration unless an initial value of the interfacial area concentration is given. The research results by Tally et al. [5-1] should be re-assessed carefully.

Extensive efforts have been made to develop a reliable interfacial area transport equation [5-6] but several shortcomings are also pointed out [5-7, 5-8] such that (1) the interfacial area transport equation may not predict an accurate interfacial area value unless the initial value is accurately given, (2) the interfacial area transport equation includes too many adjustable constants and each interfacial area transport mechanisms are hardly validated, (3) constants for interfacial area sink and source terms are geometrically dependent, (4) the scalability of the interfacial area transport equation to high-pressure system has not been validated due to the lack of experimental data, (5) the applicability of the interfacial area transport equation to transient phenomena has not been validated due to the lack of experimental data. In addition to these, the number of field equations in a code increases from six to ten if two-group interfacial area transport equation is adopted. Due to the above challenges, a simplified approach to predict an accurate interfacial area concentration may be necessary. Recently, reliable, robust and simple correlations of the interfacial area concentration have been developed based on the two-group approach [5-9, 5-10, 5-11]. The two-group gas momentum equations can be also simplified to a single gas momentum equation with the aid of Andersen approach [5-2]. If the relative velocities for group-1 and group-2 bubbles are similar, the single gas momentum equation can be further simplified. The simplified gas momentum equation may not consider the effect of the difference in relative velocities for group-1 and group-2 bubbles on the interfacial drag force but can simulate the dynamic change of the drag coefficient due to the presence of group-2 bubbles.

In view of the above, the correlations of the interfacial area concentration are implemented in TRAC-BF1 code, and the effect of the predicted interfacial area concentration on void fraction is discussed. This study performs four code calculations such as (i) comparison with existing separate effect test data, (ii) sensitivity analysis by changing the interfacial area concentration value artificially, (iii) calculation at the condition where a flow regime transition occurs and (iv) transient calculation for an actual nuclear power plant. The role of the interfacial area concentration is

revealed by the four code calculation results.

5.2 One-dimensional interfacial drag model with drag coefficient and interfacial area concentration

Various types of bubbles are present in dispersed two-phase flow system such as spherical cap bubble, cap bubble, Taylor bubble, bubbles in churn flow, and so on. The interfacial drag force term, which represents the interfacial momentum transfer at the gas-liquid interface, is governed by the product of drag coefficient and interfacial area concentration that are dependent on bubble types. Hence, in order to appropriately evaluate dispersed two-phase flow dynamics, utilization of the constitutive equations for individual bubble groups is essential. When modeling the interfacial drag force term, bubbles can be grouped depending on the drag coefficient value. As was proposed by Ishii and Hibiki [5-6], spherical bubbles and distorted bubbles are classified as Group-1, while slug, cap, and churn-turbulent bubbles are classified as Group-2.

One-dimensional momentum equation for *k*-th phase (*k* = gas or liquid) in two-phase flow can be expressed as follows [5-6]:

$$\begin{aligned}\left\langle \alpha_k \right\rangle \rho_k \frac{\partial \left\langle\left\langle v_k \right\rangle\right\rangle}{\partial t} + \left\langle \alpha_k \right\rangle \rho_k \left\langle\left\langle v_k \right\rangle\right\rangle \frac{\partial \left\langle\left\langle v_k \right\rangle\right\rangle}{\partial z} = \\ -\left\langle \alpha_k \right\rangle \frac{\partial p}{\partial z} + \left\langle \alpha_k \right\rangle \left\langle M_{\tau k} \right\rangle - \left\langle \alpha_k \right\rangle \rho_k g + \left\langle M_{ik} \right\rangle - \frac{4\alpha_{kw}\tau_{kw}}{D_H}\end{aligned} \tag{5-1}$$

Here, subscript *k* denotes gas or liquid phase, and α_k, ρ_k, v_k, t, z, p, $M_{\tau k}$, g, M_{ik}, τ_{kw}, α_{kw} and D_H, respectively, are the *k*-th phase volumetric fraction, density, velocity, time, axial position, pressure, viscous and turbulent shear stress, gravitational acceleration, interfacial drag, wall shear stress, volumetric fraction near the wall, and hydraulic diameter. The operators, $\left\langle\ \right\rangle$ and $\left\langle\left\langle\ \right\rangle\right\rangle$ represent area-averaged value, and void-weighted area-averaged value, respectively.

When considering two-group bubbles, interfacial drag for each group can be expressed as follows:

$$\left\langle M_{ig1} \right\rangle = -\frac{1}{8}\left\langle a_{i1} \right\rangle C_{D1}\rho_f \psi_1 \left\langle v_{r1} \right\rangle \left|\left\langle v_{r1} \right\rangle\right| \quad \text{and} \quad \left\langle M_{ig2} \right\rangle = -\frac{1}{8}\left\langle a_{i2} \right\rangle C_{D2}\rho_f \psi_2 \left\langle v_{r2} \right\rangle \left|\left\langle v_{r2} \right\rangle\right| \tag{5-2}$$

Here, C_D, a_i , ψ and v_r represent drag coefficient, interfacial area concentration, shape factor, and relative velocity, respectively. The subscripts 1 and 2 represent Group-1 and Group-2 bubbles, respectively. The generalized interfacial drag force term shown on the right-hand-side of Eq. (5-1) can be expressed as the summation of Group-1 and Group-2 interfacial drag [5-6].

$$\left\langle M_{ig} \right\rangle = -\left\langle M_{if} \right\rangle = \left\langle M_{ig1} \right\rangle + \left\langle M_{ig2} \right\rangle \tag{5-3}$$

Now, suppose that drag coefficient for Group-1 and Group-2 are represented by the variables C_{i1} and C_{i2} as shown in Eq. (5-4). In order to solve for the relative velocity fields of Group-1 and Group-2 bubbles, it is necessary to split the momentum equation of gas-phase into two groups. To reduce the complication, Eq. (5-3) can be expressed as shown in Eq. (5-5) using Ishii and Mishima [5-12]'s one-dimensional relative velocity expression.

$$C_{i1} \equiv \frac{1}{8} C_{D1} \left\langle a_{i1} \right\rangle \rho_f \psi_1 \quad \text{and} \quad C_{i2} \equiv \frac{1}{8} C_{D2} \left\langle a_{i2} \right\rangle \rho_f \psi_2 \tag{5-4}$$

$$\begin{aligned} \left\langle M_{ig} \right\rangle = & -\left(C_{i1} \zeta_1^2 + C_{i2} \zeta_2^2 \right) \\ & \times \left(\frac{1 - C_0 \left\langle \alpha \right\rangle}{1 - \left\langle \alpha \right\rangle} \left\langle \left\langle v_g \right\rangle \right\rangle - C_0 \left\langle \left\langle v_f \right\rangle \right\rangle \right) \left| \frac{1 - C_0 \left\langle \alpha \right\rangle}{1 - \left\langle \alpha \right\rangle} \left\langle \left\langle v_g \right\rangle \right\rangle - C_0 \left\langle \left\langle v_f \right\rangle \right\rangle \right| \end{aligned} \tag{5-5}$$

Here,

$$\zeta_1 \equiv \frac{\left\langle v_{r1} \right\rangle}{\left\langle v_r \right\rangle} \simeq \frac{\left\langle \left\langle v_{gj1} \right\rangle \right\rangle}{\left(1 - \left\langle \alpha_1 \right\rangle \right) \left\langle v_r \right\rangle} \quad \text{and} \quad \zeta_2 \equiv \frac{\left\langle v_{r2} \right\rangle}{\left\langle v_r \right\rangle} \simeq \frac{\left\langle \left\langle v_{gj2} \right\rangle \right\rangle}{\left(1 - \left\langle \alpha_2 \right\rangle \right) \left\langle v_r \right\rangle} \quad . \tag{5-6}$$

C_0 and v_{gj} represent distribution parameter and drift velocity, respectively. Drift velocities of Group-1 and Group-2 bubbles are expressed under the constitutive equations shown in Eqs. (5-7) and (5-8) [5-3, 5-13].

$$\left\langle \left\langle v_{gj1} \right\rangle \right\rangle = \sqrt{2} \left(\frac{\sigma g \Delta \rho}{\rho_f^2} \right)^{1/4} \left(1 - \left\langle \alpha_1 \right\rangle \right)^{1.75} \tag{5-7}$$

$$\left\langle\left\langle v_{gj2}\right\rangle\right\rangle = \begin{cases} 0.35\sqrt{\dfrac{\Delta\rho g D_H}{\rho_f}} & \text{, for Taylor bubbles} \\ 0.54\sqrt{\dfrac{\Delta\rho g D_{base}}{\rho_f}}\left(1-\left\langle\alpha_2\right\rangle\right)^{3/2} & \\ \simeq 0.93\sqrt{\dfrac{\Delta\rho g D_{Sm2}}{\rho_f}}\left(1-\left\langle\alpha_2\right\rangle\right)^{3/2} & \text{, for Cap bubbles} \end{cases} \quad (5\text{-}8)$$

Here, σ, $\Delta\rho$ and D_{sm} represent surface tension, density difference and Sauter mean diameter, respectively. The drag diameter of cap bubble D_{base} was determined by the approximations that it possesses wake angle of 50° and is related to its Sauter mean diameter as follows [5-13]:

$$D_{base} = 2.96 D_{Sm2} \quad (5\text{-}9)$$

Eq. (5-5) is the one-group momentum equation simplified from the two-group equation, and effect of the parameters like drag coefficient, interfacial area concentration, shape factor, and relative velocity on two-phase interfacial drag can be evaluated. However, one cannot evaluate the effect of relative velocity on interfacial drag force term under the assumption of $\left\langle v_r\right\rangle \simeq \left\langle v_{r1}\right\rangle \simeq \left\langle v_{r2}\right\rangle$, Eq. (5-5) can be further simplified to obtain Eq. (5-10).

$$\left\langle M_{ig}\right\rangle = -\left(C_{i1}+C_{i2}\right)\left(\frac{1-C_0\left\langle\alpha\right\rangle}{1-\left\langle\alpha\right\rangle}\left\langle\left\langle v_g\right\rangle\right\rangle - C_0\left\langle\left\langle v_f\right\rangle\right\rangle\right)\left|\frac{1-C_0\left\langle\alpha\right\rangle}{1-\left\langle\alpha\right\rangle}\left\langle\left\langle v_g\right\rangle\right\rangle - C_0\left\langle\left\langle v_f\right\rangle\right\rangle\right| \quad (5\text{-}10)$$

Here, C_0, C_{i1}, and C_{i2} are the distribution parameter, the drag coefficient of Group-1 and Group-2 bubbles, respectively.

As was shown, in order to utilize one-dimensional momentum equation and interfacial drag force term with consideration of two group approach, it is necessary to supply constitutive equations for drag coefficient, interfacial area concentration and shape factor of each group.

5.2.1 Constitutive relation for deriving drag force coefficient

5.2.1.1 Group-1 bubbles

Suppose that Group-1 bubbles are represented by the spherically shaped small bubbles in distorted particle regime. Then, drag coefficient for Group-1 bubbles can be obtained using following expression:

$$C_{D1} = \frac{\sqrt{2}}{3} N_{\mu} N_{Re_{\infty}} \left\{ f\left(\left\langle \alpha_1 \right\rangle\right)\right\}^2 \tag{5-11}$$

Here, $f\left(\left\langle \alpha_1 \right\rangle\right)$ is a function of the Group-1 void fraction, which is given by Eq. (5-12).

$$f\left(\left\langle \alpha_1 \right\rangle\right) = \frac{1 + 17.67\left(1 - \left\langle \alpha_1 \right\rangle\right)^{1.3}}{18.67\left(1 - \left\langle \alpha_1 \right\rangle\right)^{1.5}} \tag{5-12}$$

Additionally, viscosity number N_{μ} and Reynolds number $N_{Re_{\infty}}$ are defined as follows :

$$N_{\mu} \equiv \frac{\mu_f}{\left(\rho_f \sigma \sqrt{\frac{\sigma}{g\Delta\rho}}\right)^{1/2}} \tag{5-13}$$

$$N_{Re\infty} \equiv \frac{\rho_f \left| v_{r\infty} \right| D_d}{\mu_f} \tag{5-14}$$

Here, D_d and $v_{r\infty}$ are drag diameter of the bubble defined by $3B_d / 2A_d$ where B_d and A_d are, respectively, the volume and projected area of a typical particle, and terminal relative velocity, respectively.

Interfacial area concentration of Group-1 bubble is given by,

$$\left\langle a_{i1} \right\rangle = \frac{6\left\langle \alpha_1 \right\rangle}{D_{Sm1}} \tag{5-15}$$

In case of spherical bubble, shape factor can be approximated as 1.

$$\psi_1 \equiv \frac{D_{Sm1}}{D_d} \simeq 1 \tag{5-16}$$

Substituting Eqs. (5-11), (5-15), and (5-16) into Eq. (5-4), the drag coefficient for Group-1 bubble is expressed as follows:

$$C_{i1} = \frac{1}{2} \frac{\rho_f}{Lo} \left\langle \alpha_1 \right\rangle \left\{ f\left(\left\langle \alpha_1 \right\rangle\right)\right\}^2 \tag{5-17}$$

Here,

$$Lo \equiv \sqrt{\frac{\sigma}{\Delta\rho g}} \tag{5-18}$$

5.2.1.2 Group-2 bubbles

For Group-2 bubble, large bubbles such as Taylor bubble and cap bubble are considered, which can be found in slug flow regime or cap turbulent flow regime.

(a) Slug flow regime

Drag coefficient for Taylor bubble is given by following:

$$C_{D2} = 10.9\frac{D_d}{D_H}\left(1-\left\langle\alpha_2\right\rangle\right)^3 \simeq 9.8\left(1-\left\langle\alpha_2\right\rangle\right)^3 \tag{5-19}$$

Interfacial area concentration can be determined from the model proposed by Ishii and Mishima [5-12] as follows.

$$\left\langle a_{i2}\right\rangle = \frac{4.5}{D_H}\left\langle\alpha_2\right\rangle \tag{5-20}$$

It was shown by Hibiki et al. [5-8] that shape factor approaches constant value when the cylindrical shaped Taylor bubble length becomes much larger than drag radius. When such condition is satisfied, shape factor can be approximated by,

$$\psi_2 \simeq 1.5 \tag{5-21}$$

A drag coefficient of interfacial drag force term in slug flow regime can be calculated by substituting Eqs. (5-19) through (5-21) into Eq. (5-4), which leads to the expression shown in Eq. (5-22).

$$C_{i2} = 8.3\frac{\rho_f}{D_H}\left\langle\alpha_2\right\rangle\left(1-\left\langle\alpha_2\right\rangle\right)^3 \tag{5-22}$$

(b) Cap bubbly/ Cap turbulent flow regime

Drag coefficient for cap bubble is given by following:

$$C_{D2} = \frac{8}{3}\left(1-\left\langle\alpha_2\right\rangle\right)^2 \tag{5-23}$$

Similar to the Group-1 case, as was shown in Eq. (5-15), interfacial area concentration is determined by the Sauter mean diameter of Group-2 bubble as,

$$\left\langle a_{i2} \right\rangle = \frac{6\left\langle \alpha_2 \right\rangle}{D_{Sm2}} \tag{5-24}$$

Since drag diameter of cap bubble can be approximated by Sauter mean diameter, as was shown in Eq. (5-9), the shape factor is calculated as,

$$\psi_2 = \frac{D_{Sm2}}{D_{base}} \simeq \frac{1}{2.96} = 0.338 \tag{5-25}$$

Substituting Eqs. (5-23) through (5-25) into Eq (5-4), Eq. (5-26), which represents the drag coefficient of interfacial drag force term in cap bubbly/ cap turbulent flow regimes, can be obtained.

$$C_{i2} = 5.4\frac{\rho_f}{D_{Sm2}}\left\langle \alpha_2 \right\rangle\left(1-\left\langle \alpha_2 \right\rangle\right)^2 \tag{5-26}$$

Sauter mean diameter of cap bubble can be obtained from Schlegel and Hibiki [5-10]'s model.

$$\begin{aligned} D_{Sm2} = {} & D_H \frac{4.30}{N_{We}}\Big[0.238N_{vr}\left(1+\left\langle \alpha_1 \right\rangle\left\langle \alpha_2 \right\rangle-\left\langle \alpha \right\rangle\right) \\ & +4.95\left\langle \alpha_1 \right\rangle\left\{1.39\left(1-\left\langle \alpha_2 \right\rangle\right)^{2/3}+0.471\frac{\left(1-\left\langle \alpha_1 \right\rangle\right)^{7/4}}{\left(1-\left\langle \alpha_2 \right\rangle\right)^{1/2}}-1\right\}\Big]^{-1} \end{aligned} \tag{5-27}$$

Here,

$$N_{vr} \equiv \frac{\left\langle \varepsilon \right\rangle^{1/3} Lo^{1/3}}{v_{r2}}, \quad N_{We} \equiv \frac{\rho_f v_{r2}^2 D_H}{\sigma} \tag{5-28}$$

and necessary parameters to solve for the set of equations are shown below.

$$\begin{aligned} & \left\langle \varepsilon \right\rangle = \left\langle \varepsilon_{sh} \right\rangle + \left\langle \varepsilon_{BI} \right\rangle \approx \frac{0.316}{Re_m^{0.25}}\frac{v_m^3}{2D_H} + \left\langle j_g \right\rangle g \,, \\ & Re_m = \frac{\rho_m v_m D_H}{\mu_f}\frac{1}{1-\left\langle \alpha \right\rangle}, \quad \rho_m = \rho_g\left\langle \alpha \right\rangle + \rho_f\left(1-\left\langle \alpha \right\rangle\right), \quad v_m = \frac{\rho_g\left\langle j_g \right\rangle + \rho_f\left\langle j_f \right\rangle}{\rho_m} \end{aligned} \tag{5-29}$$

$$v_{r2} = 3.0\left(\frac{\sigma g \Delta\rho}{\rho_f^2}\right)^{1/4}\left(1-\left\langle \alpha_2 \right\rangle\right)^{1/2} \tag{5-30}$$

(c) Churn turbulent flow regime

Similar to cap-bubbly flow case, drag coefficient for the large bubble in churn turbulent flow can be given by Eq. (5-23). In churn-turbulent flow regime, bubbles tend to break-up into smaller sizes due to surface instability, and such condition is generally given by the critical Weber number of 8. The critical Weber number is defined by $\rho_f v_{gj}^2 D_b \big/ \sigma$ where v_{gj} and D_b are, respectively, the drift velocity and bubble diameter. In such case, interfacial area concentration is defined as,

$$\left\langle a_{i2} \right\rangle = \frac{3}{2}\frac{1}{Lo}\frac{\left\langle \alpha_2 \right\rangle \sqrt{1-\left\langle \alpha_2 \right\rangle}}{\psi_2} \tag{5-31}$$

The shape factor appearing in the denominator of Eq. (5-31) can be eliminated by substituting it into Eq. (5-4). From Eqs. (5-4), (5-23), and (5-31), a drag coefficient of the interfacial drag force term in churn-turbulent flow regime is given as follows:

$$C_{i2} = \frac{1}{2}\frac{\rho_f}{Lo}\left\langle \alpha_2 \right\rangle \left(1-\left\langle \alpha_2 \right\rangle\right)^{5/2} \tag{5-32}$$

Table 5-1 summarizes the drag coefficient for interfacial drag force term in each bubble group and the constitutive equations utilized for the derivation.

5.2.2 Closure relations to evaluate drag force term

In order to evaluate the interfacial drag force term using Eq. (5-4), distribution parameter, as well as constitutive equations for calculating volume fraction of each bubble group, are necessary. These constitutive equations which can be used with two-fluid model are summarized in following sections.

(a) Void fraction model for Group-1 and Group-2 Bubbles

In order to calculate the drag coefficient in interfacial drag force term shown in Eqs. (5-17), (5-22), (5-26), and (5-32), it is necessary to supply Group-1 and Group-2 void fraction values. Void fraction for each group is related to total void fraction as follows,

$$\left\langle \alpha \right\rangle = \left\langle \alpha_1 \right\rangle + \left\langle \alpha_2 \right\rangle \tag{5-33}$$

and they can be calculated using the models proposed by Ozar et al. [5-9] or Schlegel and Hibiki [5-10].

Ozar et al. model

It was shown by Ozar et al. [5-9] that the constitutive equations for interfacial area concentration utilized in RELAP5 and TRAC-P cannot accurately predict the experimental data obtained in pipe diameter of 25.4 and 48.3 mm, and annulus channel with hydraulic diameter of 19.1 mm. Ozar et al. [5-9] proposed two-group interfacial area concentration model based on the experimental database developed up to void fraction value of 0.85. In addition, Ozar et al. [5-9] proposed constitutive equation for Group-1 void fraction based on Hibiki and Ishii [5-14]'s model. Void fraction models for each bubble group reported in Ozar et al. [5-9] are tabulated in Table 5-2. These models can be utilized for medium diameter pipe, but its applicability for large diameter pipe with $D_H^* \equiv D_H / Lo > 30$ and rod-bundle flow channel hasn't been confirmed as of now.

Schlegel and Hibiki model

Schlegel and Hibiki [5-10] proposed two-group interfacial area concentration model applicable to the large diameter pipe for $D_H^* > 30$. The database utilized for the constitutive equation development includes bubbly flow, cap-bubbly flow, and churn flow. Similar to Ozar et al. [5-9]'s model, the constitutive equation to calculate Group-1 void fraction was developed in their work, and it is tabulated in Table 5-3. Applicability of the model was confirmed for the experimental database developed by Yan et al. [5-15] on 8 × 8 rod-bundle test section at the air-water system under atmospheric pressure condition. However, the model's applicability hasn't been validated with the steam-water flow with prototypic pressure and temperature conditions.

(b) Distribution parameter model

Distribution parameter proposed by Ishii [5-3] can be utilized, which is defined as follows:

$$C_0 = C_\infty - \left(C_\infty - 1\right)\sqrt{\frac{\rho_g}{\rho_f}} \tag{5-34}$$

Here, C_∞ is the asymptotic distribution parameter and it is determined depending on the flow channel geometry, low flow rate condition, subcooled boiling condition, and so on. C_∞ is given based on the channel geometry, except for the pool condition and wall-peak condition for void fraction [5-16, 5-17, 5-18].

$$C_{\infty} = \begin{cases} 1.2 & , \text{ for round tube} \\ 1.1 & , \text{ for annulus and rod bundle} \end{cases} \quad (5\text{-}35)$$

5.3 Calculation case for validating the interfacial drag model with C_D approach

The interfacial drag model shown in the previous chapter (C_D approach) was embedded into TRAC-BF1 code [5-19], and its applicability as well as calculation performances were evaluated. As tabulated in Table 5-4, analysis models for two-group interfacial area concentration models and Group-1 void fraction models were utilized. Models 1 and 2 are for medium diameter pipe and annulus test section, and Models 3 and 4 are for the large diameter pipe.

First, effect of the relative velocity term was assessed using Eq. (5-5) and Eq. (5-10). Note that Eq. (5-5) assumes relative velocity difference, while Eq. (5-10) assumes constant relative velocity. Figure 5-1 depicts the calculation node utilized in TRAC-BF1 for the current analysis. Pipe length and system pressure were set to 5 m and 7 MPa, respectively. PIPE component was assigned to the section where void fraction evaluation takes place. FILL component was utilized as a section to inject liquid and saturated vapor, and placed height by the first cell of the PIPE component. Pipe diameters were set to medium diameter pipe of 0.025 m and large diameter pipe of 0.25 m, respectively, and Models 1 and 3 were utilized for the drag coefficient model.

Figures 5-2 and 5-3 show the void fraction results in axial direction for both medium and large diameter pipe using Eqs. (5-5) and (5-10). As can be seen, no significant differences between these two models were observed for void fraction comparison. Superficial liquid velocity ranged from 0.5 to 2.0 m/s in the current analysis, but the maximum difference in void fraction was at only 2 %.

It is important to consider relative velocity for each group separately to evaluate group wise interfacial drag force term, but as shown in the sensitivity analysis of Figs. 5-2 and 5-3, treating relative velocity as one group does not make significant differences. Utilization of single relative velocity term will significantly simplify the analysis, and hence, Eq. (5-10) will be utilized for the present analysis.

5.3.1 Experimental data as separate effect test

In order to validate the interfacial drag model under C_D approach, experimental database tabulated in Table 5-5 was utilized to perform the analysis.

Jeong et al. experiment

Jeong et al. [5-20] conducted void fraction measurement of the air-water two-phase flow system in annulus channel under atmospheric pressure condition. Area-averaged void fraction values in various axial positions were obtained. Outer and inner diameters of the annulus test section were 38.1 and 19.1 mm, respectively, and its hydraulic diameter was 19.0 mm. Experiments were conducted up to slug flow regime.

Shen et al. experiment

Shen et al. [5-21, 5-22] conducted experiments at 25m and 26m long large diameter pipe with 0.2 m diameter, and measured void fraction at various axial positions. The experiments were conducted at atmospheric pressure condition, but due to its large hydrostatic head, bubble expansion phenomena can be observed as bubbles pass through low to high z / D_H positions. The reported database covered from bubbly flow up to the transitional region of cap-bubbly flow regime.

Schlegel et al. experiment

Schlegel et al. [5-23, 5-24] conducted experiments using large diameter pipe up to the void fraction value of 0.85 while Shen et al. [5-21, 5-22]'s experiment covered low void fraction range (less than 0.3). The experiments covered bubbly flow, cap-bubbly flow, and churn-turbulent flow. In addition, three different pipe diameters, 0.152, 0.203, and 0.304 m, were utilized in the experiment with void fraction measurement in 3 to 5 axial positions.

5.3.2 Sensitivity analysis accounting for an uncertainty of interfacial drag force term

The interfacial drag models introduced in chapter 2 can be considered as more realistic and rigorous formulation by utilizing two-group approach in dispersed bubbly flow condition. However, there exist several problems with this approach which ultimately leads to an inaccurate expression of interfacial drag force term. First, it assumes equivalent relative velocity for each phase as well as assuming total drag coefficient to be the summation of Group-1 and Group-2 drag coefficient. In addition, bubble shape represented by the shape factor is determined by oversimplified assumption. Thirdly, a covariance of void fraction profile must be considered for the relative velocity and drag coefficient of interfacial drag force term [5-25, 5-26, 5-27]. Lastly, existence of uncertainties in constitutive equations utilized to derive interfacial drag force term cannot be neglected.

To evaluate the effect of uncertainties in interfacial drag force term towards the

area-averaged void fraction values numerically, the sensitivity analysis was performed by multiplying the factor ξ on interfacial drag force term for the 5 m length pipes with diameters of 0.025 and 0.25 m. The calculation domain, shown in Fig. 5-1, was utilized in TRAC-BF1 code. Five conditions with different ξ values of 0.2, 0.5, 1, 2, and 5 were utilized for the numerical calculation.

5.3.3 Analysis of numerical stability with crossing flow regime boundary

It is known that the interfacial drag force term in momentum equation relaxes numerical ill-posedness of one-pressure two-fluid model. The interfacial drag model introduced in section 5.2 utilizes different constitutive equations depending on the flow regime. Hence, numerical instability issue may arise as the flow condition approaches to the flow regime transition. In order to investigate this issue, numerical analysis was conducted to see whether the models are numerically stable or not.

Analysis model depicted in Fig. 5-1 was utilized with two different pipe diameters, 0.025 and 0.25 m. It is expected that the behavior of interfacial drag force term change as the Group-2 bubbles begin to form near the flow regime transition. Such transition is expected to occur when the void fraction value reaches near 0.3. To conduct the numerical analysis covering this transition region, pipe length was set to 150 m. This condition will allow gradual void fraction increase in axial direction due to the change in hydrostatic head.

5.3.4 Transient calculation for nuclear reactor plant

Since the interfacial drag force term in momentum equation is a function of each phase's relative velocity, it will affect the void fraction behavior for both steady-state and transient state. For the safety analysis of nuclear plant, change in void fraction is directly linked to the change in neutron moderator and thermal power output.

OECD/NEA [5-28] provides the database for the turbine trip experiment performed at Peach Bottom Unit 2 as part of the international benchmark program. In this analysis, transient numerical analysis was performed based on the turbine trip experimental data obtained at Peach Bottom Unit 2 Cycle 2 (Turbine Trip Test 2). In the Turbine Trip Test 2 experiment, reactor trip was initiated under the scram signal which was purposely generated to simulate the turbine trip condition. In this analysis, scram signal was bypassed for Turbine Trip Test 2 experimental data to see the effect of interfacial drag model at the severe transient condition.

Analysis condition for the Turbine Trip Test 2 in Peach Bottom Unit 2 is tabulated in Table

5-6. COS3D code, which is a three-dimensional neutronic code, was utilized to calculate the reactor power output based on neutron flux [5-29, 5-30, 5-31, 5-32]. The calculation was performed by constantly exchanging the thermal-hydraulic conditions calculated by TRAC-BF1 code, and reactor power output obtained by COS3D code. Figure 5-4 shows the nodalization of the Peach Bottom Unit 2 in TRAC-BF1 code, and Fig. 5-5 depicts the flow channel nodalization in the reactor core.

5.4 Results and Discussions

5.4.1 Validation results with separate effect tests data

Results obtained from the TRAC-BF1 code with interfacial drag model under "C_D approach" were compared with experimental database introduced in subsection 5.3.1.

Figure 5-6 shows the comparison of numerical calculation with respect to Jeong et al. [5-20]'s database. Since Jeong et al. [5-20]'s data was obtained at annulus test section with a hydraulic diameter of 19 mm, the calculation was performed using Model 1 and Model 2 tabulated in Table 5-4. Its results are shown in Fig. 5-6. The mean absolute error, m_d , standard deviation, s_d , mean relative deviation, m_{rel} , and mean absolute relative deviation, $m_{rel.ab}$ of calculated and measured void fraction values for Model 1 were, -0.018, 0.044, -0.11, and 0.15, respectively. For Model 2, it was determined as -0.021, 0.044, -0.11, and 0.16, respectively. Definitions of these statistical parameters are shown as follows:

$$m_d = \frac{1}{N}\sum_{i=1}^{N}\left(\alpha_{i,\text{cal.}} - \alpha_{i,\text{exp.}}\right), \tag{5-36}$$

$$s_d = \sqrt{\frac{1}{N-1}\sum_{i=1}^{N}\left\{\left(\alpha_{i,\text{cal.}} - \alpha_{i,\text{exp.}}\right) - m_d\right\}^2}\,, \tag{5-37}$$

$$m_{rel} = \frac{1}{N}\sum_{i=1}^{N}\frac{\alpha_{i,\text{cal.}} - \alpha_{i,\text{exp.}}}{\alpha_{i,\text{exp.}}}, \tag{5-38}$$

$$m_{rel,ab} = \frac{1}{N}\sum_{i=1}^{N}\frac{\left|\alpha_{i,\text{cal.}} - \alpha_{i,\text{exp.}}\right|}{\alpha_{i,\text{exp.}}}, \tag{5-39}$$

As can be seen, very small difference was observed for Model 1 (slug flow regime treated as Group-2) and Model 2 (churn turbulent flow regime treated as Group-2).

Figure 5-7 depicts the comparison between numerical calculation and Shen et al. [5-21, 5-22]'s experimental data. The experimental database was obtained at 20 cm diameter test section, hence, Model 3 and Model 4 tabulated in Table 5-4 were utilized for the calculation. The mean absolute error, m_d , standard deviation, s_d , mean relative deviation, m_{rel} , and mean absolute relative deviation, $m_{rel.ab}$ of calculated and measured void fraction values for Model 3 were, 0.039, 0.049, 0.13, and 0.16, respectively. For Model 4, it was determined as 0.014, 0.039, 0.0022, and 0.15, respectively. As can be seen, analysis results are comparable with Shen et al. [5-21, 5-22]'s void fraction data which were obtained at three different axial positions ranging from 8 m to 23 m. Hence, it can be said that the interfacial drag force term with void fraction propagation due to pressure gradient can predict the actual phenomena.

Figures 8 and 9 show the comparison between numerical calculation and database obtained by Schlegel et al. [5-23, 5-24]. As shown in Fig. 5-5, since the difference between Model 3 and Model 4 was found to be small, Model 3 was utilized for the comparison shown in Figs. 5-6 and 5-7. The mean absolute error, m_d , standard deviation, s_d , mean relative deviation, m_{rel} , and mean absolute relative deviation, $m_{rel.ab}$ of calculated and Schlegel et al. [5-23, 5-24]'s void fraction values were, 0.020, 0.053, 0.072, and 0.13, respectively. For Model 4, it was determined as 0.015, 0.052, 0.056, and 0.12, respectively. As can be seen from Figs. 5-8 and 5-9, the model can predict the high valued void fraction. In addition, equivalent predictive capability was achieved with the model compared with three separate experimental data with different pipe diameters.

5.4.2 Sensitivity of interfacial drag force term

In order to consider the uncertainty of interfacial drag model, void fraction values were evaluated by multiplying uncertainty factor ξ to the interfacial drag force term. In this sensitivity analysis model, the drag coefficient of $\left(C_{i1} + C_{i2}\right)$ in Eq.(5-10) is multiplied by the factor, ξ, and replaced by $\xi \times \left(C_{i1} + C_{i2}\right)$. Calculation domain shown in Fig. 5-1 was utilized for the analysis. The calculation result for pipe diameter 0.025 m is shown in Fig. 5-10, and the result for pipe diameter 0.25 m is shown in Fig. 5-11. Four different superficial liquid velocity values of $< j_f >$= 0.5, 1.0, 1.5 and 2.0 m/s were selected, and the area-averaged void fraction values ranged from 0.1 to 0.7 for the current analysis. Model 1 was selected for the analysis performed for medium diameter pipe, and Model 3 for the large diameter pipe. The interfacial drag force term multiplied by uncertainty factor ranged from a minimum of 0.2 to a maximum of 5 times the order of nominal

value. The sensitivity of the interfacial drag force term with respect to uncertainty factor tends to be large for the condition $< j_f >= 0.5$ m/s, but the change in void fraction magnitude was within $\pm$ 5 % and the change was found to be much smaller than uncertainty factor. Additionally, for the cases with $< j_f >= 1.0$ m/s and $< j_f >= 2.0$ m/s, almost no change in void fraction values were observed with respect to the change in interfacial drag force term. Interfacial drag term governs the interfacial momentum transfer at the gas-liquid interface, hence the term is likely to affect void fraction calculation results. However, contrary to that assumption, results depicted in Figs. 5-10 and 5-11 show different tendencies.

In general, steady-state and fully developed momentum equation for two-fluid model is expressed as follows:

$$-\langle\alpha\rangle\frac{\partial p}{\partial z}-\langle\alpha\rangle\rho_g g+\langle M_{ig}\rangle-\langle\alpha\rangle F_w=0 \tag{5-40}$$

$$-\left(1-\langle\alpha\rangle\right)\frac{\partial p}{\partial z}-\left(1-\langle\alpha\rangle\right)\rho_f g-\langle M_{ig}\rangle-\left(1-\langle\alpha\rangle\right)F_w=0 \tag{5-41}$$

Here, F_w is the pressure loss term due to wall friction. Eliminating pressure gradient term in Eqs. (5-40) and (5-41) yields,

$$\langle M_{ig}\rangle=-\Delta\rho g\langle\alpha\rangle\left(1-\langle\alpha\rangle\right) \tag{5-42}$$

Eq. (5-42) represents the force balance for interfacial drag force term at the steady-state condition.

Figure 5-12 shows the dependency of the left-hand side of Eq. (5-42) obtained from Model 1, on area-averaged void fraction values with conditions of $< j_f >= 2.0$ m/s, $< j_g >= 2.9$ m/s and $D_H = 0.025$ m. At the intersection point of interfacial drag force term and buoyancy term F_b, the force balance relationship shown in Eq. (5-42) is satisfied. Then, the void fraction value at the intersection point satisfies momentum equation expressed in Eqs. (5-40) and (5-41). As shown in Fig. 5-12, the interfacial drag force term is highly sensitive to the change in void fraction value. Hence, changing the interfacial drag force term using uncertainty factor does not significantly change the intersection point of buoyancy force term. As a result, it does not have a high sensitivity towards void fraction value.

5.4.3 Developing void fraction result from numerical stability assessment

As was shown in the calculation condition in subsection 5.3.3, effects of the interfacial drag

force term during flow regime transition on numerical stability were assessed using long vertical pipe with high hydrostatic head. Figure 5-13 shows the change in axial void fraction development for pipe diameters of 0.025 m and 0.25 m, respectively. As can be seen from the plot, liquid superficial velocities of $< j_f >= 0.5$ m/s and $< j_f >= 2.0$ m/s were utilized for both pipe diameters. In general, bubbly flow transition to slug flow or cap-bubbly flow is observed at the area-averaged void fraction value of 0.3. As can be seen from the plot, no discontinuous points were observed for area-averaged void fraction value in the axial direction and its development is quite smooth.

Figure 5-14 shows the void fraction transition behavior in medium diameter pipe when the air was injected at t = 0 sec for $< j_f >= 0.5$ m/s condition. The plot shows void fraction behavior in the axial direction, but even at the transient condition, void fraction behavior tends to be quite smooth. Thus, it can be said that the change in interfacial drag force term due to flow regime transition does not create numerical instability problem.

5.4.4 Results of transient analysis of nuclear power plant

For the analysis performed for Turbine Trip 2 experiment of Peach Bottom Unit 2, rated neutron flux time series and change in the void fraction at one of the central regions of fuel assembly are plotted in Figs. 5-15 and 5-16, respectively. It should be noted that as tabulated in Table 5-6, the scram signal is bypassed in this analysis. As a result, oscillatory behaviors are seen for the rated neutron flux and void fraction. Figures 5-15 and 5-16 compare the cases with Model 1 through Model 4 on interfacial drag force term, and the difference in transient behavior is evaluated.

In case of turbine trip phenomena, Turbine stop valve (TSV) was closed as a response to the safety protection system to completely stop the steam flow through turbine system. Such method has a purpose to prevent the turbine blade damage. For the cases in Figs. 5-15 and 5-16, TSV was closed after 0.5 sec of the accident. Following the closure of TSV, reactor pressure begins to increase, and from 0.5 to 1.0 sec, void fraction value tends to decrease. In Fig. 5-16, void fraction value tends to decrease after 0.5 to 1.0 sec TSV closure, which leads to an increase in rated neutron flux. As the rated neutron flux increases, a rate of decrease in void fraction begins to slow down and it tends to increase after 1 sec. Due to this increase in the void fraction, as shown in Fig. 5-15, rated neutron flux tends to decrease which eventually causes a decrease in moderator density. Similar behavior was periodically observed, and neutron flux and void fraction tends to oscillate one another at opposite phase.

Figure 5-16 shows the change in void fraction values with different interfacial drag model.

As can be seen, void fraction values calculated using Model 1 and Model 2 tend to be smaller than the one calculated by Model 3 and Model 4. This signifies that interfacial drag coefficient for Model 1 and 2 are smaller than that of Model 3 and 4. This causes overprediction of Group-2 bubble through interfacial drag coefficient. The change in rated neutron flux tends to be larger as the void fraction tends in to increase. As shown in Fig. 5-15, the first two dominant peaks of rated neutron flux for Model 1 and 2 exceed those values calculated by Model 3 and 4, which leads to a large void fraction change for Model 1 and 2. The interfacial drag force term suppresses transient void fraction fluctuation. Hence, when the drag coefficient value decreases, void fraction fluctuation tends to be larger for Model 1 and 2, which eventually causes a difference in neutron flux peak values.

5.5 Conclusions

In one-dimensional numerical simulation of two-phase flow, it is reported by previous researchers that the evaluation of interfacial drag force using IATE gives improved prediction performance [5-1]. However, in reality, reliable and adequate databases have not been developed for the source terms in IATE to accurately perform a realistic simulation of nuclear thermal-hydraulics.

In this chapter, interfacial drag model was embedded into TRAC-BF1 code based on the recently developed two-group IATE and the following conclusions were obtained.

- Interfacial drag model with consideration of two-group relative velocities and simplified drag coefficient based on constant relative velocity assumption for two groups were selected to compare the area-averaged void fraction results. The results showed that the maximum void fraction difference in these two approaches was 2 %. Hence, treating equivalent relative velocity for two groups does not make much difference in calculation results. Not considering two-group relative velocities will largely simplify the code modification process as well as calculation scheme itself, thus, it is a preferable method for one-dimensional analysis.
- Interfacial drag model utilized in the current analysis include Model 1 and Model 2 for medium diameter pipes, and Model 3 and Model 4 for large diameter pipe (Table 5-4). Model 1 and Model 3 treat Group-2 bubble as Taylor bubble and cap bubble, while Model 2 and Model 4 treat Group-2 bubble as bubbles in churn turbulent flow regime. Almost no differences were observed in area-averaged void fraction results for Model 1 and Model 2 in medium diameter pipe, and Model 3 and Model 4 in large diameter pipe.
- Area-averaged void fraction data obtained by Jeong et al. [5-20] on annulus channel, Shen et al. [5-21, 5-22] and Schlegel et al. [5-23, 5-24] on large diameter pipe was utilized as a

benchmark study. The statistical uncertainties of the prediction for these experimental data were estimated. The range of uncertainties for mean absolute error, standard deviation, mean relative deviation, and mean absolute relative deviation were, $-0.021 < m_d < 0.039$, $s_d < 0.053$, $-0.11 < m_{rel} < 0.13$, and $m_{rel,ab} < 0.16$, respectively. The difference of prediction tendency between Model 1 and Model 2 or Model 3 and Model 4 was found out to be small.

- In order to evaluate the uncertainty of interfacial drag model, area-averaged void fraction was compared by applying multiplication factor onto the drag coefficient. Interfacial drag term is a strong function of void fraction, hence, multiplying drag coefficient term by several factors would not make a noticeable difference as shown in Fig. 5-12. It was found that applying multiplication factors to drag coefficient term had a small influence towards calculation results of area-averaged void fraction value. Since the multiplication factor represents the effect of uncertainties in drag coefficient and interfacial area concentration correlation on void fraction, thus the uncertainties in interfacial area concentration value have a very limited effect towards void fraction prediction.
- In order to evaluate numerical instability caused by flow regime transition, very long pipe channel with large pressure gradient was considered in a numerical domain. The calculation results showed that smooth transition in void fraction change was observed in the axial direction. Numerical instability problem was not observed in the analysis of interfacial drag force term which includes two-group interfacial area concentration concept.
- Based on the Turbine Trip 2 experimental database obtained at Peach Bottom Unit 2, effects on the interfacial drag force term caused by the neutron flux response and void fraction transients were investigated. No noticeable difference was observed for selecting the Group-2 bubble model for slug flow regime (Model 1) or bubbly/ cap turbulent flow regime (Model 3). Likewise, no noticeable difference was observed for selecting Group-2 bubble as churn turbulent flow regime (Model 2 and Model 4). On the other hand, it was found that neutron flux response and void fraction transients were highly affected by the selection of appropriate models for medium diameter pipes (Model 1 or Model 2), and large diameter pipes (Model 3 or Model 4).

Table 5-1 Summary of constitutive relations of drag coefficient for Group-1 and Group-2 bubbles

Parameters	**Group 1** *Distorted Particle Regime*	**Group 2** *(a) Slug Flow Regime*	*(b) Cap Bubbly/Cap Turbulent Flow Regime*	*(c) Churn Turbulent Flow Regime*
Drag Coefficient, C_D	$\frac{\sqrt{2}}{3} N_\mu N_{Re_\infty} \left\{ f\left(\langle \alpha_1 \rangle\right) \right\}^2$ [5-6]	$9.8\left(1-\langle \alpha_2 \rangle\right)^3$ [5-6]	$\frac{8}{3}\left(1-\langle \alpha_2 \rangle\right)^2$ [5-6]	$\frac{8}{3}\left(1-\langle \alpha_2 \rangle\right)^2$ [5-6]
Interfacial Area Concentration, a_i [m^{-1}]	$\frac{6\langle \alpha_1 \rangle}{D_{Sm1}}$	$\frac{4.5}{D_H}\langle \alpha_2 \rangle$ [5-12]	$\frac{6\langle \alpha_2 \rangle}{D_{Sm2}}$	$\frac{3}{2}\frac{1}{Lo}\frac{\langle \alpha_2 \rangle \sqrt{1-\langle \alpha_2 \rangle}}{\psi_2}$
Shape Factor, ψ	~ 1	~ 1.5 [5-8]	~ 0.338 [5-13]	Not Necessary
Drag Force Coefficient, C_i	$\frac{1}{2}\frac{\rho_f}{Lo}\langle \alpha_1 \rangle \left\{ f\left(\langle \alpha_1 \rangle\right) \right\}^2$	$8.3\frac{\rho_f}{D_H}\langle \alpha_2 \rangle \left(1-\langle \alpha_2 \rangle\right)^3$	$5.4\frac{\rho_f}{D_{Sm2}}\langle \alpha_2 \rangle \left(1-\langle \alpha_2 \rangle\right)^2$	$\frac{1}{2}\frac{\rho_f}{Lo}\langle \alpha_2 \rangle \left(1-\langle \alpha_2 \rangle\right)^{5/2}$

Table 5-2 Void fraction model for each bubble group applicable to medium diameter pipes [5-9]

Parameters	Recommended Formulations
Group-1 Void Fraction	$\left\langle \alpha_1 \right\rangle = \begin{cases} \left\langle \alpha \right\rangle & \left\langle \alpha \right\rangle \le \left\langle \alpha_{1,max} \right\rangle \\ \left\langle \alpha_{1,max} \right\rangle + \left(\dfrac{\left\langle \alpha_{1,max} \right\rangle - \left\langle \alpha_{1,base} \right\rangle}{\left\langle \alpha_{1,max} \right\rangle - \left\langle \alpha_{crit} \right\rangle} \right) \left(\left\langle \alpha \right\rangle - \left\langle \alpha_{1,max} \right\rangle \right) & \left\langle \alpha_{1,max} \right\rangle < \left\langle \alpha \right\rangle \le \left\langle \alpha_{crit} \right\rangle \\ \left\langle \alpha_{1,base} \right\rangle & \left\langle \alpha_{crit} \right\rangle < \left\langle \alpha \right\rangle \end{cases}$
Transition Void Fraction	$\left\langle \alpha_{1,\max} \right\rangle = \begin{cases} 0.235 + 0.011 \left\langle j_f^* \right\rangle & \left\langle j_f^* \right\rangle \le 6.1 \\ 0.325 - 0.004 \left\langle j_f^* \right\rangle & \left\langle j_f^* \right\rangle > 6.1 \end{cases}$
Critical Void Fraction	$\left\langle \alpha_{crit} \right\rangle = \begin{cases} 0.511 + 0.006 \left\langle j_f^* \right\rangle & \left\langle j_f^* \right\rangle \le 6.1 \\ 0.645 - 0.015 \left\langle j_f^* \right\rangle & \left\langle j_f^* \right\rangle > 6.1 \end{cases}$
Asymptotic Value of Void Fraction	$\left\langle \alpha_{1,base} \right\rangle = \begin{cases} 0.099 - 0.009 \left\langle j_f^* \right\rangle & \left\langle j_f^* \right\rangle \le 6.1 \\ 0.05 & \left\langle j_f^* \right\rangle > 6.1 \end{cases}$

Table 5-3 Void fraction model for each bubble group applicable to large diameter pipes [5-10]

Parameters	Recommended Formulations
Group-1 Void Fraction	$\left\langle \alpha_1 \right\rangle = \left\langle \alpha_{gs} \right\rangle \dfrac{1-\left\langle \alpha \right\rangle}{1-\left\langle \alpha_{gs} \right\rangle}$
	$\left\langle \alpha_{gs} \right\rangle = \min\left\{ \left\langle \alpha \right\rangle \quad , \quad 0.63 \tanh\left(0.00145 N_{Re_\varepsilon} \left\langle \alpha \right\rangle \right) \right\}$
Energy Dissipation per Unit Mass [m^2/s^3]	$\left\langle \varepsilon \right\rangle = \left\langle \varepsilon_{sh} \right\rangle + \left\langle \varepsilon_{BI} \right\rangle \approx \dfrac{0.316}{Re_m^{0.25}} \dfrac{v_m^3}{2D_H} + \left\langle j_g \right\rangle g$
	$N_{Re_m} = \dfrac{\rho_m v_m D_H}{\mu_f} \dfrac{1}{1-\left\langle \alpha \right\rangle}, \quad \rho_m = \rho_g \left\langle \alpha \right\rangle + \rho_f \left(1-\left\langle \alpha \right\rangle \right), \quad v_m = \dfrac{\rho_g \left\langle j_g \right\rangle + \rho_f \left\langle j_f \right\rangle}{\rho_m}$

Table 5-4 Combinations of Analysis model implemented in one-dimensional two-fluid model code.

Volumetric Fraction Models	**Interfacial Drag Force Models**
Ozar et al.(2012)	Model 1 – Slug flow regime for group 2 bubbles (Eq.(5-22))
(Table 5-2)	Model 2 – Churn turbulent flow regime for group 2 bubbles (Eq.(5-32))
Schlegel and Hibiki(2015)	Model 3 – Cap bubbly/Cap turbulent flow regime for group 2 bubbles (Eq.(5-26))
(Table 5-3)	Model 4 – Churn turbulent flow regime for group 2 bubbles (Eq.(5-32))

Table 5-5 Experimental databases utilized to validate the interfacial drag force models

Researchers	Geometry	Working Fluids	Pressure, p [MPa]	Hydraulic Diameter, D_H [m]	Measurement Locations, z / D_H [-]	Measurement Technics
Jeong et al. (2008)	Annulus	Air-Water	0.1	0.019	52, 149, 230	Conductivity Probe
Shen et al. (2010; 2012)	Pipe	Air-Water	0.1	0.2	41.5, 82.8, 113	Optical Probe
Schlegel et al. (2012)	Pipe	Air-Water	0.180/ 0.280	0.152	11.7, 17.7, 33.9	Conductivity Probe
				0.203	5.4, 9.8, 26.0	
Schlegel et al. (2013)	Pipe	Air-Water	0.180/ 0.280	0.152	2.09, 9.52, 16.3, 23.6, 30.7	Conductivity Probe
				0.203	1.26, 6.77, 12.2, 17.4, 24.9	
				0.304	1.00, 4.21, 7.82, 11.4, 15.5	

Table 5-6 Calculation conditions for a power plant transient simulation

Parameters		Values Used for Analysis
Rated Power [MWt]		3293
Rated Core Flow Rate [kg/s]		12915
Number of Fuel		764 (7x7 and 8x8)
Initial Conditions	Power [MWt]	2030
	Flow Rate [kg/s]	10445
Transient Conditions	Onset of TSV Closure [s]	0.5[*1]
	Onset of BPV Opening [s]	0.85[*2]
	Power to Initiate Scram Signal [%]	Bypassed [*3]
	Feed Water Pump	2 of 2 are tripped at about 8sec

*1: TSV(Turbine Stop Valve) fully closes at 0.0 s in the turbine trip 2 test.

*2: BPV(Bypass Valve) fully opens at 0.078 s in the turbine trip 2 test.

*3 Scram signal initiates with a power reached at 95 % of rated power in the turbine trip 2 test.

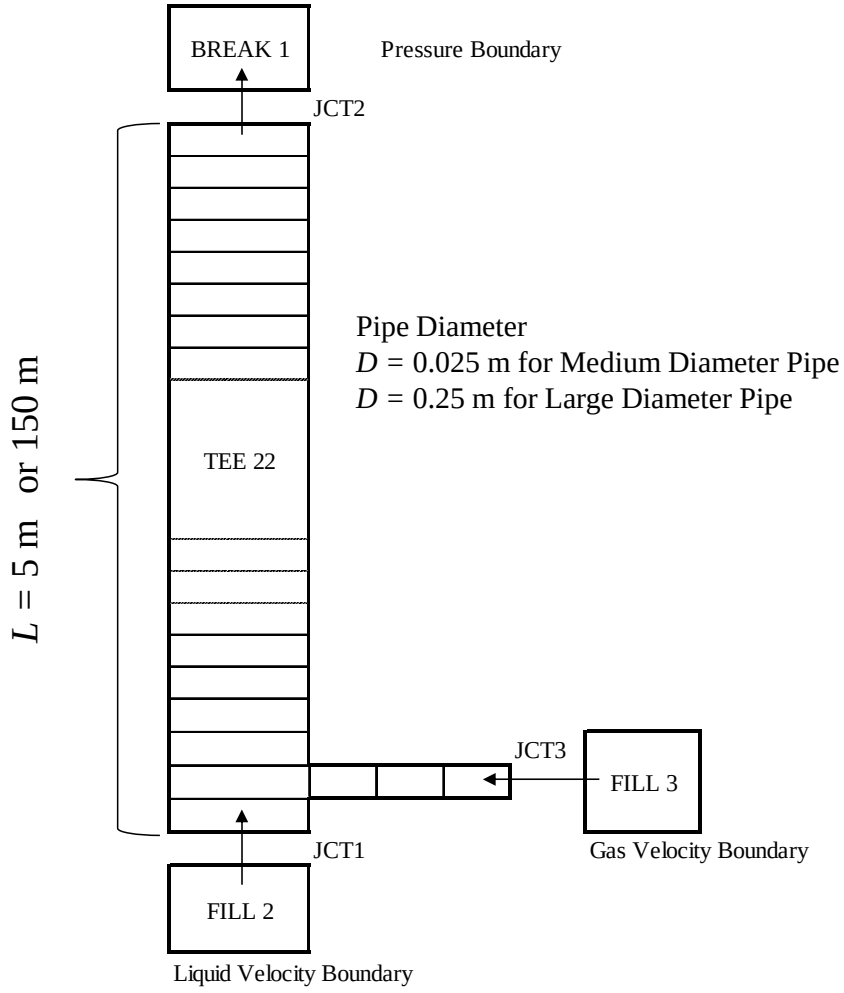

Figure 5-1 Hypothetical TRAC-BF1 calculation model for sensitivity analysis

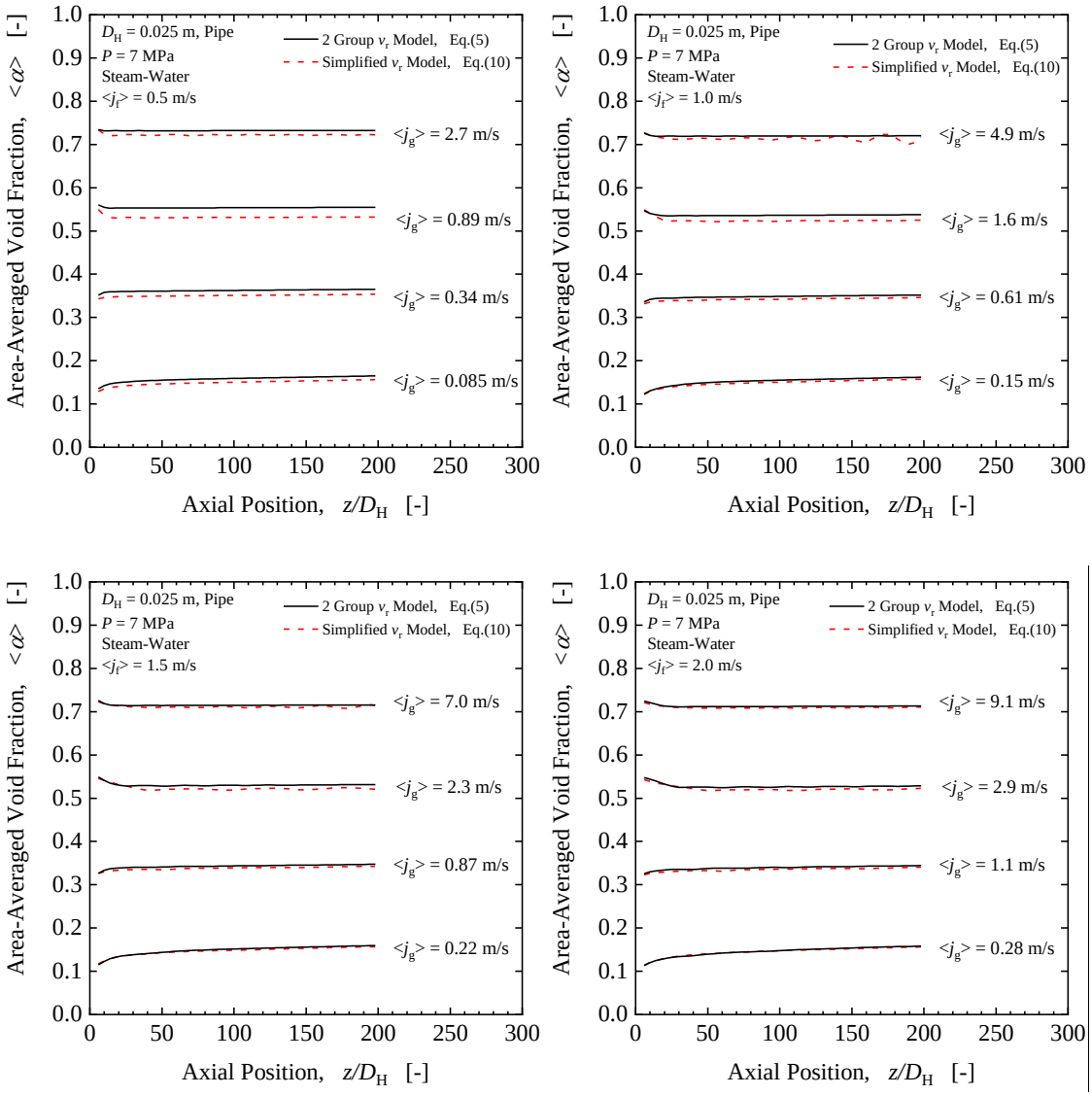

Figure 5-2 Comparisons of axial void fraction distribution between the model accounting for a difference of relative velocity and the model assuming equivalent relative velocity of each bubble group.
(Medium diameter pipe)

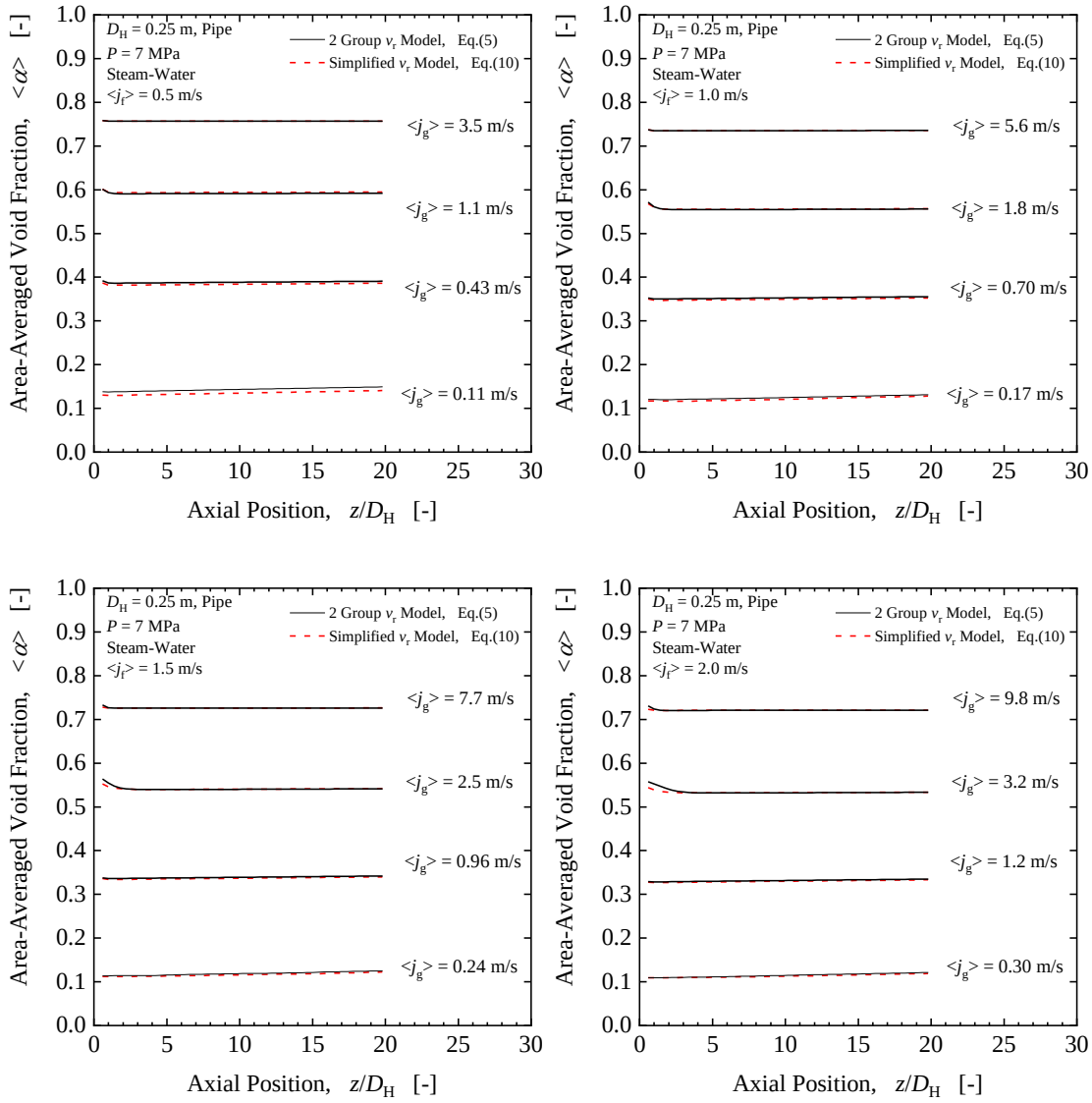

Figure 5-3 Comparisons of axial void fraction distribution between the model accounting for a difference of relative velocity and the model assuming equivalent relative velocity of each bubble group.
(Large diameter pipe)

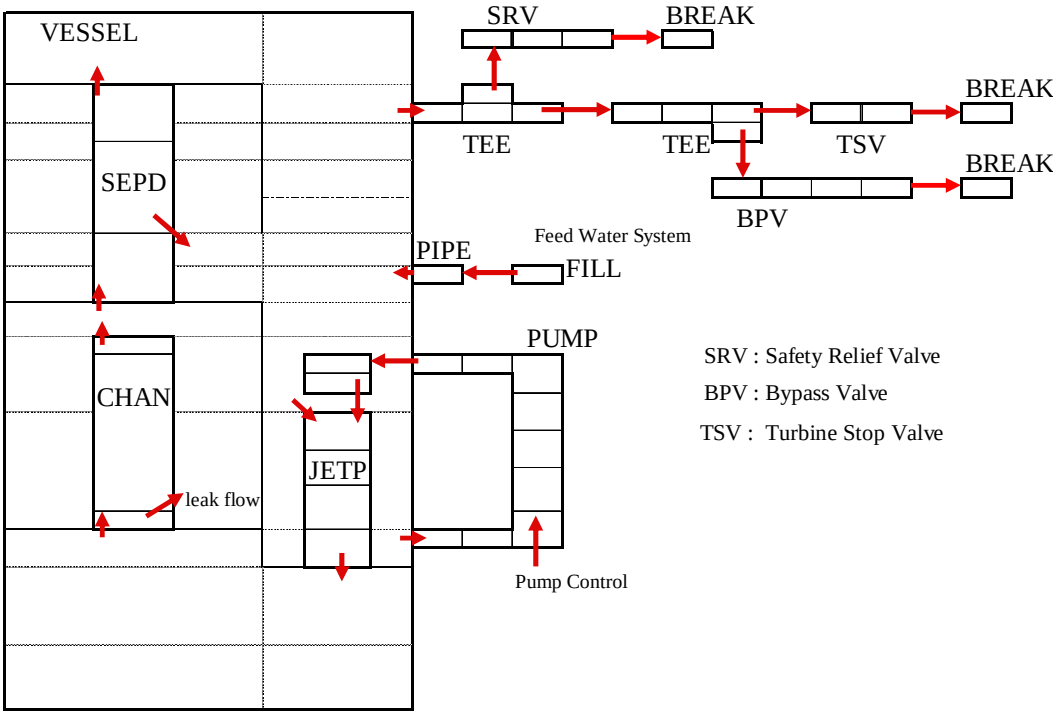

Figure 5-4 TRAC-BF1 modeling for Peach Bottom 2 plant

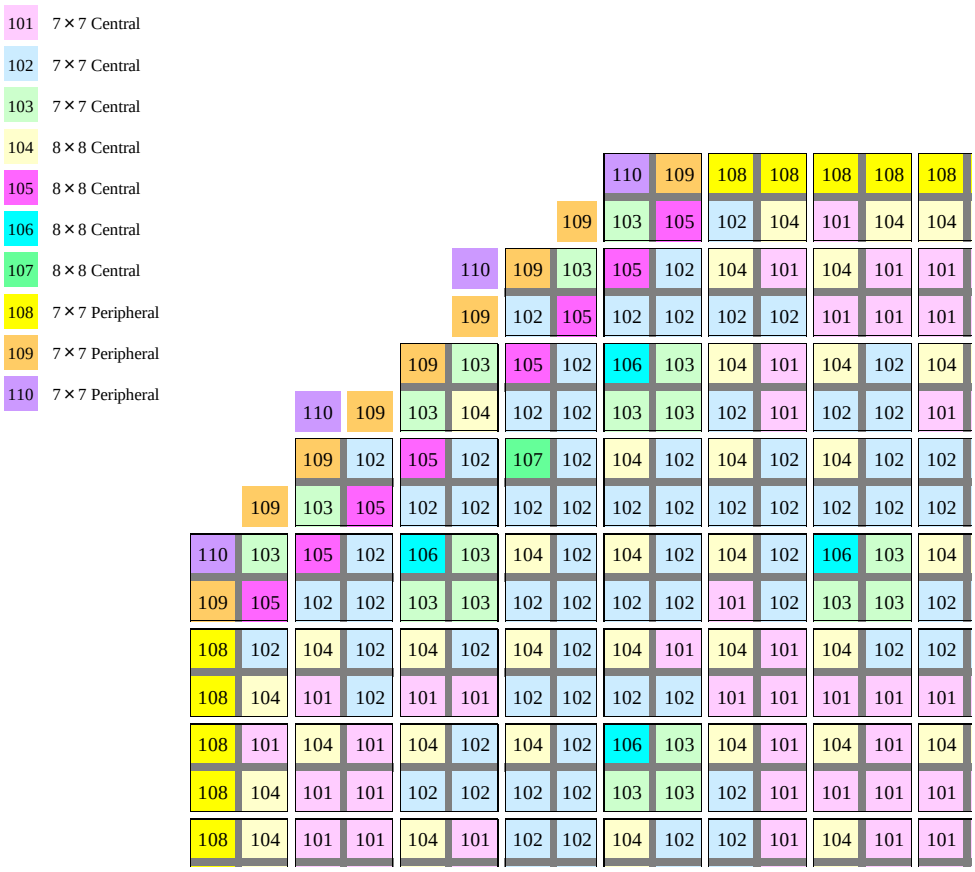

Figure 5-5 Core mapping for thermal-hydraulic model simulating cycle 2 of Peach Bottom 2 plant (1/4 Core)

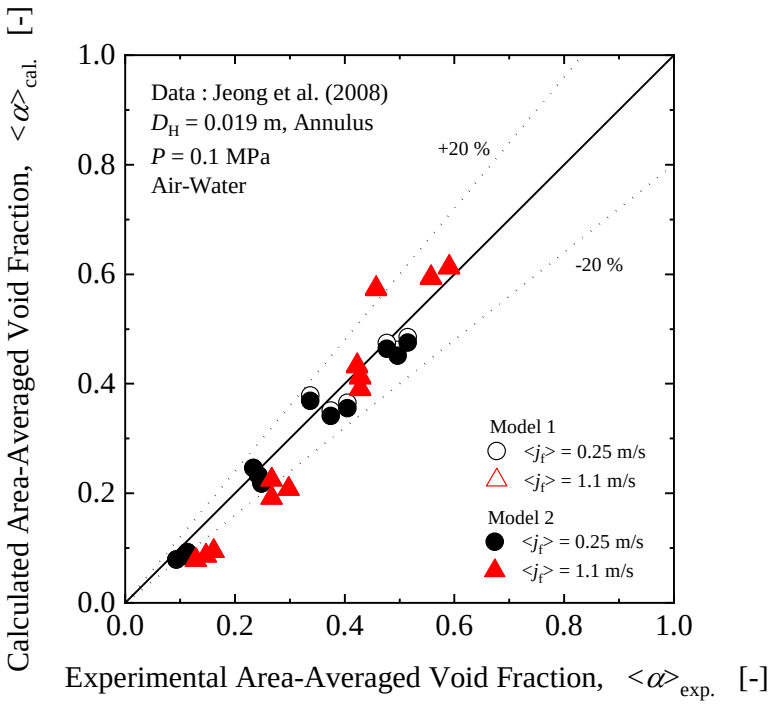

Figure 5-6 Comparison of experimental data obtained by Jeong et al. and calculation results.

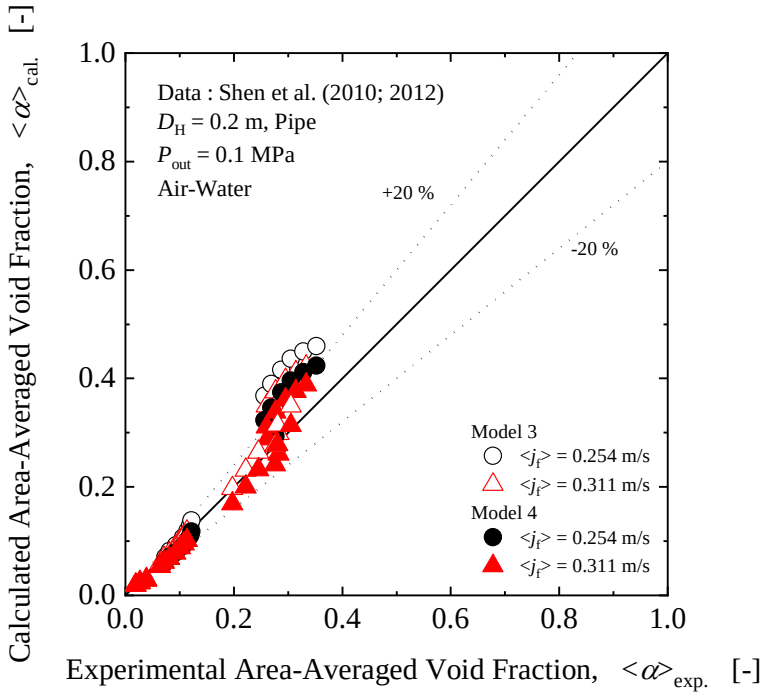

Figure 5-7 Comparison of experimental data obtained by Shen et al. and calculation results.

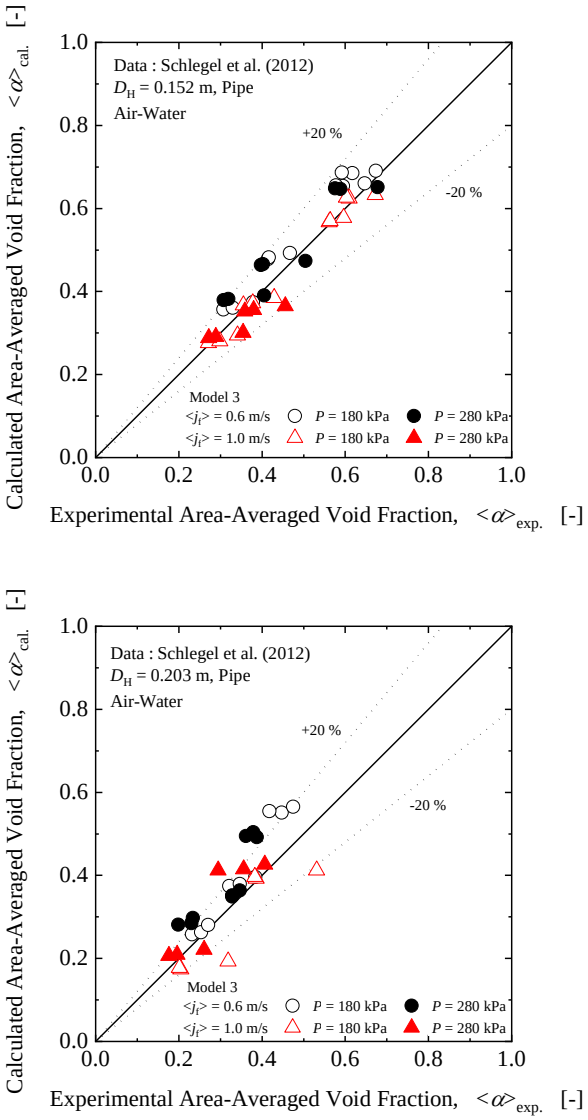

Figure 5-8 Comparison of experimental data obtained by Schlegel et al.[5-23] and calculation results.

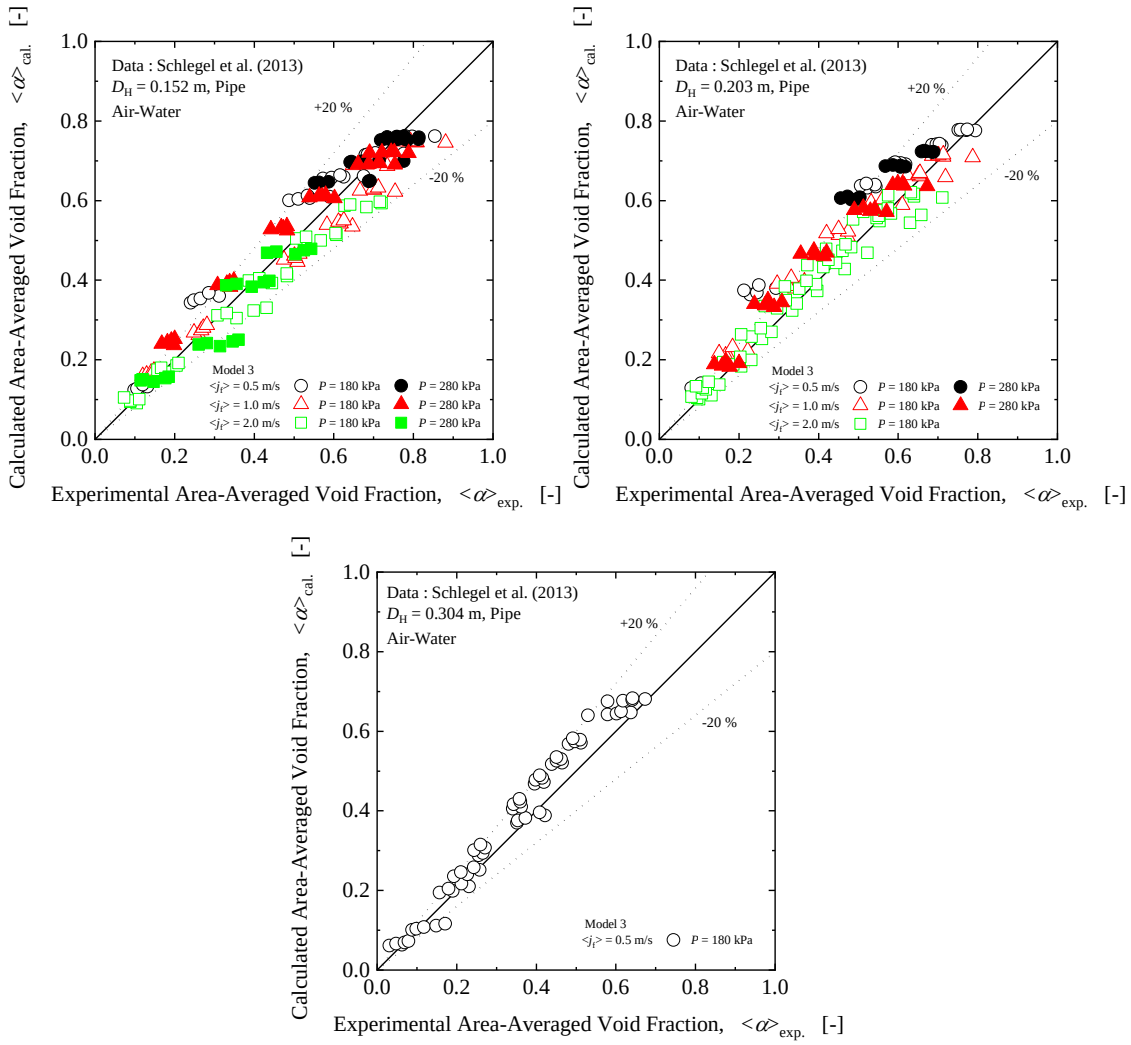

Figure 5-9 Comparison of experimental data obtained by Schlegel et al.[5-24] and calculation results.

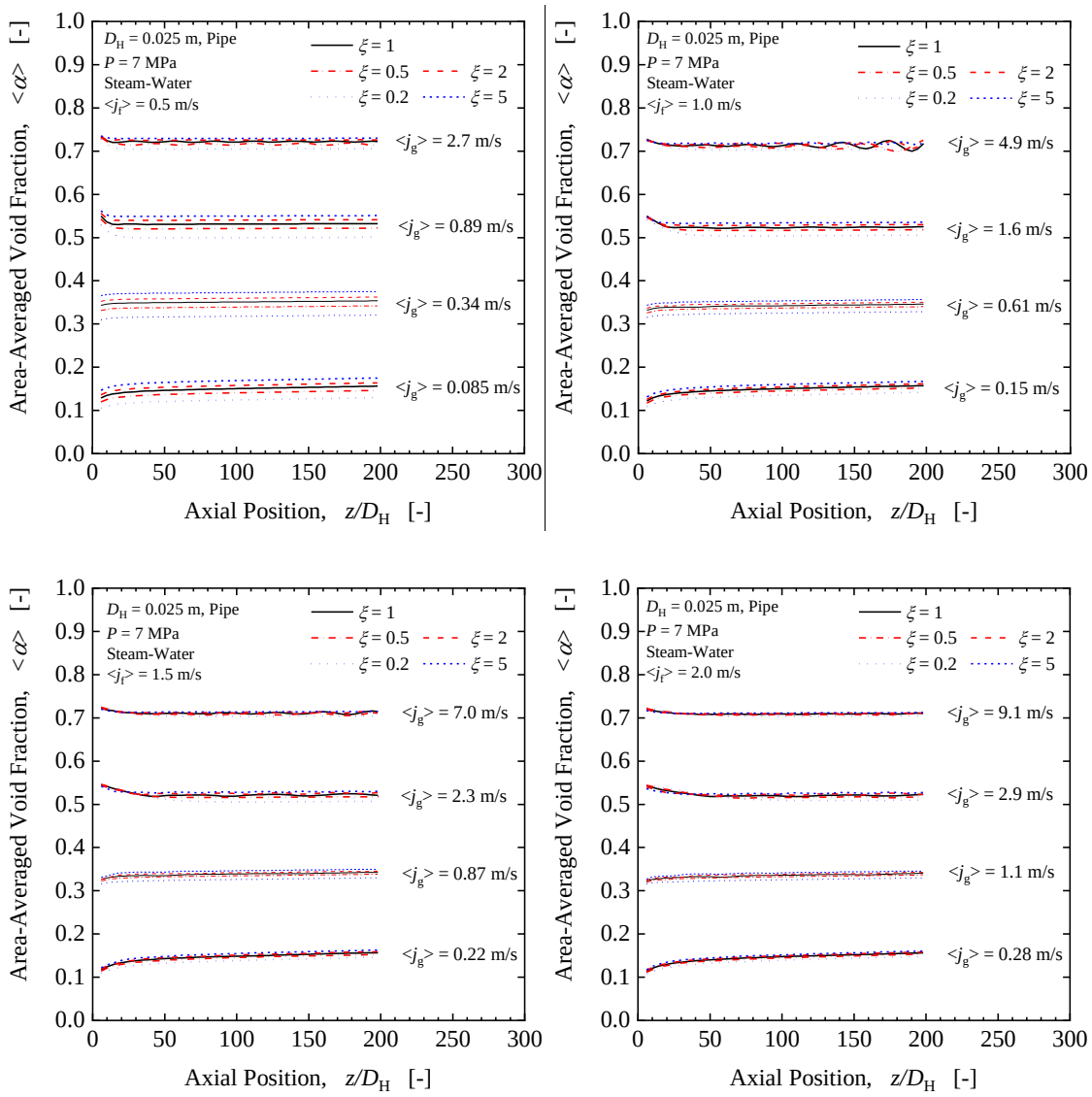

Figure 5-10 Comparisons of axial void fraction profiles with different sensitivity multiplier for the interfacial drag coefficient. (Medium diameter pipe)

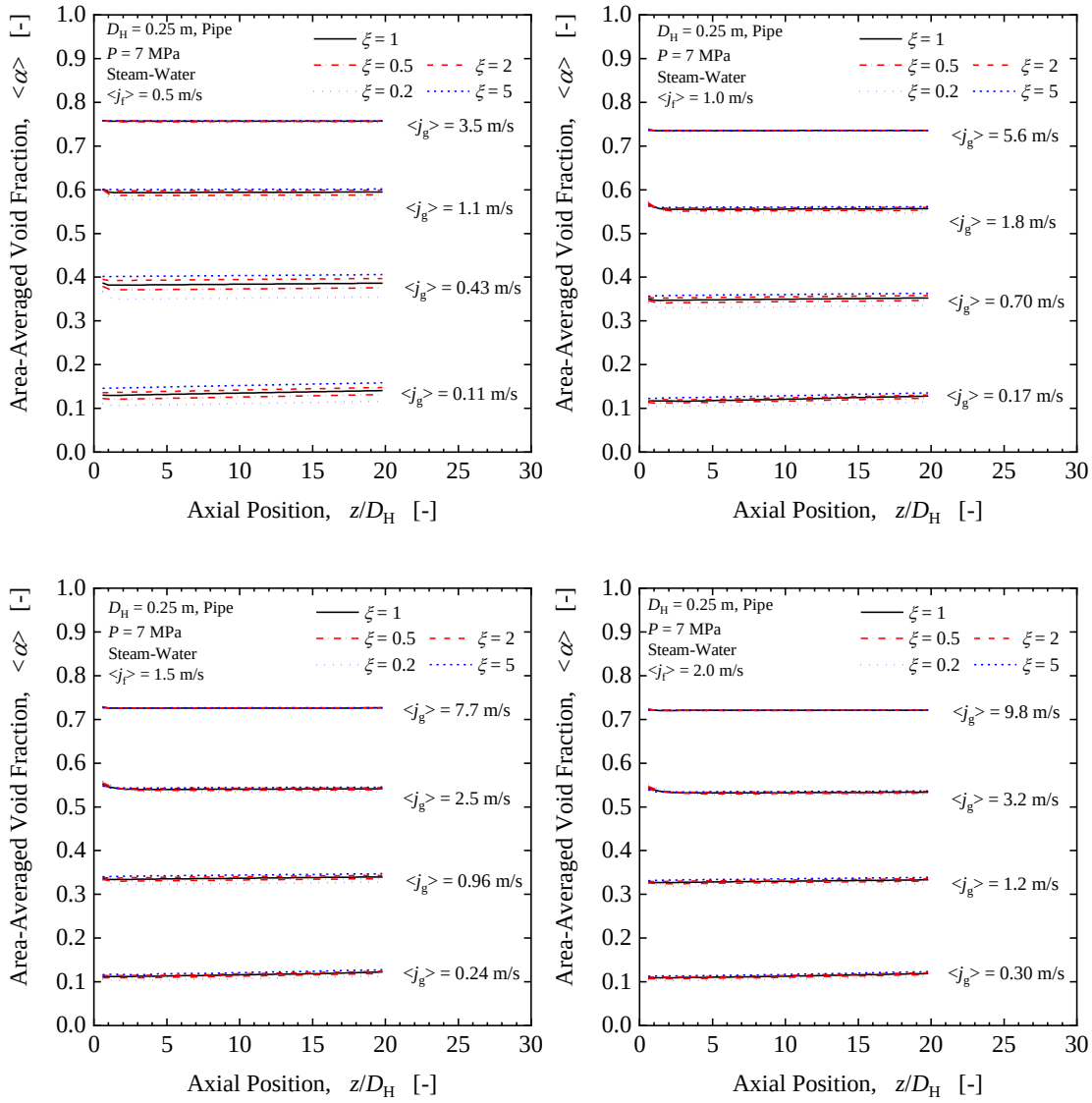

Figure 5-11 Comparisons of axial void fraction profiles with different sensitivity multiplier for the interfacial drag coefficient. (Large diameter pipe)

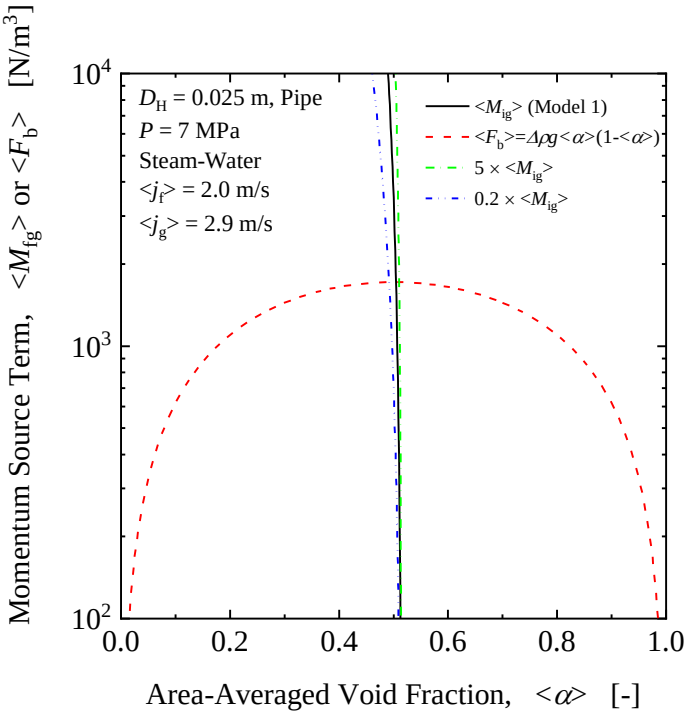

Figure 5-12 Tendencies of momentum source term of buoyancy force and interfacial drag force against an area-averaged void fraction.

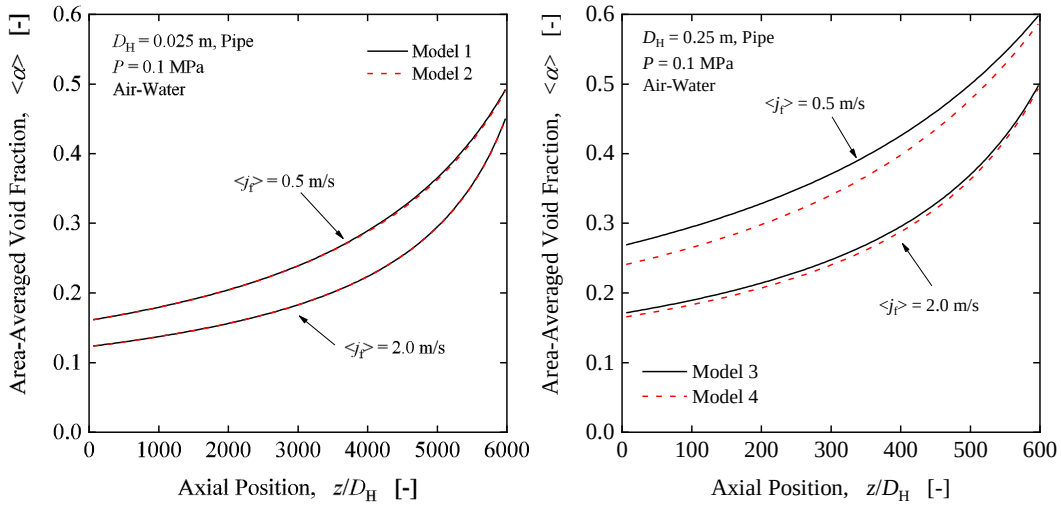

Figure 5-13 Characteristics of calculated void faction development with various interfacial drag force models

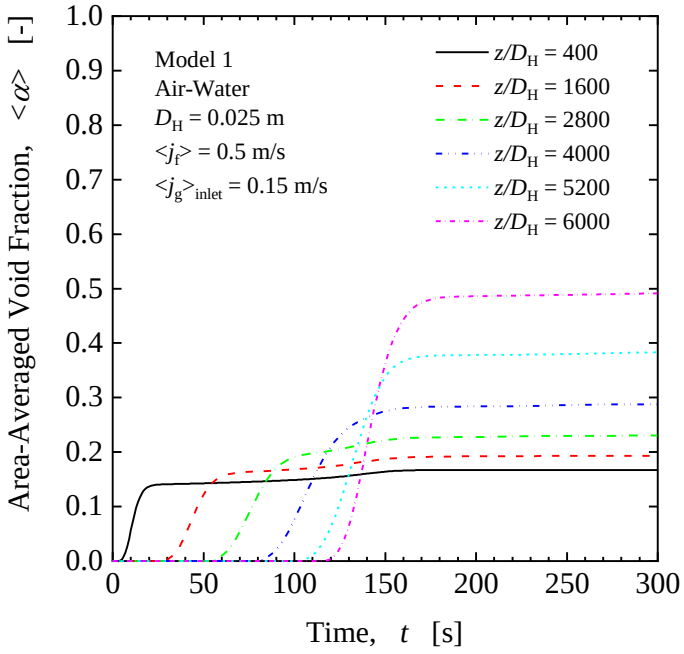

Figure 5-14 Calculation stability test results of transient void fraction development.

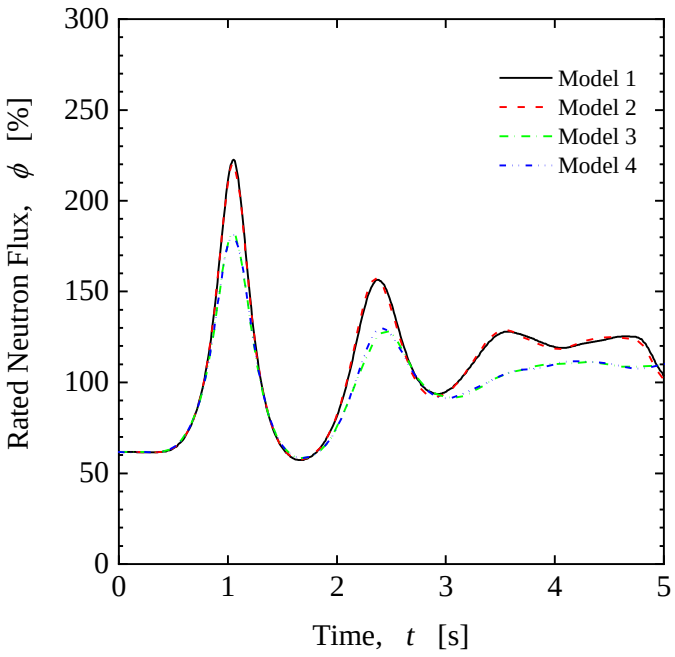

Figure 5-15 Calculation results of neutron flux of Peach Bottom 2 simulating core with the conditions of Table 5-6.

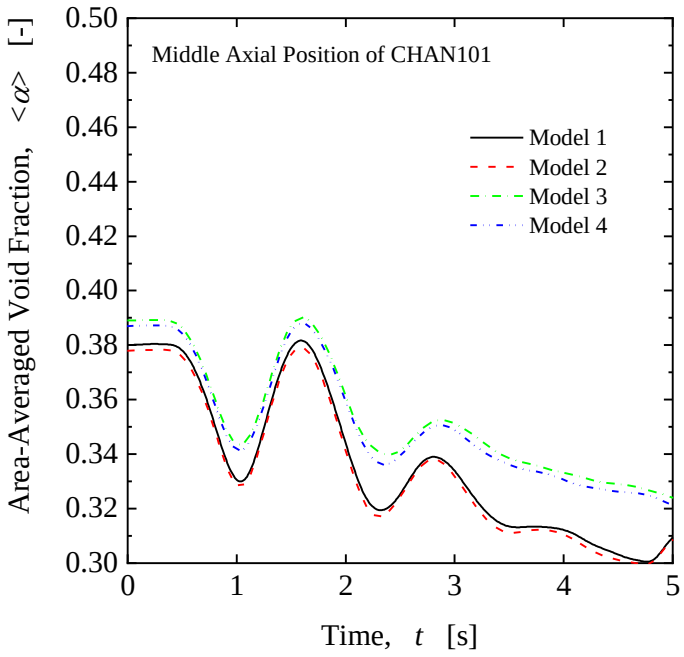

Figure 5-16 Calculation results of void fraction changes at the middle axial position of representative fuel channel of Peach Bottom 2 simulating core with the conditions of Table 5-6.

References

[5-1] Talley JD, Kim S, Mahaffy J, et al. Implementation and evaluation of one-group interfacial area transport equation in TRACE. Nuclear Engineering and Design 2011;241:865-873.

[5-2] Andersen JGM, Chu KH. BWR refill-reflood program constitutive correlations for shear and heat transfer for the BWR version of TRAC. Washington DC: US NRC; 1983. (NURG/CR-2134/GEAP-24940).

[5-3] Ishii M. One-dimensional drift-flux model and constitutive relations for relative motion between phases in various two-phase flow regimes. Argonne (IL): ANL; 1977. (ANL-77-47).

[5-4] Hibiki T, Ishii M. Distribution parameter and drift velocity of drift-flux model in bubbly flow. International Journal of Heat and Mass Transfer 2002;45:707-721.

[5-5] Hibiki T, Goda H, Kim S, et al. Axial development of interfacial structure of vertical downward bubbly flow. International Journal of Heat and Mass Transfer 2005;48:749-764.

[5-6] Ishii M, Hibiki T. Thermo-fluid dynamics of two-phase flow. 2nd ed. New York: Springer; 2011.

[5-7] Chuang TJ, Hibiki T. Vertical upward two-phase flow CFD using interfacial area transport equation. Progress in Nuclear Energy 2015;85:415-427.

[5-8] Hibiki T, Schlegel JP, Ozaki T, et al. Simplified two-group two-fluid model for three-dimensional two-phase flow computational fluid dynamics for vertical upward flow. International Journal of Heat and Mass Transfer (Forthcoming)

[5-9] Ozar B, Dixit A, Chen T, et al. Interfacial area concentration in gas-liquid bubbly to churn-turbulent flow regime. International Journal of Heat and Fluid Flow 2012;38:168-179.

[5-10] Schlegel JP, Hibiki T. A correlation for interfacial area concentration in high void fraction flows in large diameter channels. Chemical Engineering Science 2015;172-186.

[5-11] Shen X, Hibiki T. Interfacial area concentration in gas-liquid bubbly to churn flow regimes in large diameter pipes. International Journal of Heat and Fluid Flow 2015;54:107-118.

[5-12] Ishii M, Mishima K. Two-fluid model and hydrodynamic constitutive relations. Nuclear Engineering and Design 1984;82:107-126.

[5-13] Brooks CS, Paranjape SS, Ozar B, et al. Two-group drift-flux model for closure of the modified two-fluid model. International Journal of Heat and Fluid Flow 2012;37:196-208.

[5-14] Hibiki T, Ishii M. Interfacial area concentration of bubbly flow systems. Chemical Engineering Science 2002;57:3967-3977.

[5-15] Yan X, Schlegel JP, Liu Y, et al. Experimental study of interfacial area transport in air-water two phase flow in a scaled 8×8 BWR rod bundle. International Journal of Multiphase Flow

2013;50:16-32.

[5-16] Ozar B, Jeong JJ, Dixit A, et al. Flow structure of gas-liquid two-phase flow in an annulus. Chemical Engineering Science 2008;63:3998-4011.

[5-17] Ozaki T, Suzuki R, Mashiko H, Hibiki T. Development of drift-flux model based on 8×8 BWR rod bundle geometry experiments under prototypic temperature and pressure conditions. Journal of Nuclear Science and Technology 2013;50:563-580.

[5-18] Ozaki T, Hibiki T. Drift-flux model for rod bundle geometry. Progress in Nuclear Energy 2015;83:229-247.

[5-19] Borkowski JA., Wade NL. TRAC-BF1/MOD1 Models and correlations. Washington DC: US NRC; 1992. (NUREG/CR-4391/EGG-2680R4).

[5-20] Jeong JJ, Ozar B, Dixit A, et al. Interfacial area transport of vertical upward air-water two-phase flow in an annulus channel. International Journal of Heat and Fluid Flow 2008;29:178-193.

[5-21] Shen X, Mishima K, Nakamura H. Flow-induced void fraction transition phenomenon in two-phase flow. Proceedings of the 18th International Conference on Nuclear Engineering; 2010 May 17-21; Xi'an, China: ASME; 2010.

[5-22] Shen X, Hibiki T, Nakamura H. Developing structure of two-phase flow in a large diameter pipe at low liquid flow rate. International Journal of Heat and Fluid Flow 2012;34:70-84.

[5-23] Schlegel JP, Miwa S, Chen T, et al. Experimental stucy of two-phase flow structure in large diameter pipes. Experimental Thermal and Fluid Science 2012;41:12-22.

[5-24] Schlegel JP, Macke CJ, Hibiki T, et al. Modified distribution parameter for churn-turbulent flows in large diameter channels. Nuclear Engineering and Design 2013;263:138-150.

[5-25] Brooks CS, Ozar B, Hibiki T, et al. Two-group drift-flux model in boiling flow. International Journal of Heat and Mass Transfer 2012;55:6121-6129.

[5-26] Hibiki T, Ozaki T. Modeling of distribution parameter, void fraction covariance and relative velocity covariance for upward steam-water boiling flow in vertical pipe. International Journal of Heat and Mass Transfer 2017;112:620-629.

[5-27] Ozaki T, Hibiki T. Modeling of distribution parameter, void fraction covariance and relative velocity covariance for upward steam-water boiling flow in vertical rod bundle. Journal of Nuclear Science and Technology 2018;55:386-399.

[5-28] Solis J, Ivanov KN, Sarikaya B, et al. Boiling water reactor turbine trip (TT) benchmark Volume I : Final specifications. Paris, France:OECD/NEA; 2001.(NEA/NSC/DOC(2001)1).

[5-29] Nuclear Fuel Industries (NFI). Three-dimensional BWR core simulation method. Tokyo,

Japan: NFI; 1994.(NLR-03). in Japanese.

[5-30] Nuclear Fuel Industries (NFI). Core management system for BWR nuclear power plants. Tokyo Japan: NFI; 1999.(NLR-20). in Japanese.

[5-31] Ui A, Miyaji T. Peach Bottom 2 turbine trip simulation using TRAC-BF1/COS3D, a best-estimate coupled core and thermal-hydraulic code system. Nuclear Science and Engineering 2004;148:281-290.

[5-32] Ozaki T, Tsukamoto N, Nakamura R, et al. Effect of compensation error in drift-flux parameters on prediction of thermal-hydraulic parameters in nuclear safety system analysis codes. Progress in Nuclear Energy 2016;88:398-411.

6. Conclusions

One-dimensional two-fluid analysis codes are often utilized in the safety analysis of nuclear power plants. Safety analysis codes, used by plant designers or regulating authorities to simulate physical phenomena and analyze plant performance under accident scenarios, ensure the high-level of safety required in nuclear power plant operation. In this thesis, the momentum transfer term between the gas and liquid phase, namely the interfacial drag force term, is focused on due to the term's relevance to void fraction behavior and high ranking in the PIRT of many scenarios.

The existing works, focusing on the constitutive equations used to close the two-fluid model for a rod bundle, are summarized in chapter 2. As can be seen in this chapter, the constitutive equations for rod bundles are more advanced than ever especially in the flow regime map model, distribution parameter model, void fraction covariance model, and interfacial area concentration model.

The void fraction covariance model reviewed in Chapter 2 enables the exclusion of the void fraction uniformity approximation, which is implemented in existing two-fluid analysis codes. The interfacial drag force term accounting for the covariance effect was modeled and implemented in the two-fluid analysis code, and sensitivity analyses were performed for pipe geometry in Chapter 3. The results and discussion based on these sensitivity analyses, allow for the following conclusions.

1) The effect of covariance on the interfacial drag force term is especially significant for the case of high void fraction in dispersed bubbly flow and results in the interfacial drag force being reduced by almost half when the void fraction reaches 0.8. However, the sensitivity of the interfacial drag force term on the area-averaged void fraction calculated by the TRAC-BF1 code was found to be small.
2) Void fraction covariance substantially affects the drag coefficient in the interfacial drag force term, which is similar to the effect of drift-velocity on the drag coefficient. Thus, the sensitivity of covariance in an area-averaged void fraction becomes large as mixture volumetric flux decreases. The sensitivity of drift velocity is also significant in the case of low flow conditions.
3) The TRAC-BF1 code underestimates area-averaged void fraction compared to the value calculated by the simple drift-flux model when the interfacial drag force term accounts for void fraction covariance. This tendency can be explained due to the momentum source term of the liquid and gas phase, due to wall shear stress, neglecting the effect of void fraction covariance

4) The rigorous formulation of the two-fluid momentum equation is possible by accounting for the deviation of the momentum source term, which can be represented by the void fraction covariance. The area-averaged void fraction, calculated by this rigorous approach, coincides with that calculated by the drift-flux model.
5) A comparison of area-averaged void fraction response in representative transient events between the rigorous approach with covariance effect and existing approach without covariance showed a minor difference between void fraction responses. However, consideration of void fraction covariance effect in the interfacial shear force term causes a slightly enhanced oscillation behavior due to the lower coupling of liquid and gas velocity.

Chapter 4 investigates the effect of void fraction covariance in rod bundles. The conclusions, similar to those of Chapter 3, were that the void fraction covariance does not affect calculated area-averaged void fraction at steady state and constant velocity conditions. Diabatic wall conditions were also applied in this chapter and the behavior of steam flow transportation, with steam generation originating at the wall surface due to evaporation, was found to be affected by void fraction covariance. The void fraction at the heated region was slightly larger in the case considering void fraction covariance. Additionally, larger void fraction overprediction, calculated by the drift-flux model, was found in the case considering covariance, especially at the region downstream of the heated end. These differences arise due to the void fraction covariance weakening the momentum coupling between phases, causing the drag coefficient to become small. This chapter also investigated transient behaviors, by comparing area-averaged void fraction and inlet flow between the case considering void fraction covariance and the existing model. Applying some power disturbance to the system with constant pressure at the inlet and outlet boundary, allowed for simulation of the transient conditions. Conclusions drawn from the results of the transient simulations are as follows,

1) The observed dumping ratio after applying a power disturbance becomes larger in the case considering void fraction covariance. The increased dumping ratio results from a decrease of momentum coupling between phases. These results signify that void fraction covariance has some effect on the evaluation of system instability.
2) The underestimation of dumping ratio in the existing model, namely in the case approximating uniform void fraction distribution, becomes more evident as area-averaged void fraction increases. The underestimation reaches approximately 8 % when the

area-averaged void fraction at an initial steady state is 0.7.

Chapter 3 and Chapter 4 discus the rigorous formulation of the interfacial drag force term and the one-dimensional two-fluid momentum equation and the effect of void fraction covariance. While the void fraction covariance significantly affects the magnitude of the interfacial drag force term, its effects on the simulation results were limited. Therefore, the existing formulation is still valid for many simulation cases regardless of whether the formulation neglects void fraction covariance.

The interfacial drag force model, formulated based on the recently developed two-group interfacial area concentration correlation, was implemented in a two-fluid analysis code and the validity of the model was discussed in Chapter 5. The interfacial area transport equation has been proposed to prevent numerical instability caused by flow regime transition (Kelley, 1996). However, when applied in simulations of real power plants, the interfacial area transport equation has several problems, in regard to the V&V approach, that must be overcome. This thesis proposed a methodology to assess the applicability of the developed interfacial drag force model, which was based on a simplified interfacial area concentration correlation, and resulted in the following conclusions.

1) Two separate two-group interfacial drag force models were investigated. The velocity of the gas phase was rigorously determined for group-1 and group-2 bubbles, respectively. The first two-group interfacial drag force model accounts for the difference in relative velocity for each bubble group separately. So, the velocity of the gas phase was rigorously determined for group-1 and group-2 bubbles, respectively. The other model approximated that the relative velocity of group-1 and group-2 bubbles were equivalent. Comparing the models shows a maximum difference in calculated area-averaged void fraction of approximately 2%. This result implies that the second model, which approximates group-1 and group-2 relative velocity as equal, can be applied without a significant effect on simulation results. Application of the second model is beneficial, since it is easier to implement and enables a more intuitive understanding of calculation results.
2) The interfacial structure of Group-2 bubbles depend on the flow channel diameter, and thus separate interfacial drag force models should be provided for medium and large diameter pipes. The Group-2 bubble is modeled as a Taylor bubble, cap bubble, or churn

turbulent flow bubble depending on bubble shape observed in a pipe. However, there is no significant difference in the calculated area-averaged void fraction between simulations implementing the Taylor bubble model or churn turbulent bubble model in medium size pipes. Minimal differences are also observed in large diameter pipes for simulations implementing the cap bubble model or the churn turbulent bubble model.

3) Sensitivity calculations were also performed to account for model uncertainty associated with the interfacial drag force term. The uncertainty of the interfacial drag force term was represented by multiplying a constant value with the interfacial drag coefficient. The interfacial drag force term can be significantly influenced by a slight variation of area-averaged void fraction. Therefore, uncertainty associated with the interfacial drag force can be accounted for by a small change in area-averaged void fraction. The sensitivity analysis shows that uncertainties associated with values of interfacial area concentration have little effect on void fraction prediction.

4) Numerical instability may arise due to large variation of the interfacial drag force term as the two-phase flow undergoes a flow regime transition. Numerical calculations were performed and the axial development of area-averaged void fraction was investigated under the assumption of a very long pipe channel with a large pressure gradient. The calculation results show smooth void fraction transition and numerical instability was not observed, even when the two-phase flow underwent flow regime transition.

5) Based on the Turbine Trip 2 experiment performed at the Peach Bottom 2 nuclear power plant, the effect of interfacial drag force term was investigated by comparing the trends of neutron flux and void fraction obtained through use of different interfacial drag models. Use of different Group-2 bubble models in the slug flow regime or bubbly / cap turbulent flow regime resulted in negligible differences. Group-2 bubble models for the churn flow regime also showed negligible differences. However, the selection of appropriate models for use in medium diameter pipes and large diameter pipes significantly influenced neutron flux response and void fraction transients.

The conclusions obtained from Chapter 5, show that interfacial area concentration has a minimal effect on calculated values of area-averaged void fraction in a one-dimensional two-fluid analysis code. This conclusion implies that precise interfacial area concentration prediction methods and development of the interfacial area transport equation will have minimal impact on the improvement of existing one-dimensional two-fluid analysis codes. Instead, the effect of

distribution parameter on void fraction prediction and the validity and uncertainty in the existing models, needed to assure the credibility of the simulations, should be the primary focus.

Acknowledgments

First of all, I would like to express my gratitude to Prof. Michitugu Mori giving me a lot of helpful advice to complete and enhance this dissertation. I want to thank Prof. Masao Watanabe, Prof. Yuichi Murai, Assoc. Prof. Yuji Tasaka and Assistant Prof. Shuichiro Miwa for giving me comments on this dissertation through meaningful discussions.

I would also like to express the sincerest gratitude to Prof. Takashi Hibiki. Prof. Hibiki has created my fundamental knowledge about two-phase flow. This dissertation would not be completed without Prof. Hibiki's supports and encouragements.

I would like to express my appreciation to Nuclear Fuel Industries, Ltd. President Kenichi Kitagawa, Mr. Hideaki Kishita, Mr. Riichiro Suzuki, Mr. Yuichiro Kubo, and their colleague all have supported me with understanding about the extra work spent for the completion of the dissertation.

I must thank my wife, Hiroko, and daughters Yuka, Nozomi and Akina. They have patiently waited for the completion of this work. In the meantime, they warmly encourage me and I would have given up the work if there had not been their support. Finally, I express my sincere thanks to my parents for giving me a gift of the invaluable life experiences.